INTERFERENCE AND CHANNEL CONTROL TECHNIQUES FOR THE FUTURE OF WIRELESS COMMUNICATIONS

A DISSERTATION SUBMITTED TO

THE GRADUATE SCHOOL OF

ENGINEERING AND NATURAL SCIENCES

OF ISTANBUL MEDIPOL UNIVERSITY

IN PARTIAL FULFILLMENT OF THE REQUIREMENTS FOR

THE DEGREE OF

DOCTOR OF PHILOSOPHY

IN

ELECTRICAL, ELECTRONICS ENGINEERING AND CYBER SYSTEMS

By

SEDA TUSHA

August, 2020

INTERFERENCE and CHANNEL CONTROL TECHNIQUES FOR THE FUTURE OF WIRELESS COMMUNICATIONS
By SEDA TUSHA
August, 2020

We certify that we have read this dissertation and that in our opinion it is fully adequate, in scope and in quality, as a dissertation for the degree of Doctor of Philosophy.

Prof. Dr. Hüseyin ARSLAN(Advisor)

Prof. Dr. Özgür GÜRBÜZ

Prof. Dr. Hakan TOZAN

Assoc. Prof. M. Kemal ÖZDEMİR

Assoc. Prof. Ertuğrul BAŞAR

Approved by the Graduate School of Engineering and Natural Sciences:

Assoc. Prof. Dr. Yasemin Yüksel DURMAZ
Director of the Graduate School of Engineering and Natural Sciences

I hereby declare that all information in this document has been obtained and presented in accordance with academic rules and ethical conduct. I also declare that, as required by these rules and conduct, I have fully cited and referenced all material and results that are not original to this work.

Name, Last Name: SEDA TUSHA

Signature :

ABSTRACT

INTERFERENCE AND CHANNEL CONTROL TECHNIQUES FOR THE FUTURE OF WIRELESS COMMUNICATIONS

SEDA TUSHA
Ph.D. in Electrical, Electronics Engineering and Cyber Systems
Advisor: Prof. Dr. Hüseyin ARSLAN
August, 2020

Interference and random behavior of the propagation environment are the main impediments to serve a broad range of applications and use-cases in modern communication systems. Although conventional orthogonal multiple accessing (OMA) schemes are prominent for achieving high reliability, they are far from reaching the goals of 5G and beyond networks in terms of system capacity, massive connectivity, and latency. On the other hand, interest in high-frequency bands is growing due to the enormous amount of spare spectrum that has the potential to realize the aspirations of future communication systems. In addition to these considerations, next-generation communication systems require a flexible and scalable design to meet user equipment (UE) demands. For these reasons, this thesis study focuses on three pivotal research directions that control of interference in communication systems, control of channel randomness in millimeter wave (mmWave) bands, and the richness and flexibility of multidimensional signal transmission. In particular, non-orthogonal multiple accessing (NOMA) caused by partial and fully overlapping of the existing UEs, adaptive directional communication against low penetration capabilities in mmWave frequency band, and index modulation (IM)-aided multidimensional transmission for achieving flexibility are studied in the scope of this thesis.

Despite all the efforts, having effective multiple access under non-orthogonal conditions is still a conundrum in the literature. As a promising approach, waveform domain NOMA concept is introduced for serving multiple users with different requirements. The goal of waveform domain NOMA is to control interference by means of unique waveform features and consequently ensuring the separability of the overlapped UEs at the receiver. Specifically, the control of interference distribution is provided via the coexistence of appropriate waveforms while the average power of the interference remains the same. Moreover, diversity gain

is achieved through interference hopping during repetitions. Moreover, inter-carrier-interference (ICI) control for asynchronous networks and inter-numerology interference (INI) control for OFDM systems with multi-numerologies are studied via the exploitation of frequency domain IM, i.e., OFDM-IM, with the design of novel subcarrier mapping schemes.

Directional communication in mmWave bands provides opportunities to combat high level propagation loss. However, initiating communication over a certain direction makes the link vulnerable against low penetration capabilities, i.e., blockage impact. Beamwidth optimization in mmWave frequency bands is proposed in order to combat high path loss and blockage impact.

Lastly, IM-aided multidimensional communication opportunities are surveyed in a comprehensive manner. Specifically, a framework is developed for the purpose of efficient utilization of signal dimensions in order to address diverse requirements of 5G and beyond systems.

Keywords: Interference control, channel control, mmWave, blockage, low penetration capabilities, adaptive beamwidth, OFDM, OFDM-IM, waveform domain NOMA, multidimensional IM.

ÖZET

KABLOSUZ HABERLEŞMENİN GELECEĞİ İÇİN GİRİŞİM VE KANAL KONTROL TEKNİKLERİ

SEDA TUSHA
Elektrik-Elektronik Mühendisliği ve Siber Sistemler, Doktora
Tez Danışmanı: Prof. Dr. Hüseyin ARSLAN
Ağustos, 2020

Girişim ve yayılma ortamının rastgele davranışı, modern iletişim sistemlerinin hedeflerine ulaşmak için temel engellerdir. Öte yandan, geniş uygulama yelpazisini bünyesinde barındırmak için yeni nesil haberleşme sistemlerinin esnek bir yapıya sahip olması gerekmektedir. Bu yüzden, mevcut kullanıcı ekipmanlarının (UE) kısmi ve tamamen çakışmasınn kaynaklı dikey olmayan çoklu erişim (NOMA), mmWave frekans bandında düşük penetrasyon özelliklerine karşı adaptif yönlü iletişim, ve esneklik açısından çok boyutlu haberleşme imkanları bu tez kapsamında çalışılmıştır.

Gelecek vaat eden bir yaklaşım olarak, farklı gereksinimleri olan birden fazla kullanıcıya hizmet vermek için dalga formu tabanlı NOMA konsepti tanıtılmıştır. Dalga formu tabanlı NOMA'nın amacı, benzersiz dalga formu özellikleri aracılığıyla paraziti kontrol etmek ve sonuç olarak alıcıda üst üste binen UE'lerin ayrılabilirliğini sağlamaktır. Özellikle, uygun dalga formlarının bir arada bulunmasıyla parazitin ortalama gücü aynı kalırken parazit dağılımının kontrolü sağlanmıştır.

Milimetre (mmWave) dalga bantlarında yönlü iletişimi, yüksek seviyeli yayılım kaybıyla mücadele etme fırsatları sunar. Ancak, belirli bir yönde iletişim, bağlantıyı düşük penetrasyon özelliklerine, yani tıkanma etkisine karşı savunmasız hale getirir. Yüksek yol kaybı ve tıkanma etkisi ile mücadele etmek için mmWave bantları iin hüzme genişliği optimizasyonu önerilmiştir.

Son olarak, indis modulasyonu (IM) tabanlı çok boyutlu iletişim fırsatları kapsamlı bir şekilde incelenmektedir. Özellikle, 5G ve ötesindeki sistemlerin farklı gereksinimlerini karşılamak için sinyal boyutlarının verimli bir şekilde kullanılması amacıyla bir çerçeve geliştirilmiştir.

Anahtar sözcükler: Girişim kontrolü, kanal kontrolü, mmWave, tıkanma, düşük penetrasyon, adaptif hüzme genişliği, OFDM, OFDM-IM, dalga formu alanı NOMA, çok boyutlu IM.

Acknowledgement

First, I would like to deeply thank my supervisor, Dr. Hüseyin Arslan, for his continuous guidance, encouragement, and support throughout my study, and give special gratitude to him for not allowing me to quit. I would like to thank Dr. Özgür Gürbüz, Dr. Hakan Tozan, Dr. M. Kemal Özdemir, Dr. Ertuğrul Başar, Dr. Ali Görçin and Dr. Tunçer Baykaş for accepting my invitation and serving on my dissertation committee. I also thank all administrative staff in The School of Engineering and Natural Sciences at Istanbul Medipol University, especially Erol Akçay, Hasan Duman, Burak Gökay and Barış Yasin Yoldaş, for all their efforts that make this process easier for me.

It has been my pleasure and honor to be a member of the Communications, Signal Processing, and Networking Center (CoSiNC). I would like to thank all my friends in CoSiNC for their support as both friends and colleagues. I would like to give special thanks to Ahmet Yazar, and Abu Bakari Kihero for always being supportive of each other throughout this process. I would like to give special thanks to Furqan Ahmed, Ebubekir Memişoğlu, and Sohaib Solaija for their friendship, sincerity, and support. I would like to acknowledge Murat Karabacak for leading me to take the first step towards this road. I would like to thank Lamia Gülnur Kasap for her hospitality, generosity and relaxing conversations. I would like to give particular thanks to Melis Gülderen, Merve Meriç, Mine Tütüncü and Makbule Kurt for their priceless friendships in this life.

I would like to thank the members of my family in law, Fahri Tusha and Bukurije Tusha, my sisters in law Aurella Metvelaj and Almeda Tusha for all the emotional support and prayers throughout this process.

I have been always grateful to my parents Zübeyde Doğan, Recep Doğan, my dear sister Nida Doğan Çiftçi and my dear brother Ertuğrul Doğan for always being there for me in my life. I would not have been able to complete my study without their unconditional support throughout all these challenging years. I would like to give special thanks to my dear brother Akif Çiftçi for his kindness, support, generosity and exciting plans. I would like to thank my aunt Öznur Mutlu for her help, support, and prayers in my life.

Last, my deepest gratitude goes to my husband Armed Tusha for always caring

about me more than himself, for always comforting me whenever I am stressed, for always making me smile whenever I am sad, and for his immense help and support whenever I feel desperate throughout this long and winding process. Thank you for being my best friend, my best colleague, and my life companion.

Contents

Abstract **iv**

Acknowledgement **vii**

List of Figures **xi**

List of Tables **xiii**

1 Introduction **1**

1.1 Motivation 1

1.2 Scope of the Dissertation 3

1.3 Dissertation Contributions 4

1.3.1 A Novel Concept: Waveform Domain NOMA 4

1.3.2 Adaptive Beamwidth for mmWave Communications 5

1.3.3 A Multidimensional Perspective to Future Communications 5

1.3.4 Control of IUI in Asynchronous Systems 6

1.4 Dissertation Outline 7

1.5 Publications 7

2 Background **10**

2.1 5G and Beyond User Requirements 10

2.1.1 eMBB 10

2.1.2 mMTC 11

2.1.3 URLLC 13

2.1.4 Speculations for 6G and Beyond 14

2.2 Frequency Domain Index Modulation 15

2.2.1 OFDM with IM 15
2.2.2 State-of-the-art OFDM-IM Solutions 21

3 NOMA with Index Modulation for Uplink URLLC through Grant-Free Access 26
3.1 Introduction 26
3.1.1 Background on URLLC 27
3.1.2 Background on NOMA 28
3.1.3 Main contribution 29
3.2 System Model 31
3.2.1 GF Radio Access Technique 31
3.2.2 GB Radio Access Technique 33
3.2.3 Transmission Model for UE with URLLC 34
3.2.4 NOMA System Model 35
3.3 Theoretical Analysis 38
3.3.1 SINR Analysis 39
3.3.2 BER Analysis 40
3.4 Numerical Results and Discussion 42
3.5 Conclusion 51

4 Optimization of Antenna Beamwidth Under Blockage Impact in Millimeter-Wave Bands 52
4.1 Introduction 52
4.2 System Model & Power Azimuth Analysis 54
4.3 Measurement Environment and mmWave Channel Simulator . . . 56
4.3.1 Measurement Environment Description 56
4.3.2 Channel Simulator Description 58
4.4 Measurement&Simulation Results and Discussion 58
4.4.1 Measurement Results 58
4.4.2 Statistical Results 61
4.5 Conclusion 63

5 Multidimensional Index Modulation for 5G and Beyond Wireless Networks 64

5.1 Introduction 64
5.1.1 IM Can Revive Wireless Networks 65
5.1.2 Related Works 67
5.1.3 Contributions 70
5.1.4 Organization 70
5.2 Principles and Richness of Index Modulation 72
5.2.1 One-Dimensional IM 73
5.2.2 Two-Dimensional IM 83
5.2.3 Three-Dimensional IM 88
5.2.4 Hyper-Dimensional IM 89
5.3 Appropriate IM techniques for Next Generation Services 91
5.3.1 Enabling IM Techniques for Next-Generation Services . . . 95
5.3.2 Key Advantages and Disadvantages of Different IM Domains 107
5.4 Potential Challenges and Future Directions 109
5.4.1 Cognitive Radio Network through IM 110
5.4.2 Cooperative Networks through IM 111
5.4.3 Security in/with IM 112
5.4.4 Intelligent Wireless Communications through IM 113
5.4.5 Investigation of Novel IM Techniques 114
5.5 Conclusion 115

6 Conclusions **117**

Bibliography **117**

A Appendix: Copyright Notices **142**

About The Author **145**

List of Figures

2.1 Block diagram of OFDM-IM transmitter. 17
2.2 Frequency-domain representation of (**a**) OFDM-IM with $a = 3$, $b = 8$. (**b**) Classical OFDM. 18
2.3 Block diagram of OFDM-IM receiver. 20
2.4 OFDM-IM with fixed subcarrier activation ratio. 22
2.5 OFDM-GIM with variable subcarrier activation ratio. 23
2.6 Constellation diagram for (**a**) OFDM-IM (**b**) OFDM-GIM. 23

3.1 Constellation diagrams belonging to OFDM and OFDM-IM. . . . 30
3.2 GF radio access with K-repetitions for F_{UE} 32
3.3 GB radio access for S_{UE} 33
3.4 Three NOMA schemes based on OFDM for F_{UE} and S_{UE} with (a) OFDM (b) Scenario 1 for OFDM-IM (c) Scenario 2 for OFDM-IM. 37
3.5 BER performances for OFDM and OFDM-IM schemes. 43
3.6 Normalized interference power per subcarrier caused by S_{UE} on F_{UE}. 44
3.7 BER versus E_b/N_o for a single transmission of F_{UE} in the presence of NB-DI and NB-I. Impact of WB-I is represented by red color in both figures. 46
3.8 BER versus E_b/N_o for F_{UE} while $K = 2$ in the presence of NB-DI and NB-I. Impact of NB-DI and NB-I are represented with blue and red color, respectively. 47
3.9 BER versus E_b/N_o for F_{UE} under S_{UE} for $\frac{a}{b} = \frac{1}{8}$ until achieving 10^{-5} reliability by MRC receiver. Impact of WB-I, NB-DI and NB-I are represented with black, blue and red color, respectively. . 47

3.10 BER versus E_b/N_o for F_{UE} under S_{UE} for $\frac{a}{b} = \frac{3}{8}$ until achieving 10^{-5} reliability by MRC receiver. Impact of WB-I, NB-DI and NB-I are represented with black, blue and red color, respectively. . 48
3.11 BER versus E_b/N_o for F_{UE} under S_{UE} for $\frac{a}{b} = \frac{5}{8}$ until achieving 10^{-5} reliability by MRC receiver. Impact of WB-I, NB-DI and NB-I are represented with black, blue and red color, respectively. . 48
3.12 Trade-off between BER performance and latency. 49

4.1 System model where antennas with high gain are illustrated by blue color, while green color denotes to low gain antennas. 54
4.2 Measurement setup consists of the transmitter, receiver, reflectors and the blockage. 57
4.3 RSS in each azimuth angle for both LOS and penetration measurements in the absence of reflector in the system 59
4.4 RSS in each azimuth angle for both LOS and penetration measurements in the presence of reflector in the system 60
4.5 RSS in direct path regarding to Rx antenna HPBW 60
4.6 Cumulative distribution function (CDF) of observed gain as a result of optimizing HPBW. 62
4.7 Probability distribution of optimized HPBW and its corresponding observed gain. 62

5.1 Diverse IM variants for various services and channel conditions. . 66
5.2 Organization of the survey. 71
5.3 Basic implementation of IM, and the timeline of substantial IM techniques. 72
5.4 Dimensional-based categorization of the existing IM domains in the literature. 73
5.5 Corresponding fundamental IM variants for the existing multidimensional IM schemes. 90
5.6 Promising IM variants for 5G and beyond services. 105
5.7 The key advantages and disadvantages of the existing IM domains. 107

List of Tables

2.1 KPIs for next-generation services 12
2.2 An example for mapping the information bits to subcarriers by OFDM-IM and DM-OFDM while (b=4, a=2) 24
2.3 An example for mapping the information bits to subcarriers by CI-OFDM-IM while (b=4, a=2) 25

3.1 The proposed waveform pair according to communication requirements of F_{UE} and S_{UE} 29
3.2 Required number of retransmissions for F_{UE} to achieve 10^{-5} reliability, and corresponding transmission latencies under WB-I, NB-DI, and ND-I conditions 50

4.1 Optimal decision on Rx HPBW with its gain 61

5.1 Summary of the existing magazine articles on IM techniques . . . 68
5.2 One-dimensional and multidimensional IM Variants 75
5.3 IM techniques with the aid of dimension(s) exploitation 89
5.4 Data rate and computational complexity assessment of space domain IM techniques 92
5.5 Data rate and computational complexity assessment of frequency domain IM techniques 93
5.6 Data rate and computational complexity assessment of time, code, and channel domain IM techniques 94
5.7 The comparison of space and channel domain IM techniques . . . 98
5.8 The comparison of frequency, time and code domain IM techniques 100
5.9 The comparison of multidimensional IM techniques 102

Chapter 1

Introduction

1.1 Motivation

In contrast to the current 4th generation (4G) technology, where high spectral efficiency (SE) is the primary concern, 5th generation (5G) wireless networks are expected to support a broad range of applications and use-cases, which are mainly categorized under enhanced mobile broadband (eMBB), massive machine-type communication (mMTC), and ultra-reliable low-latency communication (URLLC). However, a surprisingly diverse range of requirements poses two main challenges for researchers and engineers worldwide: *1) providing service in the presence of intensive data traffic over the current communication systems,* and *2) supporting a wide range of applications and use-cases.* In order to accomplish the former *(1)*, spectrum-efficient approaches have been proposed by academia and industry, such as massive multiple-input multiple-output (MIMO) signaling, millimeter-wave (mmWave) communications, and non-orthogonal multiple access (NOMA) schemes. Besides high spectral efficiency (SE), 5G and beyond communication systems require a much more flexible structure for the latter *(2)*.

Orthogonal multiple access (OMA) always outperforms non-orthogonal multiple access (NOMA) in terms of reliability due to the distinct resource utilization

by multiple user equipments (UEs). NOMA systems suffer from inter-user interference (IUI) caused by the overlapping of the UEs in available resources. In a given system, non-orthogonality can be originated by partial and fully overlapping between the existing UEs. Generally, partial overlapping is the primary reason for IUI in previous communication systems due to out-of-band emission (OOBE) of signal energy. OOBE leads to adjacent channel interference (ACI). Besides, NOMA with partial overlapping in 5G communication systems occurs due to two fundamental reasons that are 1) inter-numerology interference (INI) in OFDM systems with multiple numerologies, and 2) asynchronous transmission. In order to serve eMBB, mMTC, and URLLC, OFDM with multiple numerologies is adopted for 5G and beyond networks, where the use of subcarrier spacings (SCSs) up to 120 kHz is allowed to shorten the symbol duration. The intermittent and sporadic traffic of UEs with mMTC results in asynchronous transmission, where time offset between UEs leads to IUI. Please note that there is no resource sharing between available UEs in the aforementioned scenarios. Distinct resource assignment to the UEs becomes more and more difficult in future communication systems because of emerging applications and use cases with diverse requirements. To exemplify, providing massive connectivity over limited resources for mMTC requires the sharing of available resources by the existing UEs. In the same vein, grant-free (GF) access for URLLC leads to overlapping of multiple UEs over the resources. Therefore, controlled NOMA schemes with partial and fully overlapping are extensively studied in the last decade. As an example of NOMA with full-overlapping, one of the well-known approaches is power domain NOMA, where multiplexing is employed in the power domain at Tx and successive interference cancellation (SIC) is utilized for demultiplexing at Rx. Despite all the efforts, power domain NOMA leads to catastrophic reliability when the overlapped UEs have similar channel gains. Even if the UEs have different channel gains, the power difference between them is not sufficient to separate them at the Rx side in real conditions. Although non-orthogonal transmission becomes difficult to avoid in future communication systems due to the aforementioned reasons, having effective multiple access under non-orthogonal conditions is still a conundrum in the literature, which encourages the researchers to seek new strategies that allow the utilization of available resources by multiple UEs.

mmWave communication is considered as one of the key technologies to meet high data rates demand of 5G and beyond networks due to the vast amount of spectrum. In high-frequency bands, transmitted signal exposes to a high path-loss and suffers from low penetration capabilities, i.e., blockage effect, due to millimetric wavelength. Rich scattering environment in microwave frequency bands enables the communication under non-light-of-side (NLOS) conditions. However, the sparse channel characteristics of mmWave frequencies require different solutions than that of microwave frequency bands in order to combat these challenges.

In light of the above considerations, firstly, interference sources in 5G and beyond networks are very diverse and the effect of interference alters considering its source. Therefore, interference control plays a key role in achieving 5G goals. Secondly, the control of mmWave channel is required to overcome a high path-loss and low penetration capabilities faced in high-frequency bands. Thirdly, multidimensional signal transmission schemes become more attractive for satisfying a broad range of user demands in modern communications systems.

1.2 Scope of the Dissertation

The scope of this thesis is to design flexible interference and channel control techniques for non-orthogonal transmission and mmWave communication in next-generation systems. The introduced techniques ensure flexibility in physical (PHY) layer to serve the different objectives of 5G and beyond systems. Specifically, this thesis study focuses on the coexistence of multiple UEs with diverse requirements via waveform domain NOMA, the directional communication with adaptive beamwidth against low penetration capabilities in mmWave frequency bands, and the multidimensional communication via index modulation (IM) to accommodate a broad range of services in future communication systems.

1.3 Dissertation Contributions

The conducted research studies in this thesis focus on the control of interference and channel effects faced in the next-generation communication system and the main contributions are summarized in the following.

1.3.1 A Novel Concept: Waveform Domain NOMA

Although conventional power domain NOMA is heavily studied in the last decade, it is far from satisfying the 5G expectations due to the unresolvable interference at the receiver. On the other hand, the accommodation of numerous applications with diverse demands inherently leads to non-orthogonal transmission in beyond 5G networks. Therefore, it is time to change the perspective to NOMA for serving a wide variety of services. In this sense, waveform-domain NOMA concept is proposed in this thesis. The concept aims to serve multiple users with different requirements that perform transmission over the same time and frequency resources. In waveform-domain NOMA, unique features of the overlapped waveforms in time and frequency dimensions ensure the separability of the superimposed UEs at the receiver. Specifically, the use of OFDM and index modulated OFDM (OFDM-IM) is introduced for the coexistence of UE with grant-free ultra-reliable low-latency communication (URLLC) and UE with grant-based latency-tolerant service, respectively. Available resources are shared among the services when URLLC occurs. This scheme exploits two critical things that 1) narrowband dominant interference compared to the whole band interference, and 2) interference hopping. The utilization of OFDM-IM leads to narrowband dominant interference on OFDM with frequency hopping as the active subcarriers are dependent on information bits. On the other hand, the superposition of two OFDM signals results in wideband interference. In this sense, although the average power of interference to be faced is the same, interference distribution is controlled to achieve reliable communication.

1.3.2 Adaptive Beamwidth for mmWave Communications

In this study, beam expansion and optimization approach is proposed as a solution to alleviate blockage impact at mmWave frequency bands. Directional communication in mmWave bands provides opportunities to combat with high-level propagation loss. However, initiating communication over a certain direction makes the link vulnerable against blockage impact. In this study, an investigation on antenna directionality is conducted through indoor measurements and statistical analysis to elaborate directional link performance under blockage effect. Measurements are conducted at 60 GHz frequency band by using 15° half power beamwidth (HPBW) antennas at transmitter and receiver . Beam expansion approach is evaluated by power azimuth spectrum (PAS) analysis. The proposed approach is also analyzed statistically using mmWave channel simulator.

1.3.3 A Multidimensional Perspective to Future Communications

IM provides a novel way for the transmission of additional data bits via the indices of the available transmit entities compared to classical communication schemes. This study examines the flexible utilization of existing IM techniques in a comprehensive manner to satisfy the challenging and diverse requirements of 5G and beyond services. After spatial modulation (SM), which transmits information bits through antenna indices, application of IM to OFDM subcarriers has opened the door for the extension of IM into different dimensions, such as radio frequency (RF) mirrors, time slots, codes, and dispersion matrices. Recent studies have introduced the concept of multidimensional IM by various combinations of one-dimensional IM techniques to provide higher spectral efficiency (SE) and better bit error rate (BER) performance at the expense of higher transmitter (Tx) and receiver (Rx) complexity. Despite the ongoing research on the design of new IM techniques and their implementation challenges, proper use of the available IM techniques to address different requirements of 5G and beyond networks is an open

research area in the literature. For this reason, we first provide the dimensional-based categorization of available IM domains and review the existing IM types regarding this categorization. Then, we develop a framework that investigates the efficient utilization of these techniques and establishes a link between the IM schemes and 5G services, namely eMBB, mMTC, and URLLC. Additionally, this work defines key performance indicators (KPIs) to quantify the advantages and disadvantages of IM techniques in time, frequency, space, and code dimensions. Finally, future recommendations are given regarding the design of flexible IM-based communication systems for 5G and beyond wireless networks.

1.3.4 Control of IUI in Asynchronous Systems

The major challenge in current technology using OFDM is to provide services for a large number of UEs, who transmit at different times or distances from the BS. Asynchronicity between the users results in inter-user interference (IUI). OFDM systems are highly sensitive to IUI because of strict synchronization requirements to maintain subcarrier orthogonality. In this study, OFDM-IM is proposed as an eligible solution to alleviate IUI caused by asynchronous transmission in uncoordinated networks. In OFDM-IM, data transmission is performed not only by modulated subcarriers but also by the indices of active subcarriers. Unlike classical OFDM, fractional subcarrier activation leads to less IUI in OFDM-IM technology. Moreover, a novel subcarrier mapping scheme (SMS) named as Inner Subcarrier Activation (ISA), which gives activation priority to inner subcarriers, is proposed to further alleviate adjacent user interference in asynchronous OFDM-IM based systems. It is shown through theoretical analysis and computer-based simulation results that OFDM-IM is superior to conventional OFDM under time misalignments between the users, and its performance is further improved with the aid of ISA.

1.4 Dissertation Outline

This thesis consists of six chapters. Chapter 1 provides the motivation and summarizes the main contributions of the thesis. In Chapter 2, the essential background is presented for readers. Chapter 3 presents waveform-domain NOMA for uplink URLLC through GF access. In Chapter 4, the optimization of antenna beamwidth is introduced to combat low penetration capabilities in mmWave communication systems. Chapter 5 provides a comprehensive overview of multidimensional communication via IM. In Chapter 6, concluding remarks and open issues are presented.

1.5 Publications

Journals:

1. **S. Dogan**, A. Tusha and H. Arslan, "OFDM with Index Modulation for Asynchronous mMTC Networks", in *Sensors*, no. 4: 1280, Apr. 2018.

2. **S. Dogan**, A. Tusha and H. Arslan, "NOMA With Index Modulation for Uplink URLLC Through Grant-Free Access", in *IEEE Journal of Selected Topics in Signal Processing*, vol. 13, no. 6, pp. 1249-1257, Oct. 2019. **(Chapter 3)**

3. **S. Dogan**, A. Tusha, E. Basar and H. Arslan, "Multidimensional Index Modulation for 5G and Beyond Wireless Networks", Submitted to *Proceedings of The IEEE*, pp. 1-30, 2020. (Decisioned with Revise and Resubmit). **(Chapter 2 - Chapter 5)**

4. A. Tusha, **S. Dogan** and H. Arslan, "IQI Mitigation for Narrowband IoT Systems With OFDM-IM", in *IEEE Access*, vol. 6, pp. 44626-44634, Aug. 2018.

5. A. Tusha, **S. Dogan** and H. Arslan, "A Hybrid Downlink NOMA With

OFDM and OFDM-IM for Beyond 5G Wireless Networks" in *IEEE Signal Processing Letters*, vol. 27, pp. 491-495, 2020.

Conferences:

1. **S. Dogan**, M. Karabacak and H. Arslan, "Optimization of Antenna Beamwidth under Blockage Impact in Millimeter-Wave Bands", *Proc. IEEE International Symposium on Personal, Indoor and Mobile Radio Communications (PIMRC)*, Bologna, 2018, pp. 1-5. **(Chapter 4)**

2. A. Tusha, **S. Dogan** and H. Arslan, "Single Carrier Transmission for URLLC with Adaptive Radio Resource Utilization", *Proc. International Wireless Communications & Mobile Computing Conference (IWCMC)*, Tangier, Morocco, 2019, pp. 26-30.

3. M. S. J. Solaija, **S. Dogan**, S. Bykcorak and H. Arslan, "Hybrid Terrestrial-Aerial Network for Ultra-Reliable Low-Latency Communication", *Proc. IEEE International Symposium on Personal, Indoor and Mobile Radio Communications (PIMRC)*, Istanbul, Turkey, 2019, pp. 1-6.

4. A. Tusha, **S. Dogan** and H. Arslan, "Performance Analysis of Frequency Domain IM Schemes under CFO and IQ Imbalance", *Proc. IEEE International Symposium on Personal, Indoor and Mobile Radio Communications (PIMRC)*, Istanbul, Turkey, 2019, pp. 1-5.

Book Chapters:

1. **S. Dogan**, A. Tusha, E. Basar and H. Arslan, "Index Modulation-based Flexible Waveform Design", Flexible and Cognitive Radio Access Technologies for 5G and Beyond, Telecommunication Series, The Institution of Engineering and Technology, 2020, pp. 1-20 (In Press). **(Chapter 2)**

2. A. Tusha, **S. Dogan** and H. Arslan, "Non-orthogonal Radio Access Technologies", Flexible and Cognitive Radio Access Technologies for 5G and Beyond, Telecommunication Series, The Institution of Engineering and Technology, 2020, pp. 1-20 (In Press).

Patents:

1. **S. Dogan**, A. Tusha, and H. Arslan, "A system for controlling interference on non-orthogonal multiple access in next-generation communication systems," PCT Patent Application, Application Date: July 2019. **(Chapter 3)**

2. A. Tusha, **S. Dogan**, and H. Arslan, "Single carrier transmission with adaptive roll-off factor for ultra reliable and low latency communication systems," PCT Patent Application, Application Date: February 2019.

3. A. Tusha, **S. Dogan**, and H. Arslan, "Multi-user SC transmission through intelligent frame design for 5G and beyond communication systems," Turkish Patent and Trademark Office Patent Pending, File No: 2019/21291, Application Date: December 2019.

4. M. S. J. Solaija, **S. Dogan**, and H. Arslan, "A method of providing macro-diversity for reliable communication," Turkish Patent and Trademark Office Patent Pending, File No:2019/21319, Application Date: December 2019.

Chapter 2

Background

2.1 5G and Beyond User Requirements

In this section, three main services of fifth generation (5G) networks, i.e., enhanced mobile broadband (eMBB), massive machine-type communication (mMTC), and ultra-reliable low-latency communication (URLLC), and their use scenarios are briefly explained, along with their widely accepted key performance indicators (KPIs) and benchmarks in the 3rd Generation Partnership Project (3GPP) standards. Additionally, forecasts for sixth generation (6G) and beyond systems are mentioned. The KPIs and their values in the standards are given in Table 2.1.

2.1.1 eMBB

High data rate use-cases and applications, such as virtual reality, broadband internet access, and high definition video streaming, are grouped under the eMBB service, which can be considered as the continuation of the current fourth generation (4G) technology [1]. For these applications, peak data rates up to 10 Gbit/s

are required for the uplink (UL) and downlink (DL) transmission of a user equipment (UE) [2]. Hence, to support the increased data rate requirements, bandwidths of at least 100 MHz and 1 GHz are proposed for sub-6 GHz and above 6 GHz bands, respectively. Furthermore, supporting a high data rate transmission for three different mobility classes must be considered: pedestrian speeds up to 10 km/h, vehicular speeds from 10 km/h to 120 km/h, and high-speed vehicular speeds from 120 km/h to 500 km/h. Therefore, increasing the spectral efficiency (SE) via the development of new flexible communication schemes has become a critical demand. eMBB applications are expected to perform scheduled transmissions due to their characteristics, namely delay-tolerant and continuous. Hence, the eMBB service requires a spectrum-efficient waveform and modulation design at the cost of a moderate level of transmission latency and system complexity.

2.1.2 mMTC

In the context of Internet-of-Things (IoT), a connection of a massive number of UEs to a network is expected in the next-generation systems [3, 4]. The coexistence of numerous machine-type and mobile UEs in the network puts pressure on service providers to satisfy the diverse demands [5]. Various applications of the IoT, such as smart cities, connected vehicles, smart agriculture, public safety, and asset tracking, require different levels of coverage area, battery life, and connection capability [6]. Unlike the human-oriented higher data rate communication in the 4G systems, providing service for massive machine-type UEs with lower data rate is the primary focus of mMTC. Although mMTC is latency-tolerant, long waiting time occurs due to the scheduling of a large number of UEs. Therefore, random access mechanisms are proposed as promising solutions for mMTC [7]. However, the current orthogonal frequency division multiplexing (OFDM) technology requires strict synchronization between the UEs to avoid inter-user-interference (IUI) [8]. mMTC use-cases with ultra low power consumption and wide coverage area are grouped into narrowband IoT (NB-IoT) by the 3GPP [9–11]. The standards adopt orthogonal frequency division multiple access (OFDMA) and single

Table 2.1: KPIs for next-generation services

Service	**KPIs**	**Definitions**
eMBB	Data rate	Supporting peak data rates of 10 Gbit/s and 20 Gbit/s for UL and DL transmission, respectively.
	Mobility	Achieving desired data rate for a given mobility class (10 km/h $\leq V \leq$ 500 km/h).
mMTC	Connection capability	Number of mMTC UEs per a cell (1.000.000 UEs per km^2).
	Power Consumption	At least 10 years of lifetime for a device by sending 20 bytes and 200 bytes for UL and DL transmission, respectively.
	Coverage	Maximum coupling loss that corresponds to total loss including antenna gain, path loss and shadowing for baseline data rate of 160 bit/s (max_{CL} = 164 dB).
URLLC	Latency	The elapsed time for successful transmission and reception of a packet (0.25 ms $\leq$ latency $\leq$ 1 ms).
	Reliability	Successful reception of a packet with the reliability range of ($10^{-5} \leq$ BLER $\leq 10^{-9}$).

carrier frequency division multiple access (SC-FDMA) for DL and UL transmission and introduce SCS of 3.75 kHz for UL transmission over random access channels. Narrowband transmission, which leads to a low data rate, is performed to reduce power consumption and to guarantee a lifetime exceeding 10 years. In order to reduce the cost, mMTC UE is equipped with a single antenna, and half-duplex transmission is adopted. Retransmission of a packet is allowed to improve the coverage area at the expense of at most 10ms transmission latency.

2.1.3 URLLC

In 5G and beyond wireless systems, achieving ultra-reliability and low-latency is a crucial as well as a very challenging task. URLLC use-cases and applications need to guarantee block error rate (BLER) values up to 10^{-9} within the latency bounds of 0.25 ms [12–14]. The latency refers to the round trip time required for the successful transmission and reception of the transmitted data packet. In the current systems, the long handshaking process between a UE and base station (BS), data processing time, and transmission time interval (TTI) are the major barriers in achieving low-latency communications [15]. Moreover, the smallest resource unit is a subframe that consists of 14 OFDM symbols corresponding to a TTI of 1 ms for 15 kHz SCS. This rules out the possibility of any transmission faster than 1ms. Thus, mini-slot concept is adopted in 5G NR to meet the different latency requirements. For DL transmission, no latency occurs due to the handshaking since base station (BS) manages the communication. However, the handshaking process between UE and BS is mandatory in UL transmission to establish reliable communication at the cost of an extra delay that corresponds to 3 TTIs. This is in addition to the reduction in SE and EE due to the signaling overhead and the processing complexity, respectively. Hence, the UL latency for 4G systems is almost doubled compared to DL. Moreover, UL with grant-based (GB) transmission further leads to the waste of resources due to its sporadic nature. In GB access, BS assigns available resources to a UE continuously. However, UE with URLLC utilizes the resources intermittently. In the literature, grant-free (GF) access is extensively investigated to avoid the latency caused by

the handshaking process [16]. However, UEs with GF transmission are exposed to collisions that reduce system reliability. Hence, interference immune multiple accessing schemes are required for achieving URLLC.

2.1.4 Speculations for 6G and Beyond

As in 5G systems, underlying applications, and used cases will be the driving factors in 6G and beyond wireless networks [17]. For instance, 6G is expected to open the door for a wide range of unprecedented services such as self-driving cars, virtual reality, flying vehicles, human-body, and holographic communications [18]. Hence, the future of wireless system operators must simultaneously deliver much higher data rates, higher security, and communication reliability within a shorter latency compared with the aforementioned scenarios of 5G. For example, a five times increase of average data consumption per UE and down to 0.1 ms latency are expected by 2024 [19]. Moreover, a service of joint eMBB and URLLC with security constraints, and other combinations of eMBB, mMTC and URLLC are envisioned to represent these new applications and use-cases. In this context, artificial intelligence, machine learning, reconfigurable intelligent surfaces (RIS), unmanned aerial vehicles (UAVs), and terahertz (THz) communications are mainly speculated among potential technologies in beyond 5G [20]. Extensive research is afforded by both academia and industry for beyond 5G wireless networks in the industrialized countries. In China, several research groups are established to enhance intelligent manufacturing. Horizon 2020 ICT-09-2017 project considers mmWave and THz spectrum as a possible solution for scenarios with joint eMBB and latency limitations. Moreover, in [21], IM is considered as complementary technology to conventional OFDM-based multiplexing in order to achieve flexibility in 6G systems.

2.2 Frequency Domain Index Modulation

Due to the need for flexible wireless architectures to address these requirements, the index modulation (IM) concept has gained significant interest from the researchers worldwide. In contrast to classical communications techniques, where all the available radio resources are used for data transmission, only a fraction of the resource entities, i.e., time slots, antennas, or subcarriers, is utilized through IM. Extra information bits are carried by the indices of active resources to compensate for the decrease in SE due to the partial activation of radio resources.

In this section, the frequency-domain IM scheme, which is widely recognized as orthogonal frequency division multiplexing with index modulation (OFDM-IM), is presented as a complementary waveform to orthogonal frequency division multiplexing (OFDM), which is the main multi-carrier communication technology of 5G standard. Indexing of the subcarriers in the frequency domain is proposed to improve both SE and energy efficiency of the conventional OFDM systems. Moreover, state-of-the-art OFDM-IM solutions are presented.

2.2.1 OFDM with IM

The current OFDM technology utilizes all the available subcarriers for the purpose of efficient resource utilization. In case of frequency-domain IM, not all the subcarriers transmit M-ary symbols, but the indices of active subcarriers convey additional information bits. Subcarrier index modulation OFDM (SIM-OFDM) is an initial attempt in the literature that introduces frequency-domain IM [22]. SIM-OFDM divides incoming m data bits into two parts with the same length. On-off keying data bits corresponding to the first part decide the status of N subcarriers considering the number of one and zero bits. If the number of ones is higher than the number of zeros, subcarrier activation is performed based on the ones and vice versa. Therefore, the number of active subcarriers (A) is variable for each OFDM block. The remaining bits are modulated by conventional M-ary with quadrature amplitude modulation (QAM) / phase-shift keying (PSK) and

conveyed by activated subcarriers. In SIM-OFDM, there are control subcarriers for carrying the information of majority bit-value (1 or 0) to the receiver. However, it is assumed that this information is always transmitted correctly. To avoid error propagation stemming from the wrong majority bit-value at the receiver, OFDM block is split into $G = \frac{N}{2}$ subblocks through enhanced SIM-OFDM (ESIM-OFDM), and a single-subcarrier ($a = 1$) per subblock is activated [23]. Hence, the total number of activated subcarriers for each OFDM block is fixed and equals $A = aG$. Nevertheless, the performance of SIM-OFDM and ESIM-OFDM are not satisfactory, and their implementations are impractical. Thus, it is important to emphasize that the general concept for frequency-domain IM is firstly introduced in [24] and called OFDM-IM.

A block diagram of an OFDM-IM transmitter is shown in Figure 2.1. OFDM block is equally divided into G subblocks that consist of $b = \frac{N}{G}$ subcarriers, and a out of b subcarriers are selected to transmit M-ary data symbols [24]. It is important to note that IM can not be directly applied over the OFDM block, since the number of block realizations can get extremely large due to practical N values from 128 to 2048 [25]. Each OFDM-IM subblock consists of $p = \frac{m}{G}$ bits, which is divided into p_1 and p_2 bits. The indices of active subcarriers are defined by $p_1 = \lfloor \log_2(C(b, a)) \rfloor$ bit stream, while the remaining $p_2 = a\log_2(M)$ bit stream is mapped to the conventional M-ary symbols that are carried by the activated subcarriers. The indices of active subcarriers for g-th subblock are defined as follows

$$\mathbf{i}_g = \begin{bmatrix} i(1) & i(2) & \dots & i(a) \end{bmatrix}_{1\times a}, \tag{2.1}$$

where $i(\gamma) \in \{1, 2, \dots, b\}$ for $g = 1, \dots, G$. The transmitted symbols by the active subcarriers of the g-th subblock is represented as

$$\mathbf{s}_g = [s(1) \quad s(2) \quad \dots \quad s(a)]_{1\times a}, \tag{2.2}$$

where $s(\gamma) \in \mathcal{S}$, where $\mathcal{S}$ is the set of M-ary symbols $\mathcal{S} = \{s_0 \quad s_1 \quad \cdots \quad s_{M-1}\}$, and the $(b-a)$ inactive subcarriers are set to zero. Hence, the transmission vector for the g-th subblock is

$$\mathbf{x}_g = [0 \quad s(1) \quad \dots \quad 0 \quad \dots \quad s(\gamma) \quad 0]_{1\times b}, \tag{2.3}$$

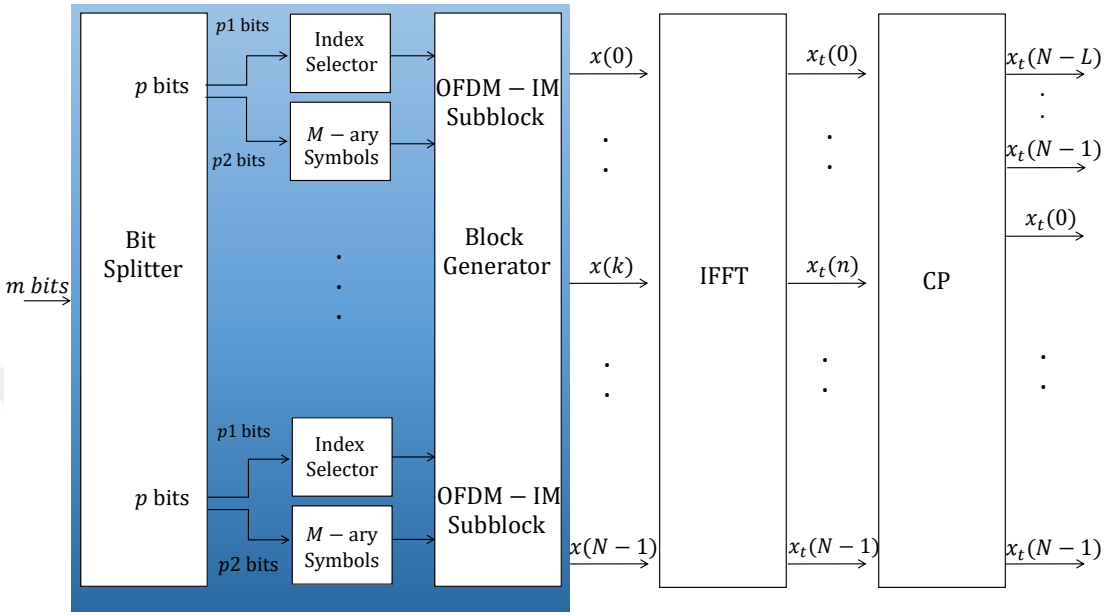


Figure 2.1: Block diagram of OFDM-IM transmitter.

where the position of $s(\gamma)$ is defined by $i(\gamma)$. In the case of $a = b$, $\mathbf{x}_g$ turns into the classical OFDM signal. OFDM block is generated via the composition of all G subblocks as follows

$$\mathbf{x} = [\mathbf{x}_1 \quad \dots \quad \mathbf{x}_g \quad \dots \quad \mathbf{x}_G]_{1\times N}, \tag{2.4}$$

where $x_g(\gamma) \in \{0, \mathcal{S}\}$. Therefore, the total number of conveyed bits per OFDM-IM subblock is calculated as

$$p = p_1 + p_2 = \lfloor \log_2(C(b,a)) \rfloor + a\log_2(M), \tag{2.5}$$

while the number of transmitted bits per OFDM block is

$$m = Gp = G\bigg(\lfloor \log_2(C(b,a)) \rfloor + a\log_2(M) \bigg), \tag{2.6}$$

where $\lfloor . \rfloor$ and $C(b,a)$ denote floor function and binomial coefficient, respectively. Frequency-domain representation of OFDM-IM and OFDM signals are illustrated in Figure 2.2. As seen in this figure, partial subcarrier activation is performed via OFDM-IM, and extra information bits are transmitted through the indices of active subcarriers with $\mathbf{i}_g = [1, 5, 7]$. Later, time-domain samples of OFDM block are obtained by inverse fast Fourier transform (IFFT) process as

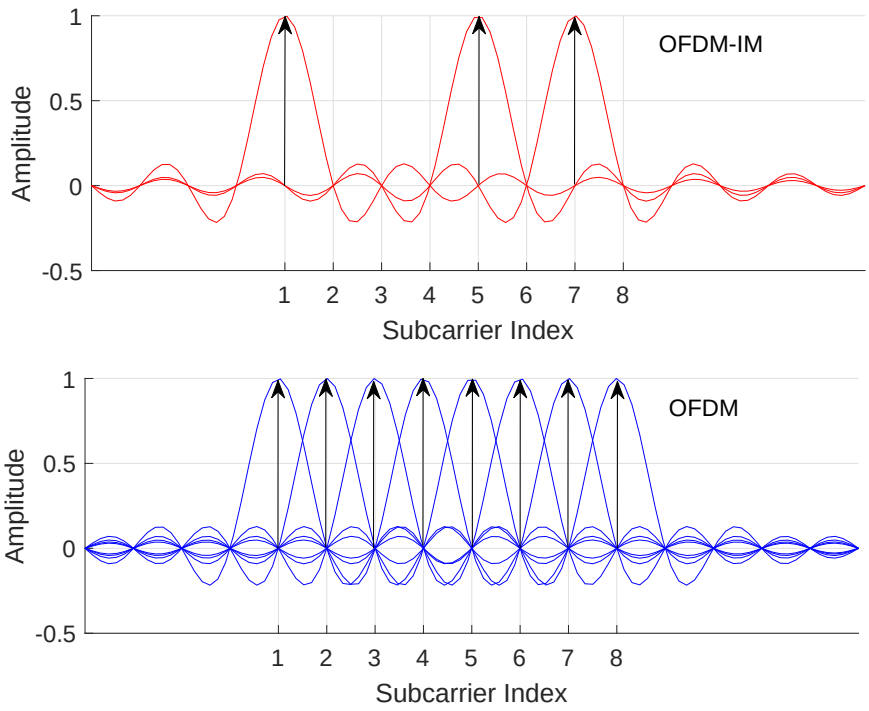


Figure 2.2: Frequency-domain representation of (**a**) OFDM-IM with $a = 3,\ b = 8$. (**b**) Classical OFDM.

$$x_t(n) = \sum_{k=0}^{N-1} x(k) e^{j2\pi nk/N}, \quad 0 \leq n \leq N-1. \tag{2.7}$$

Before the transmission of $x_t(n)$, a cyclic prefix (CP) with length L is appended to the signal to avoid inter-symbol interference (ISI) due to the time dispersion of multi-path channel. After $x_t(n)$ leaves the transmitter (Tx), it undergoes through an independent and identically distributed multi-path Rayleigh fading channel as

$$y_t(n) = \sum_{l=0}^{L-1} h_t(l) x_t(n-l) + w(n), \tag{2.8}$$

where L denotes the number of channel taps, and path gains $h_t(l)$ are Gaussian random variables with $\mathcal{CN}(0, \frac{1}{L})$. $w(n)$ represents additive white Gaussian noise (AWGN) with zero mean and variance σ_w^2. After CP removal, fast Fourier transform (FFT) process is performed over the received signal $y_t(n)$ as follows

$$y(k) = \sum_{n=0}^{N-1} y_t(n) e^{-j2\pi nk/N}, \quad 0 \leq k \leq N-1. \tag{2.9}$$

In frequency-domain, $y(k)$ for k-th subcarrier corresponds to

$$y(k) = x(k)h(k) + w(k), \tag{2.10}$$

where $h(k) \sim \mathcal{CN}(0,1)$ and $w(k) \sim \mathcal{CN}(0, N_0)$ represent frequency response of multi-path channel and AWGN noise, respectively. Later, OFDM block is divided into OFDM-IM subblocks as shown in Figure 2.3. In order to recover data bits conveyed by both the modulated subcarriers and their indices, maximum likelihood (ML) and log-likelihood ratio (LLR) receiver are proposed for OFDM-IM transmission [24].

2.2.1.1 Maximum Likelihood Detector

ML decoder completes a full search over all possible subblock realizations to perform a joint decision of the data bits transmitted via the subcarriers' indices and M-ary symbols. ML receiver for g-th subblock is given as

$$(\hat{\mathbf{i}}_g, \hat{\mathbf{s}}_g) = \arg\min \sum_{\xi=0}^{a-1} |y_g(k) - h_g(k) s_g(\xi)|^2. \tag{2.11}$$

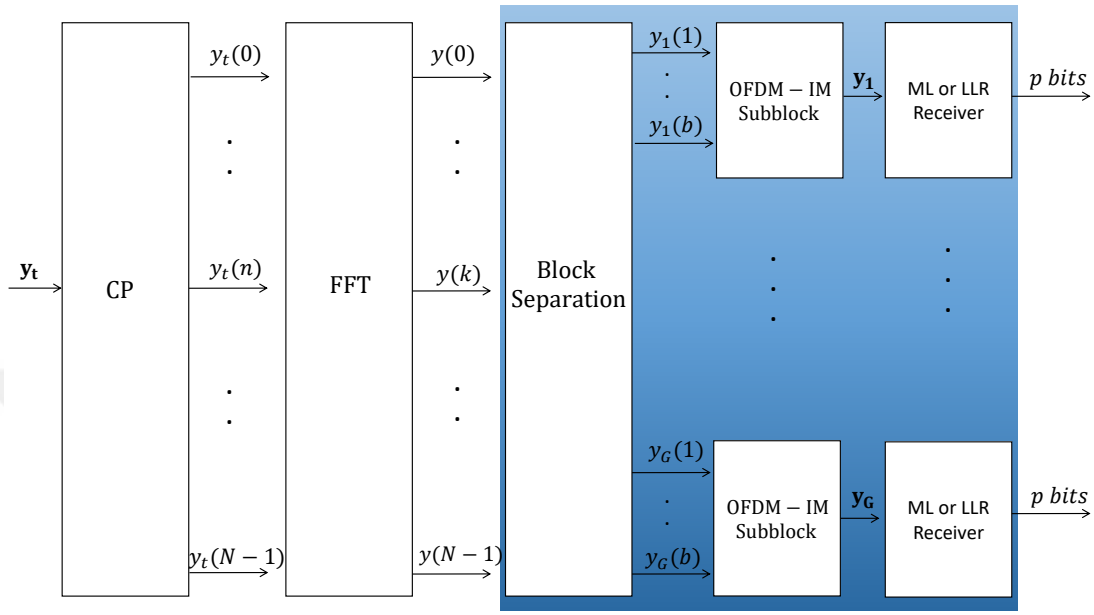


Figure 2.3: Block diagram of OFDM-IM receiver.

Due to the exhaustive search, ML receiver suffers from high complexity with the order of $\mathcal{O}(2^{\lfloor \log_2(C(b,a)) \rfloor} M^a)$. To exemplify, a total of $2^{\lfloor \log_2(C(b,a)) \rfloor} M^a = 2^7 2^5 = 4096$ possible subblock realizations are searched in case of $b = 10$, $a = 5$, and $M = 2$.

2.2.1.2 Log-likelihood Ratio Detector

In order to reduce the complexity of ML technique, log-likelihood ratio (LLR) detector is proposed to estimate the indices of active subcarriers. The logarithmic ratio of a posteriori probabilities is calculated as

$$\lambda(k) = ln\left(\frac{\sum_{i=0}^{M-1} P\Big(x(k) = s_i \mid y(k)\Big)}{P\Big(x(k) = 0 \mid y(k)\Big)}\right), \tag{2.12}$$

where $P\big(x(k) = 0\big) = \frac{b-a}{b}$ and $\sum_{i=0}^{M-1} P\big(x(k) = s_i\big) = \frac{a}{b}$ denote a posteriori probability of a given subcarrier being used or null, respectively. Moreover, after

utilizing Bayes' rule $\lambda(k)$ values can be represented as

$$\lambda(k) = \ln(a) - \ln(b-a) + \frac{|y(k)^2|}{N_0} + \ln\left(\sum_{i=0}^{M-1} \exp\left(-\frac{|y(k) - h(k)s_i|^2}{N_0}\right)\right). \tag{2.13}$$

In each subblock, a subcarriers with maximum λ values denote the indices of utilized subcarriers. Later, these indices are mapped to p_1 bits, while p_2 information bits are obtained via the conventional demodulation of M-ary symbols.

2.2.2 State-of-the-art OFDM-IM Solutions

Promising advantages of OFDM-IM, such as high SE, high energy efficiency, and improved reliability, to meet the diverse requirements of 5G and beyond communication networks shed light on the investigation of novel frequency-domain IM techniques [26]. In this section, state-of-the-art advances for OFDM-IM including generalized, dual/multiple modes, and interleaved schemes are elaborated. Furthermore, their implementation difficulties in practical scenarios are discussed.

2.2.2.1 Interleaved OFDM-IM

OFDM with interleaved subcarrier index modulation (OFDM-ISIM) is proposed to ensure that subcarriers in an OFDM-IM subblock pass through the uncorrelated fading channels. For this reason, OFDM-ISIM performs subcarrier-level block interleaving [27]. The performance of OFDM-IM systems depends on the correct detection of active subcarriers. The use of interleaving in OFDM-IM maximizes the Euclidean distance between two subblock realizations and thus provides better performance than the conventional OFDM-IM, which has no interleaving process. Since the implementation of frequency-domain interleaving corresponds to only a matrix multiplication, it is applied in the recently introduced OFDM-IM techniques.

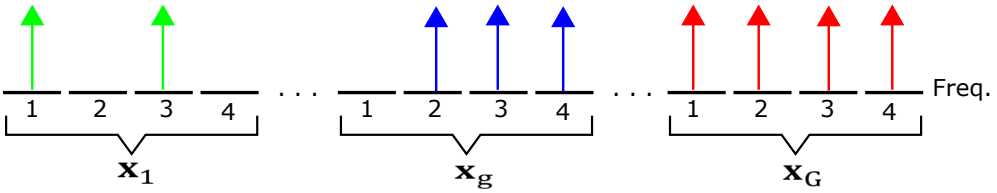


Figure 2.4: OFDM-IM with fixed subcarrier activation ratio.

2.2.2.2 Generalized OFDM-IM

OFDM-IM outperforms OFDM in terms of SE in case low-order modulation is used. Otherwise, OFDM-IM may not provide higher SE than OFDM due to inactive subcarriers. Therefore, generalized OFDM-IM (OFDM-GIM) aims to increase the SE of conventional OFDM-IM without compromising its advantages [28].

In conventional OFDM-IM, the number of active subcarriers in a subblock is fixed to a. Generalized OFDM-IM (OFDM-GIM) provides a degree of freedom to achieve flexible OFDM-IM-based communication systems with high SE by activating a different number of subcarriers in each subblock. Mapping of information bits to subcarriers in OFDM-IM and OFDM-GIM are illustrated in Figure 2.4 and Figure 2.5, respectively. In OFDM-GIM, $\mathbf{v}$ is the set of allowed numbers of active subcarriers in each OFDM-IM subblock and expressed as

$$\mathbf{v} = [v(1)\ v(2)\ \cdots\ v(\sigma)]_{1\times\sigma}, \tag{2.14}$$

where $v(\sigma) \in \{1, 2, \cdots, b\}$. In case of $v(\sigma) = b$, all the subcarriers are activated in the subblock, as in the conventional OFDM transmission. For example, $\mathbf{v} = [2\ 3]_{1\times 2}$ means that $\sigma = 2$, and two or three subcarriers can be activated for a given subblock. Therefore, the number of bits transmitted over the l-th subblock is

$$p = \lfloor \log_2(C(b, v(\sigma))) \rfloor + v(\sigma)\log_2(M). \tag{2.15}$$

In order to activate the different number of active subcarriers in a subblock, the length of p_1 and p_2 bit streams are changed for the selected $v(\sigma)$, while p

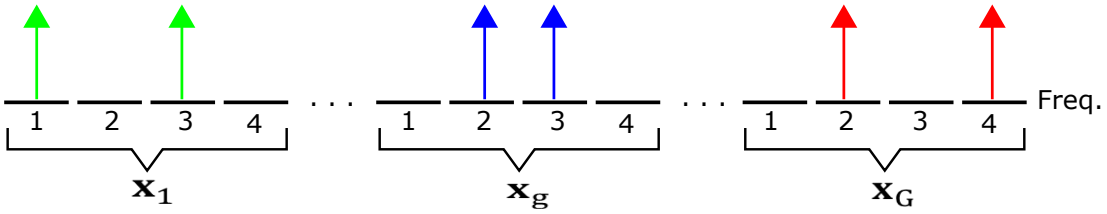


Figure 2.5: OFDM-GIM with variable subcarrier activation ratio.

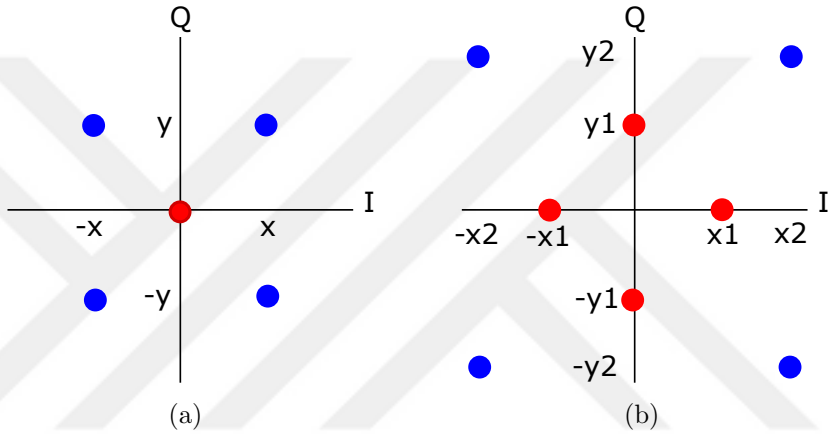


Figure 2.6: Constellation diagram for (**a**) OFDM-IM (**b**) OFDM-GIM.

is fixed for all subblocks to avoid error propagation stemming from subblock asynchronization. In the conventional OFDM-IM, ML and LLR receiver can be used for the detection of data bits carried by both indices and M-ary symbols. As in (2.11), ML detector performs a search over all possible subblock realizations. Since the number of subblock realizations in OFDM-GIM is higher than that of the conventional OFDM-IM, ML detector leads to heavy complexity. In order to use LLR receiver for OFDM-GIM, $\lambda(k)$ values in (2.12) are calculated for the set of $v(\sigma)$ as

$$\begin{aligned} \lambda(k) = \ln(v(\sigma)) - \ln(b - v(\sigma)) + \frac{|y(k)^2|}{N_0} + \\ \ln\left(\sum_{i=0}^{M-1} \exp\left(-\frac{1}{N_0} |y(k) - \sqrt{\frac{n}{v(\sigma)}} h(k) s_i|^2 \right) \right), \end{aligned} \tag{2.16}$$

where $v(\sigma)$ that minimizes the distance between estimated transmit signals and received signal denotes the correct number of active subcarriers for each subblock.

Table 2.2: An example for mapping the information bits to subcarriers by OFDM-IM and DM-OFDM while (b=4, a=2)

OFDM-IM		
p_1	$\mathbf{i}_g$	$\mathbf{x}_g$
[00]	1,2	$[s_i \;\; s_j \;\; 0 \;\; 0]$
[01]	2,3	$[0 \;\; s_i \;\; s_j \;\; 0]$
[10]	3,4	$[0 \;\; 0 \;\; s_i \;\; s_j]$
[11]	1,4	$[s_i \;\; 0 \; 0 \;\; s_j]$

DM-OFDM		
p_1	$\mathbf{i}_g$	$\mathbf{x}_g$
[00]	1,2	$[\mathcal{S}_1(i) \;\; \mathcal{S}_1(j) \;\; \mathcal{S}_2(i) \;\; \mathcal{S}_2(j)]$
[01]	2,3	$[\mathcal{S}_2(i) \;\; \mathcal{S}_1(i) \;\; \mathcal{S}_1(j) \;\; \mathcal{S}_2(j)]$
[10]	3,4	$[\mathcal{S}_2(i) \;\; \mathcal{S}_2(j) \;\; \mathcal{S}_1(i) \;\; \mathcal{S}_1(j)]$
[11]	1,4	$[\mathcal{S}_1(i) \;\; \mathcal{S}_2(i) \;\; \mathcal{S}_2(j) \;\; \mathcal{S}_1(j)]$

2.2.2.3 Dual-Mode OFDM

In OFDM-IM, subcarriers within a subblock are split into two parts as active and inactive ones according to the incoming data bits. Likewise, dual-mode OFDM (DM-OFDM) also divides subcarriers into two parts, but both of them are activated by the use of different modulation sets $\mathcal{S}_1$ and $\mathcal{S}_2$ for a and $b-a$ subcarriers, respectively [29]. An example mapping of information bits to subcarriers for OFDM-IM and DM-OFDM is given in Table 2.2.

The number of transmitted bits by DM-OFDM subblock is

$$p = \lfloor \log_2(C(b,a)) \rfloor + a\log_2(M_1) + (b-a)\log_2(M_2), \tag{2.17}$$

where M_1 and M_2 denote the size of $\mathcal{S}_1$ and $\mathcal{S}_2$, respectively. Figure 2.6 shows the constellation diagrams for OFDM-IM and DM-OFDM. OFDM-IM has a constellation point at 0 due to inactive subcarriers. If Euclidean distance between the possible subblock realizations is higher than that of OFDM-IM, DM-OFDM provides better BER performance, and vice versa. At the receiver, ML or LLR detector can be used for the recovering of the transmitted data. The minimum distance between the different subblock realizations is calculated to decide the used modulation set for a subcarrier. As an advanced version of DM-OFDM, multiple-mode OFDM (MM-OFDM) is proposed in the literature [30]. MM-OFDM uses multiple QAM/PSK sets within a subblock to enhance the SE.

Table 2.3: An example for mapping the information bits to subcarriers by CI-OFDM-IM while (b=4, a=2)

CI-OFDM-IM		
p_1	$\mathbf{i}_g$	$\mathbf{x}_g$
[00]	1,2	$[s_i^R + \mathrm{j}s_j^I \quad s_j^R + \mathrm{j}s_i^I \quad 0 \quad 0]$
[01]	2,3	$[0 \quad s_i^R + \mathrm{j}s_j^I \quad s_j^R + \mathrm{j}s_i^I \quad 0]$
[10]	3,4	$[0 \quad 0 \quad s_i^R + \mathrm{j}s_j^I \quad s_j^R + \mathrm{j}s_i^I]$
[11]	1,4	$[s_i^R + \mathrm{j}s_j^I \quad 0 \quad 0 \quad s_j^R + \mathrm{j}s_i^I]$

2.2.2.4 Coordinate Interleaved OFDM-IM

Coordinate interleaved (CI) OFDM-IM (CI-OFDM-IM) combines OFDM-IM and space-time block codes with coordinate interleaving [31]. CI-OFDM-IM achieves an additional diversity gain through the transmission of real and imaginary parts of a complex data symbol over two active subcarriers via the CI orthogonal design. A rotated square M-ary QAM constellation is used in CI-OFDM-IM for the modulation. In Table 2.3, an example mapping of information bits to subcarriers is shown for CI-OFDM-IM. Additional to coordinate interleaving, block interleaving is also used in CI-OFDM-IM. In this way, CI-OFDM-IM provides better performance than both OFDM-IM and OFDM-ISIM. At the receiver, ML or LLR detector can be utilized for the detection of both active subcarriers and M-ary symbols.

Chapter 3

NOMA with Index Modulation for Uplink URLLC through Grant-Free Access

3.1 Introduction

Next generation of wireless communication systems is expected to support three main services, named as enhanced mobile broadband (eMBB), massive machine-type communication (mMTC) and ultra-reliable low-latency communication (URLLC) [14, 16, 32–34]. As an extension of fourth generation (4G) Long Term Evolution (LTE) systems, eMBB services are the most envisioned one with moderate reliability and high data rate requirements [35]. In mMTC, serving a massive number of users emerges as a difficulty for fifth generation (5G) New Radio (NR) systems. However, URLLC is the most challenging with the requirements of both ultra-reliability and low-latency for NR [15]. According to the requirements defined by International Telecommunication Union (ITU), URLLC applications such as industrial automation, health safety or intelligent transportation, need to guarantee 10^{-5} reliability within 1ms [36].

In LTE uplink transmission, grant-based (GB) radio access has been adopted to allocate user equipments (UEs) over orthogonal resources. In this way, zero interference between UEs occurs since each UE performs its transmission over dedicated resources. Hence, GB access guarantees reliable transmission for URLLC. However, the reliability comes at the cost of latency due to signaling overhead of scheduling and granting processes. Hence, grant-free (GF) radio access has been proposed as an attractive solution to reduce the latency of GB access. In GF transmission, UEs do not require handshaking with the BS to start a transmission. Therefore, collision between UEs occurs and it results in low-reliable data transmission. Due to the aforementioned reasons, researchers face with dilemma of finding solutions for URLLC by either reducing the latency of GB access or increasing the reliability of GF access [14–16, 35].

3.1.1 Background on URLLC

Since the latency is not a primary concern for 4G systems, redesign of frame structure, resource assignment, and multiple access schemes is needed to sustain emerging communication systems with URLLC. In LTE, the smallest transmission time interval (TTI) consists of 14 time domain OFDM symbols with 15 kHz subcarrier spacings (SCS), and TTI corresponds to 1 ms. In order to reduce the transmission latency for URLLC, mini-slot concept that consists of 2, 4 or 7 OFDM symbols is introduced for 5G NR systems. Moreover, SCS of 15 kHz, 30 kHz and 60 kHz for below 6 GHz, and 60 kHz, 120 kHz for above-6 GHz are proposed to meet different demands of UEs. Therefore, shorter TTI by larger SCS is adopted to reduce the required latency for URLLC in LTE Rel. 14 and Rel. 15 [12, 13, 37].

Due to latency caused by scheduling and granting processes of GB access, there is no room to have a sufficient number of retransmissions for reaching 10^{-5} bit error rate (BER) within 1 ms. Hence, in LTE Rel. 14 semi-persistent scheduling (SPS) has been proposed as a faster solution in comparison to GB transmission [13, 38]. In SPS, available resources are persistently assigned to a single URLLC

UE for certain time intervals without extra signaling. However, pre-assignment of resources leads to a waste of resources due to sporadic nature of URLLC traffic [39]. Hence, simultaneous use of resources by a group of URLLC UEs is proposed rather than by a single UE usage [13]. In LTE Rel. 15, various types of GF schemes such as Reactive, K-Repetitions and Proactive have been assessed to fulfill the requirements of URLLC [40, 41]. It is shown that GF techniques are superior to GB transmission in terms of latency, even for a reasonable UE load [40]. However, GF random access causes collision that results in non-orthogonal resource sharing between the UEs. Therefore, non-orthogonal multiple accessing (NOMA) has been proposed for contention-based transmission schemes [41–44]. Intelligently overlapping of the UEs at the transmitter allows to separate them at the receiver.

3.1.2 Background on NOMA

The history of NOMA dates back almost twenty years, although it is introduced as a new concept. Signal separability, which is achieved by utilizing different characteristics of superimposed signals, has been the main concern for co-channel use scenarios in FDMA/TDMA based systems. In [45], relative timing delay between co-channel signals is exploited as a separability metric to detect the signals individually. In heterogeneous networks, separation of the desired signal from dominant interference (DI) is achieved by utilizing power offset between the signals [46]. Moreover, in [47] two co-channel signals are treated as desired signals by utilizing inherent signal separation that is obtained by overlapping of multi-carrier signal and single-carrier signal. Likewise, in [48] NOMA scheme based on orthogonal code-division multiple access and time-division multiple access is proposed to serve additional UEs over the same resources.

Recently, NOMA concept has been heavily investigated by both academia and industry from the perspective of system capacity [49]. Therefore, different NOMA schemes such as power domain and code domain have been assessed in the recent studies [50–52]. In this work, we emphasize that non-orthogonal transmission for

Table 3.1: The proposed waveform pair according to communication requirements of F_{UE} and S_{UE}

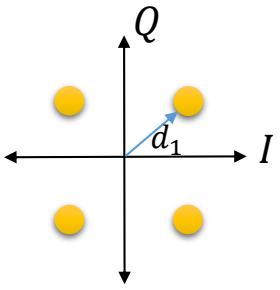
UE	Access Type	Waveform	Reliability	Latency
F_{UE}	GF	OFDM	High	Low
S_{UE}	GB	OFDM-IM	Moderate	Moderate

5G systems is required not only for increasing the system capacity but also for fulfilling different requirements of UEs. In [53], coexistence of orthogonal multiple accessing (OMA) and NOMA is proposed both to satisfy the requirements of URLLC and to avoid the loss of spectral efficiency (SE) due to sporadic traffic structure of URLLC.

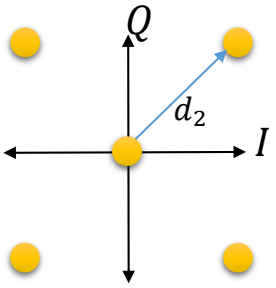
3.1.3 Main contribution

In this study, sharing of the available resources is proposed between two UEs who have different transmission requirements. First user (F_{UE}) performs URLLC on the resources where second user (S_{UE}) has ongoing latency-tolerant communication with moderate reliability. S_{UE} can be considered as a classical LTE UE which requires up to 10^{-2} reliability and 10 ms latency. Hence, GF access and GB access are adopted for F_{UE} and S_{UE}, respectively. Due to GF access of F_{UE}, collision occurs between the UEs. OFDM based transmission for both F_{UE} and S_{UE} results in wideband interference (WB-I) which prevents the URLLC for F_{UE}. Therefore, use of different waveform for F_{UE} and S_{UE} utilizing NOMA concept is proposed to alleviate the effect of collision on F_{UE}. Orthogonal frequency division multiplexing (OFDM) for F_{UE} and OFDM with index modulation (OFDM-IM) for S_{UE} are suggested to control the interference. Table 3.1 shows the proposed waveform pair according to the communication requirements of F_{UE} and S_{UE}.

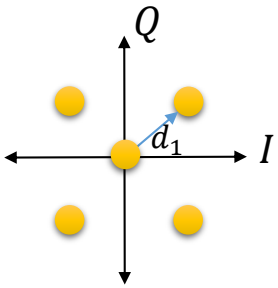
OFDM-IM carries information not only by modulated subcarriers but also by indices of active subcarriers [24]. In Fig 3.1, constellation diagrams for classical OFDM and two OFDM-IM scenarios are illustrated. OFDM-IM schemes provide BER improvement by both increased Euclidean distance and reduction of



(a) Conventional OFDM



(b) Scenario 1 for OFDM-IM



(c) Scenario 2 for OFDM-IM

Figure 3.1: Constellation diagrams belonging to OFDM and OFDM-IM.

conventional modulation bits [54]. In the recent years, the superiority of OFDM-IM versus OFDM in terms of RF impairments, Doppler spread, asynchronous transmission and inter-carrier interference has been extensively investigated by the researchers [8, 11, 24, 55–58]. The main contributions of this study are listed as follows:

1. URLLC is performed over the same resources that are already utilized by latency-tolerant communication not only for avoiding loss of SE but also for achieving tight requirements of URLLC.

2. GF access is adopted to meet the latency requirement of F_{UE}, while OFDM-IM for S_{UE} is proposed to increase the reliability of OFDM transmission.

3. The interference caused by S_{UE} on F_{UE} is controlled by inherent flexibility of OFDM-IM. F_{UE} experiences narrowband and dominant interference (NB-DI), while the power of inactive subcarriers is distributed over active

subcarriers, as in Fig. 3.1(b). On the other hand, S_{UE} causes narrowband interference (NB-I) over F_{UE} if the power of inactive subcarriers is suppressed, as in Fig. 3.1(c). In both cases, F_{UE} is partially affected by S_{UE} due to fractional subcarrier activation in OFDM-IM.

4. Reliability of F_{UE} for a single transmission is increased by NB-(D)I. Hence, a lower number of retransmissions, which is associated with lower latency compared to classical NOMA with pure OFDM, are required to achieve 10^{-5} reliability of URLLC.

5. Closed-form expressions for signal-to-interference-plus-noise ratio (SINR) and bit error rate (BER) probability are derived for the proposed system.

The remainder of the chapter is outlined as follows. Section 3.2 describes GB and GF radio access techniques, and the proposed NOMA scheme. Section 3.3 includes theoretical analysis for SINR and BER performances. Section 3.4 presents computer based simulation results and discussions. Finally, Section 3.5 contains the conclusion remarks.

3.2 System Model

This section considers an uplink multiple access system with two UEs. Firstly, GF and GB radio access techniques are explained in terms of the transmission latency. Later, OFDM-IM transmission model for S_{UE}, and non-orthogonal transmission model due to the collision of F_{UE} with OFDM and S_{UE} with OFDM-IM are presented in detail.

3.2.1 GF Radio Access Technique

In the literature, there have been discussed two types of GF transmission. In the first scheme, BS completes the assignment of available resources between UEs

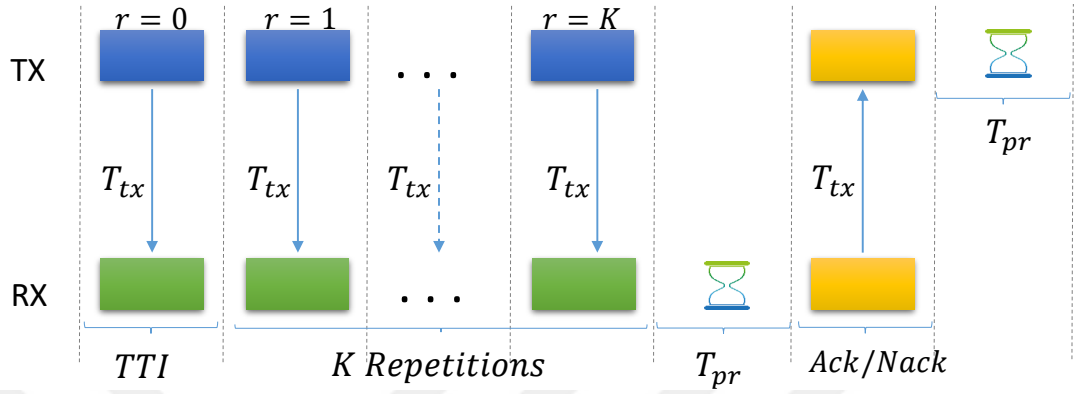


Figure 3.2: GF radio access with K-repetitions for F_{UE}

before the data packet arrives to the UE. Therefore, scheduling process is not considered as latency, and the UEs perform data transmission over dedicated resources, such as SPS [40]. However, pre-allocation of the resources for intermittent URLLC leads to loss of SE. Secondly, GF access over the shared resources is proposed for URLLC UEs. In this case, collision emerges between the URLLC UEs, and data retransmission becomes mandatory in order to improve the transmission reliability.

GF access with K-repetitions over the shared resources is used for F_{UE} in this work. K-repetitions reduces the latency in comparison to classical Hybrid Automatic Repeat Request (HARQ) scheme [40]. As illustrated in Fig. 3.2, a UE retransmits its data without waiting for feedback from the BS. The UE waits for the feedback after K retransmissions are completed. Hence, the latency L_{GF} caused by GF access is expressed as follows

$$L_{GF} = 2T_{tx} + \underbrace{\sum_{r=1}^{K} T_{tx}}_{\text{due to retransmissions}} + 2T_{pr}, \tag{3.1}$$

$$= T_{tx}(K+2) + 2T_{pr}, \tag{3.2}$$

where T_{tx} denotes a single TTI, while T_{pr} refers to processing time for the transmitted data. In this study, T_{pr} is assumed the same for both UE and BS, and

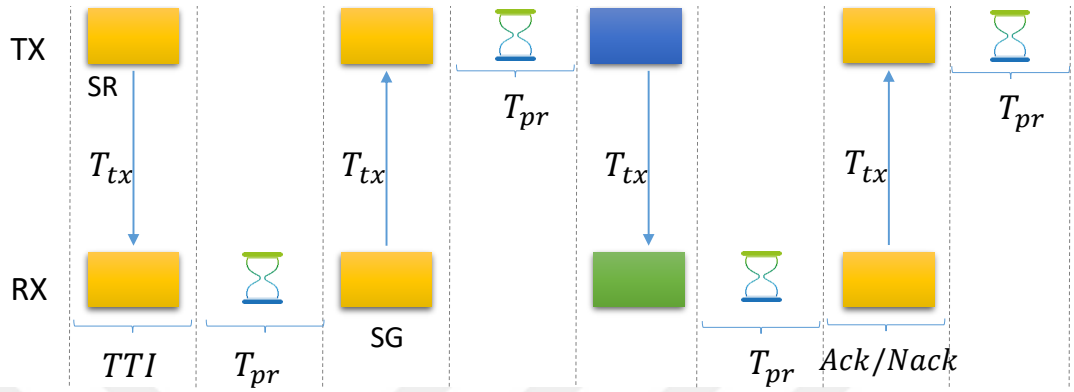


Figure 3.3: GB radio access for S_{UE}

equals 1 TTI. TTI is defined by SCS in the current standard. Larger SCS corresponds to smaller TTI, that results in less latency for the transmission.

3.2.2 GB Radio Access Technique

In LTE systems, UEs in a network are dynamically scheduled through GB transmission. Initially, each UE sends a scheduling request (SR) to the BS upon a data packet reaches the UE, as shown in Fig. 3.3. Once the BS processes SR of the UE, it responds with a scheduling grant (SG) which defines resources for uplink transmission of the UE. Dynamically allocation of the available resources between the UEs corresponds to orthogonal transmission, and thus it provides reliable transmission with the latency penalty. Therefore, the latency (L_{GB}) for a single transmission via GB access is calculated as follows

$$L_{GB} = \underbrace{2T_{tx}}_{\text{due to SR and SG}} + 4T_{pr} + 2T_{tx}. \tag{3.3}$$

3.2.3 Transmission Model for UE with URLLC

In this study, OFDM-IM based communication is proposed for S_{UE} to control interference over F_{UE} with URLLC. Different from classical OFDM, data transmission in OFDM-IM is performed not only by modulated subcarriers but also by indices of active subcarriers. It is considered N size OFDM-IM block, where subcarriers are equally split into G subblocks. Each subblock consists of $b = \frac{N}{G}$ subcarriers, and a out of b subcarriers are utilized for data transmission. Indices of the active subcarriers for s-th subblock can be represented as

$$\xi_s = [i_s(1), \ldots, i_s(r), \ldots, i_s(a)]_{1\times a}, \tag{3.4}$$

where $i_s(r) \in [1, 2, \ldots, b]$. In each subblock, $p_1 = \lfloor log_2 C(b, a) \rfloor$ bits are transmitted by the active subcarrier indices ξ_s, and $p_2 = a(log_2 M)$ bits are transmitted by the modulated subcarriers with M-ary symbols $S = [s_1, \ldots, s_M]$. $C(b, a)$ and $\lfloor . \rfloor$ denote binomial coefficient and floor function, respectively. The number of transmitted bits per OFDM-IM subblock equals $p = (p1 + p2)$ bits. An OFDM-IM block is generated after concatenation of G OFDM-IM subblocks, and it is expressed as

$$Z = [Z(0), \ldots, Z(k), \ldots, Z(N-1)]_{1\times N}. \tag{3.5}$$

OFDM-IM signal Z consists of both zeros and M-ary symbols due to partial activation of the subcarriers. Note that several methods have been proposed in the literature for mapping of incoming data bits to the subcarrier indices [8,24,59]. The total number of bits carried by OFDM-IM symbol equals $m = Gp$.

Time domain OFDM-IM signal is achieved through conventional Inverse Fast Fourier Transform (IFFT) process as

$$z(n) = \sum_{k=0}^{N-1} Z(k) e^{\frac{j2\pi nk}{N}}, \quad 0 \leq n \leq N-1. \tag{3.6}$$

After cyclic prefix (CP) is added to the time domain signal $z(n)$, it is emitted into a Rayleigh multipath channel as follows

$$y_i(n) = \sum_{l=0}^{L-1} h^{'}(l) z(n-l), \tag{3.7}$$

where $h'(n) = \sum_{l=0}^{L-1} h'(l)\delta(n-l)$. L is the number of channel taps, and $h'(l)$ denotes path gains, which are complex Gaussian random variables with $\mathcal{CN}(0, \frac{1}{L})$. In this study, it is assumed that CP size is larger than number of channel taps to prevent inter-symbol interference.

3.2.4 NOMA System Model

Conventional OFDM based communication with N subcarriers is considered for F_{UE} as seen in Fig. 3.4. $N(log_2 M)$ information bits are mapped to M-ary data symbols, which modulate subcarriers and form the frequency-domain signal $X(k)$. Later, $X(k)$ is transformed to time-domain signal by IFFT process as follows

$$x(n) = \sum_{k=0}^{N-1} X(k) e^{\frac{j2\pi nk}{N}}, \quad 0 \leq n \leq N-1. \tag{3.8}$$

As in (3.7), $x(n)$ reaches the BS after passing through a Rayleigh multipath channel $h(l)$ as

$$y_d(n) = \sum_{l=0}^{L-1} h(l) x(n-l), \tag{3.9}$$

where $h(n) = \sum_{l=0}^{L-1} h(l)\delta(n-l)$ refers to the channel of F_{UE}, and expected value of the channel gains are the same $\mathbb{E}[|h|^2] = \mathbb{E}[|h'|^2]$.

Received signal at the BS is expressed as the superposition of OFDM signal y_d with the interferer signal y_i as follows

$$r(n) = y_d(n) + y_i(n) + w(n), \tag{3.10}$$

where $w(n)$ denotes additive white Gaussian noise (AWGN) with $\mathcal{CN}(0, \sigma_o^2)$. After CP removal, FFT process is used to obtain frequency domain samples of the overlapped signal R(k), which is obtained as

$$R(k) = \sum_{n=0}^{N-1} r(n) e^{\frac{-j2\pi nk}{N}}, \quad 0 \leq k \leq N-1. \tag{3.11}$$

The received baseband signal on k-th subcarrier is

$$R(k) = \underbrace{X(k)H(k)}_{F_{UE}} + \underbrace{Z(k)H^{'}(k)}_{S_{UE}} + W(k), \tag{3.12}$$

where $W(k)$ denotes the frequency response of $w(n)$, while $H(k)$ and $H^{'}(k)$ correspond to channel frequency response (CFR) of $h(n)$ and $h^{'}(n)$, respectively.

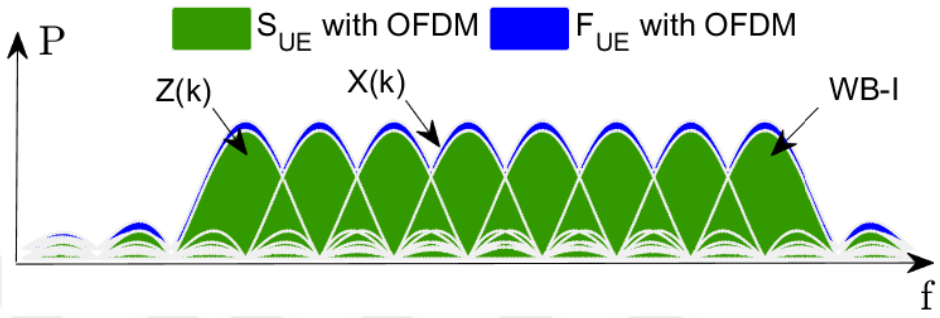
As shown in Fig. 3.4, three different scenarios are considered for S_{UE}.

3.2.4.1 OFDM

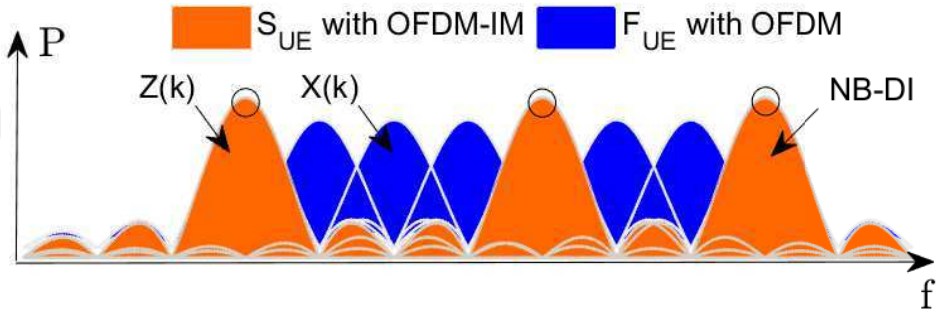
Use of OFDM technology for S_{UE} is firstly evaluated as a reference scenario. Unit transmission power P_{tx} is equally distributed to all subcarriers of S_{UE}. Hence, F_{UE} is exposed to WB-I as seen in Fig. 3.4(a). The received signal $R(k)$ on k-th subcarrier of F_{UE} equals (3.12).

3.2.4.2 Scenario 1 for OFDM-IM

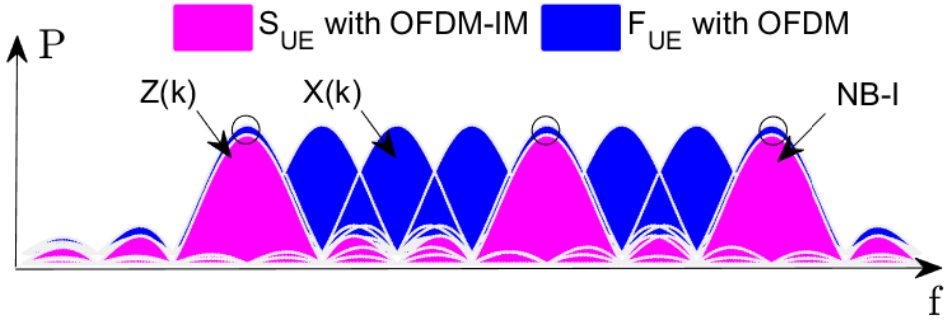
As shown in Fig. 3.4(b), WB-I is converted to NB-DI when OFDM-IM uses the same transmission power P_{tx} with OFDM. Thus, P_{tx} is allocated between active subcarriers. Due to partial subcarrier activation on OFDM-IM, the received signal $R(k)$ on k-th subcarrier of F_{UE} equals (3.12) for k-th active subcarrier of S_{UE}, $(Z(k) \neq 0)$. On the other hand, F_{UE} is only affected by AWGN for inactive subcarriers $(Z(k) = 0)$, and (3.12) converts to



(a) In the presence of WB-I



(b) In the presence of NB-DI



(c) In the presence of NB-I

Figure 3.4: Three NOMA schemes based on OFDM for F_{UE} and S_{UE} with (a) OFDM (b) Scenario 1 for OFDM-IM (c) Scenario 2 for OFDM-IM.

$$R(k) = \underbrace{X(k)H(k)}_{F_{UE}} + W(k). \tag{3.13}$$

3.2.4.3 Scenario 2 for OFDM-IM

In Fig. 3.4(c), WB-I is converted to NB-I when power of active subcarrier for OFDM-IM is the same as OFDM. Therefore, transmission power is changed by subcarrier activation ratio $\frac{a}{b}$. The received signal $R(k)$ on k-th subcarrier of F_{UE} depends on k-th subcarrier of S_{UE} being utilized or not utilized as in (3.12) and (3.13), respectively.

Since the available resources are shared between UEs, maximum ratio combining (MRC) receiver is used to enhance robustness of the desired user F_{UE} against the interferer S_{UE}. After K retransmissions, output of the combiner $R_{MRC}(k)$ is expressed as follows

$$R_{MRC}(k) = \sum_{i=1}^{K} \zeta_i(k) R_i(k) = \boldsymbol{\zeta}^{\boldsymbol{H}} \boldsymbol{r}, \tag{3.14}$$

where $\zeta_i(k)$ denotes combining weight factor for k-th subcarrier of i-th retransmission to maximize SINR, with $\boldsymbol{\zeta} = [\zeta_1(k), \zeta_2(k), ..., \zeta_M(k)]^T$ and $\boldsymbol{r} = [R_1(k), R_2(k), ..., R_M(k)]^T$.

3.3 Theoretical Analysis

This section includes theoretical analysis for SINR and BER performances of F_{UE} under WB-I, NB-DI, and NB-I conditions.

3.3.1 SINR Analysis

As illustrated in Fig. 3.4, SINR on k-th subcarrier of F_{UE} depends on the status of k-th subcarrier of S_{UE} being active or inactive. Instantaneous SINR for F_{UE} on k-th active subcarrier equals

$$\gamma_{act}(k) = \frac{|X(k)|^2 |H(k)|^2}{|Z(k)|^2 |H'(k)|^2 + N_0}, \tag{3.15}$$

where N_0 denotes the noise variance in frequency domain.

3.3.1.1 Under WB-I conditions

As explained in Section 3.2.4.1, F_{UE} experiences WB-I due to S_{UE} with OFDM. Therefore, the interference signal power $P_I = |Z(k)|^2$ equals the desired signal power $P_D = |X(k)|^2$ for all subcarriers. Average SINR for the reference NOMA scheme, which is a superposition of the two OFDM signals, is expressed as

$$\gamma_{WB-I} = \frac{\gamma_D}{\gamma_I + 1}, \tag{3.16}$$

where $\gamma_D = \gamma_I = \frac{E_s \mathbb{E}[|h|^2]}{N_0}$ represent the average signal-to-noise ratio (SNR) and E_s is the energy for M-ary symbol.

3.3.1.2 Under NB-DI conditions

If S_{UE} transmits unit power P_{tx} for the communication, power of the inactive subcarriers is spread over the active ones. Therefore, amount of interference associated with each active subcarrier increases with a factor of $\frac{b}{a}$ in comparison to OFDM scenario. The average SINR for F_{UE} equals

$$\gamma_{NB-DI} = \frac{\gamma_D}{\frac{b}{a}\gamma_I + 1}. \tag{3.17}$$

As seen in Fig. 3.4(b), F_{UE} faces with asymmetric interference caused by fractional subcarrier activation of S_{UE}.

3.3.1.3 Under NB-I conditions

Symbol energy of S_{UE} with OFDM-IM is reduced from $\frac{b}{a}E_s$ to E_s by suppressing power of the inactive subcarriers, as seen in Fig. 3.4(c). Therefore, the transmitted power by S_{UE} is $\frac{a}{b}P_{tx}$. The average SINR for F_{UE} equals $\gamma_{NB-I} = \gamma_{WB-I}$ since γ_I is γ_D for active subcarriers.

In the case of k-th inactive subcarrier, instantaneous SNR for F_{UE} is,

$$\gamma_{inact}(k) = \frac{|X(k)|^2|H(k)|^2}{N_0}, \tag{3.18}$$

and its average SNR is γ_D. Additionally, total SINR for F_{UE} at the output of MRC receiver can be written as,

$$\overline{\gamma}_{total} = \sum_{r=1}^{K} \overline{\gamma}_r, \tag{3.19}$$

where $\overline{\gamma}_r$ denotes average SINR for r-th transmission of F_{UE}.

3.3.2 BER Analysis

Closed-form expressions of BER performances for BPSK and M-ary quadrature amplitude modulation (M-QAM) over Rayleigh fading channel are available in the literature. BER for BPSK is calculated as

$$P_b(E) = \frac{1}{2}\Big(1 - \mu_c\Big), \tag{3.20}$$

while BER for M-QAM is expressed as follows [60]

$$P_b(E) \;=\; 2\Big(\frac{\sqrt{M}-1}{\sqrt{M}}\Big)\Big(1 - \mu_c\Big) + \Big(\frac{\sqrt{M}-1}{\sqrt{M}}\Big)^2.\Big[\frac{4}{\pi}\mu_c tan^{-1}\Big(\mu_c\Big) - 1\Big], \tag{3.21}$$

where $\mu_c = \sqrt{\frac{q\overline{\gamma}}{1+q\overline{\gamma}}}$. $q = 1$ and $q = \frac{3\log_2 M}{2(M-1)}$ for BPSK and M-QAM, respectively.

The probability of k-th subcarrier being active and inactive should be considered to compute average BER performance for a transmission of F_{UE} as in (3.12) and (3.13), respectively. In first case ($C1$), F_{UE} suffers from both S_{UE} and AWGN for k-th active subcarrier ($Z(k) \neq 0$). Therefore, the probability of F_{UE} being affected by S_{UE} equals the subcarrier activation probability $P(C1) = \frac{a}{b}$. In the second case ($C2$), performance of F_{UE} is only degraded by AWGN. Hence, the probability of F_{UE} being affected by only AWGN is $P(C2) = \frac{b-a}{b}$. The overall BER probability of the proposed NOMA scheme is calculated as

$$P_b(E) = P_b(E|C1)P(C1) + P_b(E|C2)P(C2), \tag{3.22}$$

$$= \frac{a}{b}{P_b}^{C1}(E) + \frac{b-a}{b}{P_b}^{C2}(E), \tag{3.23}$$

where ${P_b}^{C1}(E)$ and ${P_b}^{C2}(E)$ are calculated by using (3.20) and (3.21) for BPSK and M-QAM, respectively. The average SINR $\overline{\gamma}$ for ${P_b}^{C1}(E)$ is replaced with γ_{NB-I} (3.16) or γ_{NB-DI} (3.17) to consider impact of S_{UE}. On the other hand, the average SNR $\overline{\gamma}$ for ${P_b}^{C2}(E)$ equals γ_D. As an example, ${P_b}^{C1}(E)$ and ${P_b}^{C2}(E)$ for BPSK while F_{UE} experiences NB-DI is written as

$${P_b}^{C1}(E) = \frac{1}{2}\Big(1 - \sqrt{\frac{\gamma_{NB-DI}}{1+\gamma_{NB-DI}}}\Big), \tag{3.24}$$

$${P_b}^{C2}(E) = \frac{1}{2}\Big(1 - \sqrt{\frac{\gamma_D}{1+\gamma_D}}\Big). \tag{3.25}$$

By substituting (3.24) and (3.25) on (3.23), $P_b(E)$ is obtained as

$$P_b(E) = \frac{a}{2b}\Big(1 - \sqrt{\frac{\gamma_{NB-DI}}{1+\gamma_{NB-DI}}}\Big) + \frac{(b-a)}{2b}\Big(1 - \sqrt{\frac{\gamma_D}{1+\gamma_D}}\Big). \tag{3.26}$$

F_{UE} always interferes with S_{UE} in case of S_{UE} performs OFDM based communication (b = a). Therefore, $P(C1) = 1, P(C2) = 0$, and $P_b(E) = {P_b}^{C1}(E) = \frac{1}{2}\Big(1 - \sqrt{\frac{\gamma_{WB-I}}{1+\gamma_{WB-I}}}\Big)$.

Under the assumption that interference is treated as noise, BER performance of the URLLC UE with BPSK after K retransmissions can be written as

$$P_b^K(E) = P_b(E)^K \sum_{k=0}^{K-1} \binom{K+k-1}{k} (1 - P_b(E))^k, \tag{3.27}$$

while BER performance for M-QAM is expressed as in (3.28) [60]. $P_b(E)$ equals (3.23) for the proposed system.

$$\begin{aligned} P_b^K(E) = 4\Big(\frac{\sqrt{M}-1}{\sqrt{M}}\Big)\Big(\frac{1-\mu_c}{2}\Big)^K \cdot \sum_{k=0}^{K-1} \binom{K+k-1}{k} \Big(\frac{1+\mu_c}{2}\Big)^K - 4\Big(\frac{\sqrt{M}-1}{\sqrt{M}}\Big)^2 \\ \Bigg(\frac{1}{4} - \frac{\mu_c}{\pi}\Big(\Big[\frac{\pi}{2} - \arctan(\mu_c)\Big] \cdot \sum_{k=0}^{K-1} \frac{\binom{2k}{k}}{4(1+q\overline{\gamma})^k} - \sin(\arctan(\mu_c)) \\ \cdot \sum_{k=0}^{K-1} \sum_{i=1}^{k} \frac{\binom{2k}{k}}{\binom{2(k-i)}{k-i} 4^i (2(k-i)+1)(1+q\overline{\gamma})^k} \cdot [\cos(\arctan(\mu_c))]^{2(l-i)+1}\Big)\Bigg). \end{aligned} \tag{3.28}$$

3.4 Numerical Results and Discussion

In this section, performance of the proposed system, which corresponds to overlapping of OFDM with OFDM-IM, is evaluated in terms of F_{UE}, and it is compared with the reference scenario, where OFDM is used for both F_{UE} and S_{UE}. Two UEs fully overlap in time and frequency domain if URLLC occurs. Otherwise, latency-tolerant UE will have a collision-free transmission. Therefore, performance analysis for S_{UE} is not considered in the manuscript. Additionally, required reliability for S_{UE} can be achieved through use of different modulation and coding schemes (MCS) or interference cancellation techniques. Firstly, computer based simulations are used to validate theoretical calculations of SIR and BER analysis for F_{UE}. Later, output of MRC receiver is obtained to increase

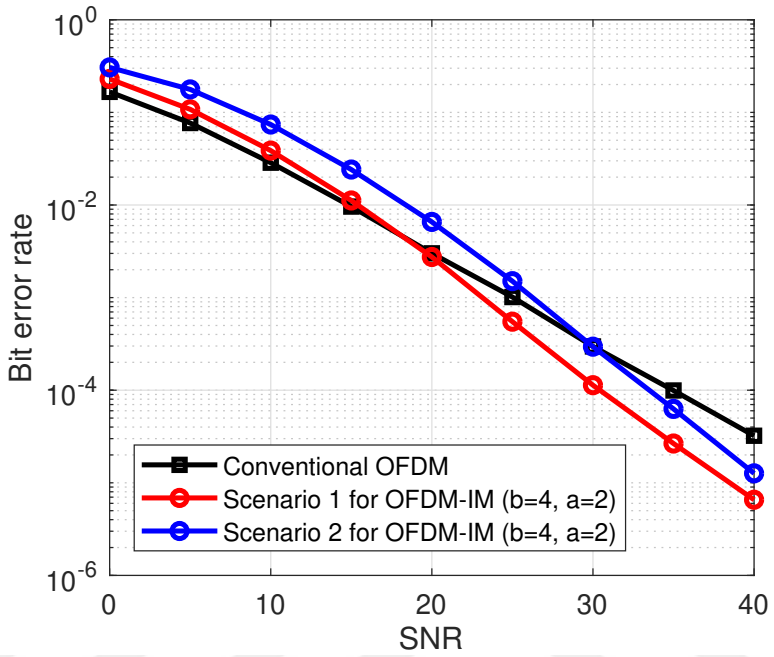


Figure 3.5: BER performances for OFDM and OFDM-IM schemes.

reliability level of F_{UE} to 10^{-5} by considering various subcarrier activation ratios for S_{UE} with OFDM-IM. The latency performance for F_{UE} is calculated by the number of required retransmissions to reach the desired reliability. The system parameters used in the simulations are N = 128, L = 10 and CP = 16. BPSK modulation is used to carry data symbols. OFDM-IM subblock size is fixed $b = 8$, and different activation ratios $(\frac{a}{b})$ are considered for S_{UE}. It is assumed that perfect channel state information (CSI) is available at the receiver. BER performances for classical OFDM and two OFDM-IM schemes are illustrated in Fig. 3.5. Scenario 1 (NB-DI) Scenario 2 (NB-I) for OFDM-IM with (b = 4, a = 2) provide better BER performances than OFDM after SNR = 15 dB and SNR = 30 dB due to having P_{tx} and $\frac{a}{b}P_{tx}$ transmission power, respectively.

Fig. 3.6 shows the average interference on F_{UE} due to WB-I, NB-DI, and NB-I by considering different number of active subcarriers within the subblock. F_{UE} is exposed to the same amount of interference in case of WB-I and NB-DI since the transmitted total power P_{tx} is the same. The average interference under NB-DI is independent from the number of active subcarriers as power of inactive subcarriers

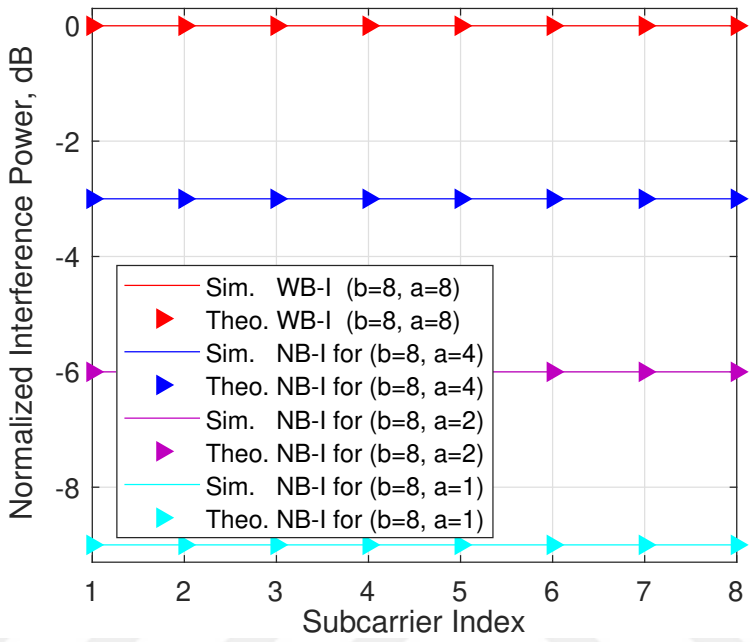


Figure 3.6: Normalized interference power per subcarrier caused by S_{UE} on F_{UE}.

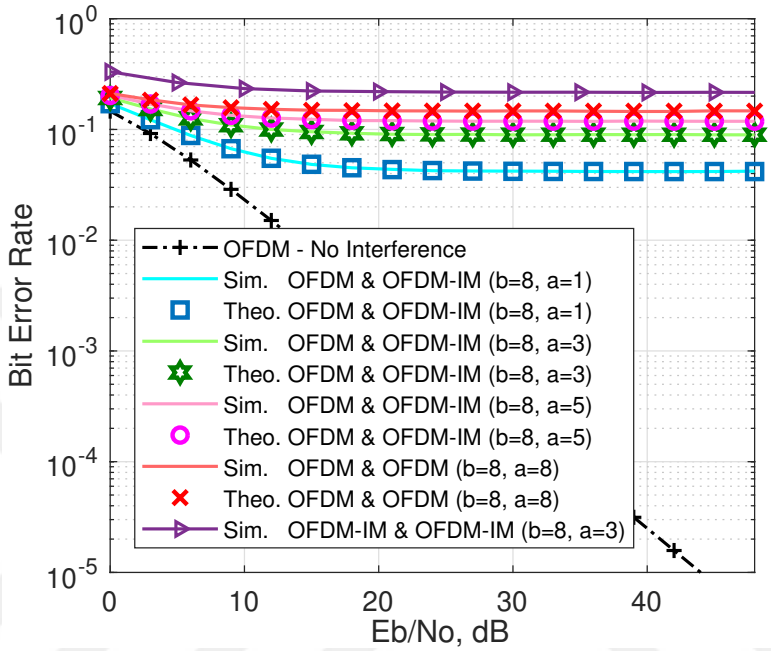
is distributed over the active ones, while the amount of interference under NB-I is proportional to the activation ratio. In Fig. 3.6, 3dB more degradation on the average interference is observed between lines starting from red line (b = 8, a = 8) to light blue line (b = 8, a = 1) as the activation ratio increases two times per line.

The advantage of NB-DI against WB-I is easily seen in Fig. 3.7(a). F_{UE} with OFDM under WB-I offers worse performance compared with OFDM under NB-(D)I. BER performance of F_{UE} improves under NB-DI due to reduced number of active subcarriers. As the activation ratio decreases, energy of the interferer S_{UE} becomes more dominant, while increasing activation ratio spreads NB-DI and generates WB-I. As shown in Fig. 3.7(b), F_{UE} under NB-I has the best performance since NB-I has the same distribution with NB-DI, and it is not dominant. Additionally, use of OFDM-IM for both UEs is considered in order to reveal the importance of the proposed scheme. OFDM-IM with (b = 8, a = 3) is considered for both UEs to maintain the same SE with OFDM, and log-likelihood ratio detector is used at the receiver [24]. Due to random interference features of

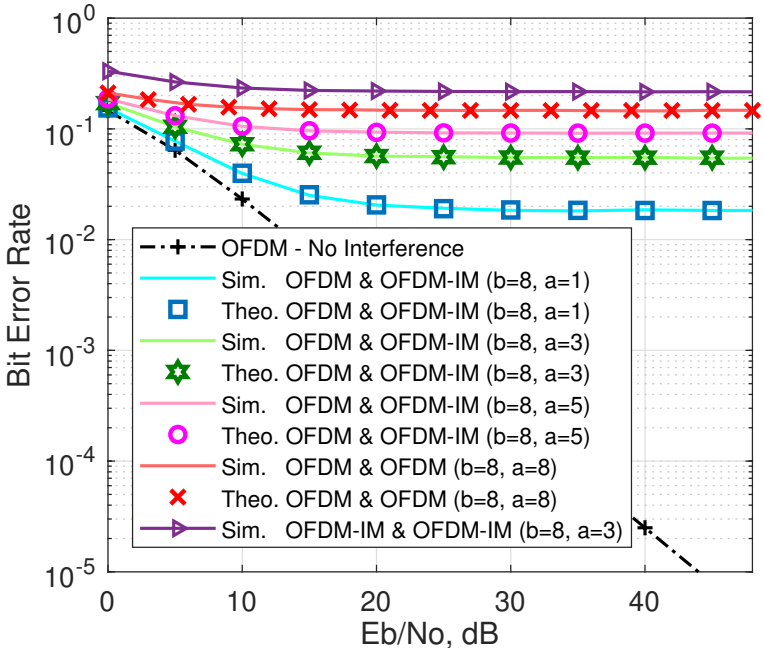
S_{UE} with OFDM-IM, correct detection of active subcarriers for F_{UE} with OFDM-IM becomes difficult and it leads to wrong symbol decision. Therefore, F_{UE} has the worst BER performance.

MRC receiver is used by F_{UE} to obtained the reliability level for URLLC. Fig. 3.8 shows that regarding (3.27) a tight upper bound is achieved for the performance of F_{UE} after K retransmissions. As illustrated in Fig **??**, maximum retransmissions (K = 9) due to WB-I is required for F_{UE} to achieve 10^{-5} BER. In Fig. 3.9, subcarrier activation ratio ($\frac{a}{b} = \frac{1}{8}$) is used to illustrate the advantage of NB-(D)I on the BER performance against WB-I. F_{UE} requires (K = 5) and (K = 3) retransmissions to reach 10^{-5} BER under NB-DI and NB-I conditions, respectively. Therefore, it can be easily said that for a given amount of interference, localized interference structure is preferable against the spread interference structure. OFDM-IM with activation ratio ($\frac{a}{b} = \frac{1}{8}$) provides lower SE than OFDM. In Fig.3.10, S_{UE} with activation ratio ($\frac{a}{b} = \frac{3}{8}$) offers the same SE with OFDM, and it results in wider interference caused by the increased number of active subcarriers. Hence, F_{UE} needs two more retransmissions in comparison to S_{UE} with ($\frac{a}{b} = \frac{1}{8}$) for each case to obtain the required reliability. In Fig. 3.11 S_{UE} uses subcarrier activation ratio of ($\frac{a}{b} = \frac{5}{8}$), which is associated with higher SE than S_{UE} with OFDM. BER performance of F_{UE} becomes worse due to higher number of active subcarriers. However, F_{UE} still needs less number of retransmissions (K = 8) for NB-DI and (K = 6) for NB-I in comparison to WB-I (K = 9).

The required number of repetitions to achieve the baseline URLLC target 10^{-5} reliability for F_{UE} are summarized in Table 3.2. Additionally, regarding (5.2), transmission latencies are calculated for two different mini-slot configurations. As shown in Table 3.2, lower latencies are achieved by the proposed NOMA scheme in comparison to WB-I. The latency under WB-I is 13 TTI, which equals 6.5 ms and 1.85 ms for 7-OFDM symbols and 2-OFDM symbols, respectively. For the same SE (i.e. OFDM-IM with (b = 8, a = 3)), F_{UE} requires K = 7 retransmissions that correspond to 5.5 ms for 7-OFDM symbols and 1.57 ms for 2-OFDM symbols. 15% and 30% improvement on the latency for F_{UE} are achieved by NB-I and NB-DI, respectively. Moreover, 30% and 46% improvement on the latency are observed for F_{UE} under NB-DI and NB-I caused by OFDM-IM with



(a) In the presence of NB-DI



(b) In the presence of NB-I

Figure 3.7: BER versus E_b/N_o for a single transmission of F_{UE} in the presence of NB-DI and NB-I. Impact of WB-I is represented by red color in both figures.

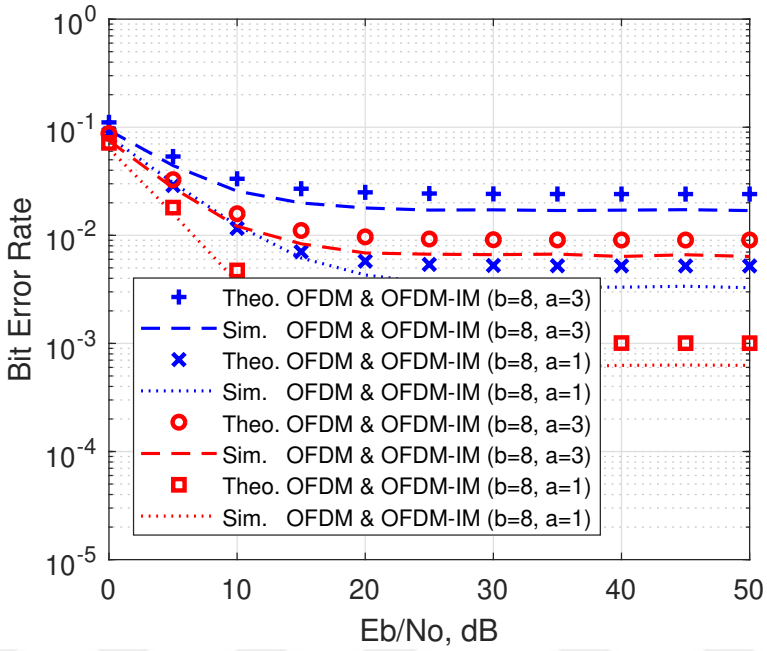


Figure 3.8: BER versus E_b/N_o for F_{UE} while $K = 2$ in the presence of NB-DI and NB-I. Impact of NB-DI and NB-I are represented with blue and red color, respectively.

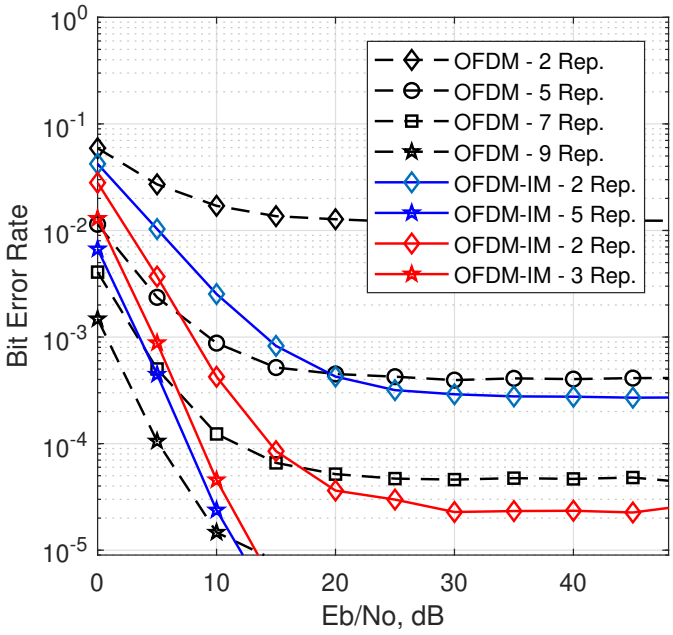


Figure 3.9: BER versus E_b/N_o for F_{UE} under S_{UE} for $\frac{a}{b} = \frac{1}{8}$ until achieving 10^{-5} reliability by MRC receiver. Impact of WB-I, NB-DI and NB-I are represented with black, blue and red color, respectively.

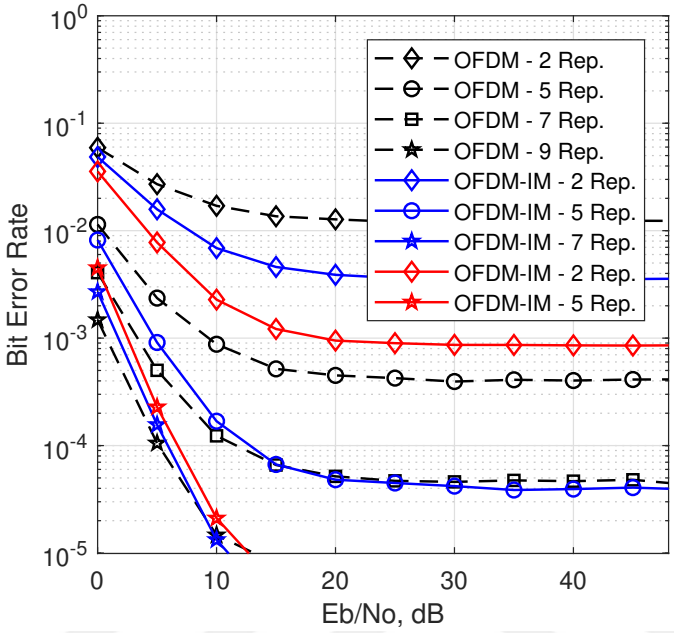


Figure 3.10: BER versus E_b/N_o for F_{UE} under S_{UE} for $\frac{a}{b} = \frac{3}{8}$ until achieving 10^{-5} reliability by MRC receiver. Impact of WB-I, NB-DI and NB-I are represented with black, blue and red color, respectively.

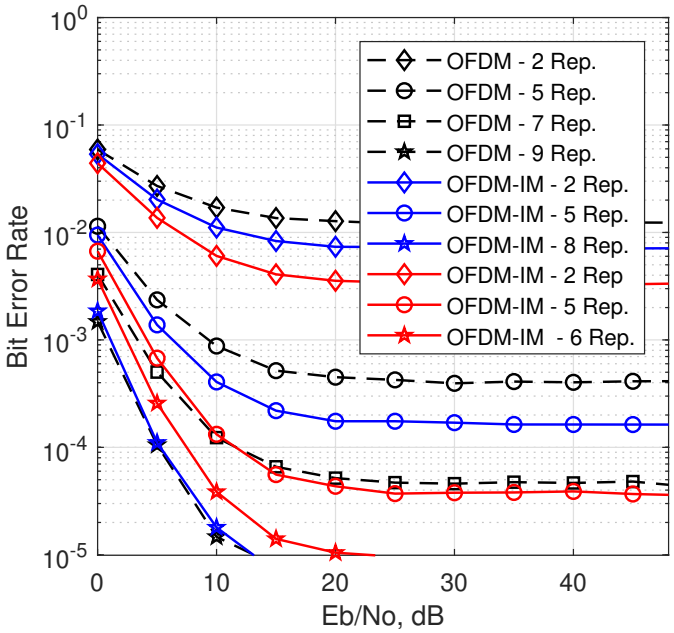


Figure 3.11: BER versus E_b/N_o for F_{UE} under S_{UE} for $\frac{a}{b} = \frac{5}{8}$ until achieving 10^{-5} reliability by MRC receiver. Impact of WB-I, NB-DI and NB-I are represented with black, blue and red color, respectively.

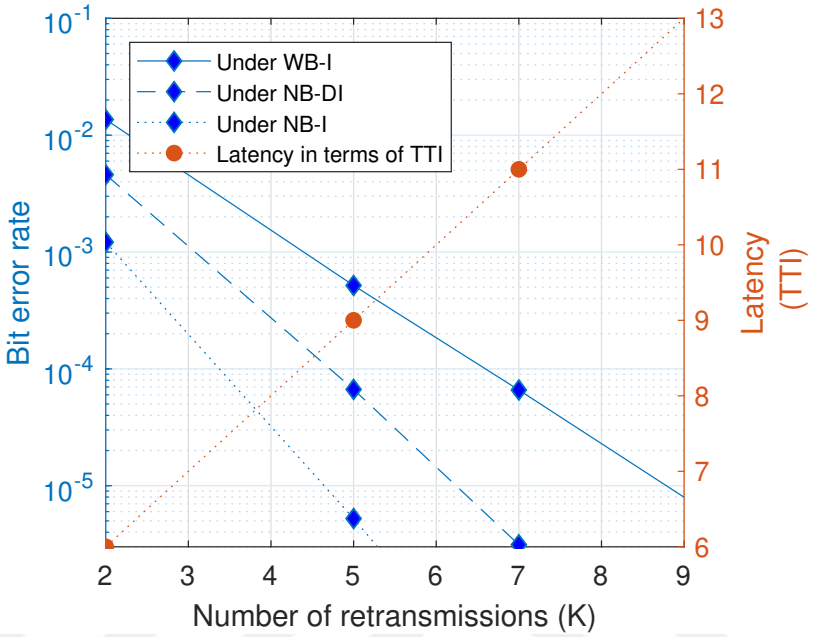


Figure 3.12: Trade-off between BER performance and latency.

(b = 8, a = 1). It is expected that achieved gain by the proposed system can be further increased via optimization of OFDM-IM subblock size and number of active subcarriers. Note that GF access is adopted for URLLC in this study. In the case of GB access, the latency according to (5.1) equals 8 TTI for a single transmission, and use of dedicated resources for URLLC results in loss of SE. Moreover, Fig. 3.12 shows performances of the URLLC UE at SNR = 15 dB for the retransmissions and corresponding latency in terms of TTI. It is easily seen that as the number of retransmission increases, BER performances of the URLLC UE improves at the expense of latency.

In contrast to classical NOMA where two UEs perform OFDM based transmission, the proposed NOMA scheme provides the flexibility to determine the expected latency of a system not only by frame structure or SCS but also by waveform selection. Furthermore, the proposed waveform-domain NOMA concept can also support multiple URLLC UEs if the collision probability is less than required failure probability $P_f = 10^{-2}$ for a single transmission [39].

Table 3.2: Required number of retransmissions for F_{UE} to achieve 10^{-5} reliability, and corresponding transmission latencies under WB-I, NB-DI, and ND-I conditions

WB-I			
Activation Ratio	b=8, a=8		
No. Rep	K=9		
Latency Cal. by (5.2)	13 TTI		
7-OFDM Sym.	6.5 ms		
2-OFDM Sym.	1.85 ms		
NB-DI			
Activation Ratio	b=8, a=1	b=8, a=3	b=8, a=5
No. Rep	K=5	K=7	K=8
Latency Cal. by (5.2)	9 TTI	11 TTI	12 TTI
7-OFDM Sym.	4.5 ms	5.5 ms	6 ms
2-OFDM Sym.	1.28 ms	1.57 ms	1.71 ms
NB-I			
Activation Ratio	b=8, a=1	b=8, a=3	b=8, a=5
No. Rep	K=3	K=5	K=6
Latency Cal. by (5.2)	7 TTI	9 TTI	10 TTI
7-OFDM Sym.	3.5 ms	4.5 ms	5 ms
2-OFDM Sym.	1 ms	1.28 ms	1.42 ms

3.5 Conclusion

URLLC is the most challenging service with the requirements of both ultra-reliability and low-latency for 5G NR systems. GF access over shared resources has been proposed to achieve tight latency of UEs with URLLC in recent studies. However, it leads to collision between the URLLC UEs. In this study, sharing of the available resources between URLLC and latency-tolerant communication has been proposed both to provide ultra-reliable transmission with low-latency and to avoid inefficient spectrum utilization. A novel non-orthogonal resource sharing scheme based on OFDM and OFDM-IM has been introduced and assessed to reduce the impact of the collision for URLLC. The flexible nature of OFDM-IM has provided opportunities to design an adaptable system by taking different communication requirements into account. Frequency-flat-interference (WB-I) on URLLC due to OFDM has been transformed to frequency-selective interference (NB-(D)I) by fractional subcarrier activation in OFDM-IM. Therefore, URLLC is partially affected by latency-tolerant communication. The advantage of IM over classical M-ary modulation has been shown for contention-based transmissions within the scope of the study. As our future work, existence of multiple URLLC UEs, and optimal receiver with interference cancellation by utilizing NB-DI characteristics will be considered. Moreover, detailed analysis for the proposed NOMA scheme will be investigated under imperfect CSI.

Chapter 4

Optimization of Antenna Beamwidth Under Blockage Impact in Millimeter-Wave Bands

4.1 Introduction

Millimeter wave (mmWave) frequency bands have attracted considerable attention owing to their wide band opportunities for both multi giga-bit data rate and higher capacity requirements of 5G and beyond communication systems [61–64]. Therefore, in recent years mmWave channel characteristics have been analyzed by both academia and industry for the sake of exploring behavior of a transmitted signal at mmWave bands [65–69]. High free space path loss and penetration loss are addressed as critical issues for the mmWave communications. While directional communication is used to solve path loss problem, high penetration loss is still a challenging problem in practical communication scenarios.

Concentrating energy towards a specific region by directional communication

eliminates multipath in the environment and poorly scatters the transmitted signals [63, 66, 70]. Therefore, the communication is easily interrupted by any obstacle on antenna direction. In [71], authors have investigated human blockage impact by performing extensive measurement in a laboratory environment. It is shown that human blockage causes up to 25 dB attenuation at line-of-sight (LOS) path, and use of horn antennas result in poor multipath reflection as well as the reduced angular diversity. Also, increased rate of call drops has been observed due to lack of angular spreading. In [72], it is demonstrated that when LOS path is shadowed by a metallic blockage, the reflected waves become as important as the direct path for power delivery to the receiver. LOS path experiences up to 36 dB loss due to a metal surface.

In the recent study [73], authors have performed extensive measurement at 73 GHz in order to analyze fading effect caused by human blockers in crowded urban scenarios. Fading effects are analyzed through antennas with 7°, 15° and 60° half power beamwidth (HPBW) at the transmitter (Tx) and receiver (Rx). Both reduced fade time durations and lower mean signal attenuation are observed for large beam antennas in comparison to narrow beam antennas since more energy is captured from reflected waves. In [74] and [75], additional relay points have been introduced as a costly solution to provide diversity against shadowing and to recover the power loss caused by the blockage.

As a common result of the aforementioned studies, LOS path exposes to more signal attenuation in comparison to indirect paths or non-line-of-sight (NLOS) paths under blockage conditions. The motivation of this study is to provide robustness for mmWave links against blockage by enhancing angular domain diversity with the aid of indirect paths. For this purpose, investigations are conducted on angular dispersion and its relation to antenna radiation pattern when the direct path is blocked by a human body or a metallic prism. Beam expansion and optimization approach is proposed to improve the spreading in angular domain. Beam expansion is evaluated through power azimuth spectrum (PAS) analysis, and its optimization is performed by considering signal strength at the receiver. The performance analysis is conducted by indoor channel measurements, and also statistical analysis is provided by using mmWave channel model presented

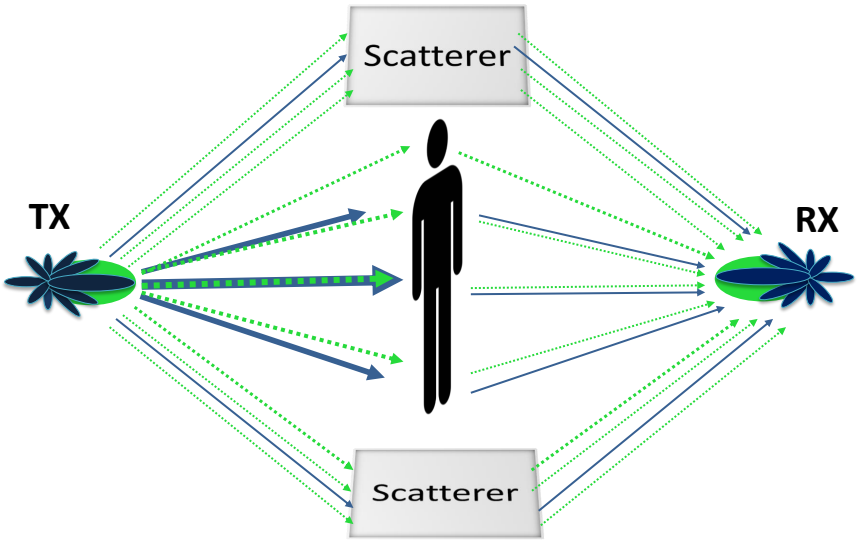


Figure 4.1: System model where antennas with high gain are illustrated by blue color, while green color denotes to low gain antennas.

in [76–78].

The rest of the chapter is organized as follows. Section 4.2 describes the system model and how PAS analysis is performed. The measurement environment and used mmWave channel simulator are explained in Section 4.3. Section 4.4 presents the results and discussions. Finally, Section 4.5 summarizes the contributions and concludes the chapter.

4.2 System Model & Power Azimuth Analysis

We consider a multipath channel environment as shown in Fig. 4.1. In this study, beam expansion and optimization are conducted only at the Rx, since beam analysis at the Tx is also expected to have a similar conclusion. When the Tx and Rx antenna beams are oriented towards each other, the analytical expression of the received signal can be written as,

$$r(t) = \sum_{l=0}^{L-1} a_l \sqrt{G(\theta_l - \psi)} x(t) + n(t), \tag{4.1}$$

where $r(t)$, $x(t)$ and $n(t)$ denote the received signal, transmitted signal and noise, respectively. Term a_l represents coefficient of the lth propagation path ($l \in \{1, 2, \ldots, L\}$), where the propagation paths are independent. $G(\theta)$ shows radiation pattern of the Rx antenna. Arrival angle of the lth path is θ_l, $-\pi \leq \theta_l \leq \pi$, in azimuth domain and ψ denotes azimuth angle offset from main lobe direction ($\theta = 0°$). Note that there is no multipath departure angle effect in (4.1), since multipath arrival angle dispersion is assumed as time invariant while the environment and antennas are fixed. Received signal strength (RSS) P_r at azimuth angle ψ is given in [79] as,

$$P_r(\psi) = \int_{\theta} \mathcal{S}_{\mathcal{A}}(\theta) G(\theta - \psi) d\theta + N_0, \tag{4.2}$$

where $\mathcal{S}_{\mathcal{A}}(\theta)$ and N_0 denote power azimuth spectra and additive white Gaussian noise (AWGN) power in the system, respectively. Antenna radiation pattern $G(\theta)$ experiences symmetry over $-\pi \leq \theta \leq \pi$. Thus, the integration process in (4.2) transforms into a circular convolution as,

$$P_r(\theta) = \mathcal{S}_{\mathcal{A}}(\theta) \circledast G(\theta) + N_0, \tag{4.3}$$

where $\circledast$ denotes the circular convolution.

For a given fixed measurement environment, the multipath distribution in azimuth plane is assumed as stationary. Utilizing the circular convolution properties, PAS is easily estimated with Fourier domain division, which is obtained from (4.3) as,

$$\hat{\mathcal{S}}_{\mathcal{A}}(\theta) = \mathcal{F}^{-1}\Big\{\frac{\mathcal{F}\{P_r(\theta)\}}{\mathcal{F}\{G(\theta)\}}\Big\}, \tag{4.4}$$

where $\mathcal{F}\{.\}$ and $\mathcal{F}^{-1}\{.\}$ represent the Fourier transform and inverse Fourier transform, respectively. By applying (4.4) to the received measurement results, PAS is obtained for a given measurement scenario. Later, beam optimization at the receiver is performed by emulating different antenna pattern $\mathcal{G}_{\theta_{3dB}}(\theta)$ in the simulation environment. Antenna pattern $\mathcal{G}_{\theta_{3dB}}(\theta)$ using realistic gains on commonly

accepted model given in [76] is expressed as,

$$\mathcal{G}_{\theta_{3dB}}(\theta) = \max\left[\mathcal{G}_0 e^{\alpha\theta^2+\beta\phi^2}, \frac{\mathcal{G}_0}{100}\right], \tag{4.5}$$

$$\alpha = \frac{4\ln 2}{\theta_{3dB}}, \quad \beta = \frac{4\ln 2}{\phi_{3dB}}, \quad \mathcal{G}_0 = \left(\frac{41253\eta}{\theta_{3dB}\phi_{3dB}}\right), \tag{4.6}$$

where θ denotes azimuth angle offset while θ_{3dB} and ϕ_{3dB} refer to azimuth half power beamwidth (HPBW) and elevation HPBW in degrees, respectively. ϕ_{3dB} is 0° in the measurement campaign. $\mathcal{G}_0$ is antenna gain at boresight. α and β parameters depend on the azimuth and elevation HPBW, respectively. $\eta = 0.7$ is a typical average antenna efficiency coefficient for the rectangular horn antennas.

Optimal beam pattern in the presence of an obstacle is chosen by performing the inverse process of (4.4) for the emulated antenna patterns. Therefore, optimum HPBW at the Rx is estimated as,

$$\hat{\theta}_{3dB} = \text{argmax}_{\theta_{3\text{dB}}}\left\{\hat{\mathcal{S}}_{\mathcal{A}}(\theta) \circledast \mathcal{G}_{\theta_{3\text{dB}}}(\theta)|\theta = 0^\circ\right\}. \tag{4.7}$$

4.3 Measurement Environment and mmWave Channel Simulator

In this work, investigations are performed in two steps. Firstly, indoor measurements at 60 GHz is performed, and then the measurement results are statistically validated by using well-known mmWave channel model.

4.3.1 Measurement Environment Description

Indoor measurements are conducted in the 5G and beyond laboratory at Istanbul Medipol University, and the measurement setup is illustrated in Fig. 4.2. Using 21 dBi directional antennas (15° HPBW) at the both end, power levels of 60 GHz

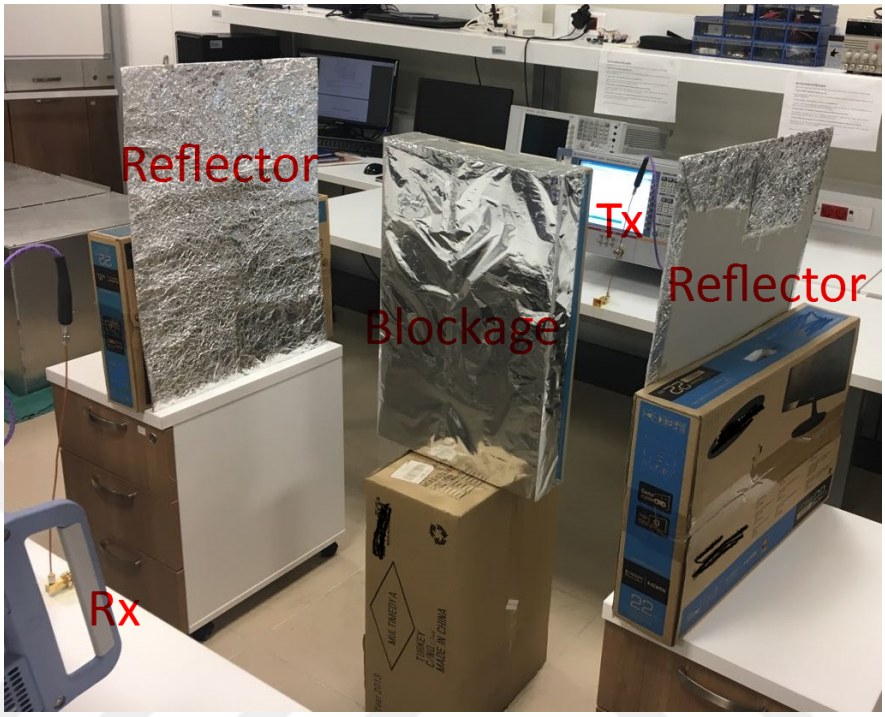


Figure 4.2: Measurement setup consists of the transmitter, receiver, reflectors and the blockage.

continuous wave is measured. The separation distance between the Tx and Rx antennas, which are at the same height and fixed locations, is 1.80 m. Dimensions of the measurement environment are 10.8 $m \times 9\ m \times 3\ m$. The human blocker with dimensions 1.67 $m \times 0.50\ m \times 0.20\ m$ and aluminum prism with the size of 0.63 $m \times 0.1\ m \times 0.4\ m$ are used to investigate antenna pattern effect in NLOS scenarios. The human body dimensions are in the order of body height, shoulder to shoulder length, and depth. The blockages are located in the middle of Tx and Rx to obstruct LOS path. Evaluation of environment scattering richness is performed using the reflectors, which are placed at a distance of $1m$ from the blockage edges as shown in the Fig. 4.2. The measurement system consists of vector signal analyzer (R&S FSW67), which is used to evaluate the signal and vector network analyzer (R&S ZVA67), which is used to generate the carrier signal.

4.3.2 Channel Simulator Description

In this study, mmWave channel simulator named as NYUSIM is used to evaluate beam expansion and optimization approach in the presence of blockage impact [76–78]. In the simulator, time clusters (TCs) and spatial lobes (SLs) are used to generate channel impulse response (CIR). A TC consists of paths which are close in time domain, while SL defines the paths whose arrival/departure directions are close in the space domain. Further information about the channel simulator can be found in [76–78]. In order to evaluate beam optimization approach, NLOS environment is considered, and Tx and Rx antennas are oriented to direction of SL pairs which provide the highest signal strength at the receiver. Then, weighting factors regarding various antenna pattern are applied to the incoming multipath at the receiver. Various Rx antenna beamwidths are evaluated for a given Tx antenna beamwidth and environment, as expressed in (4.7).

4.4 Measurement&Simulation Results and Discussion

4.4.1 Measurement Results

To investigate the angular spread of the received power under blockage effect, the measurements are performed by rotating the Rx antenna in the azimuth plane by an increment step of 5°. Two different types of blockage, i.e., the human and metal surface, are investigated during our measurements while LOS measurements are used as a reference to analyze them. Fig. 4.3 and Fig. 4.4 illustrate polar plots of relative received power level at the each azimuth angle by considering the reflectors in the environment. The radius of the polar plots refers to RSS in dB level. Firstly, the measurements are conducted in the absence of reflectors, and the results are shown in Fig. 4.3. It is observed that the human blocker and metal surface cause nearly 25 dB and 40 dB loss, respectively which also follows the

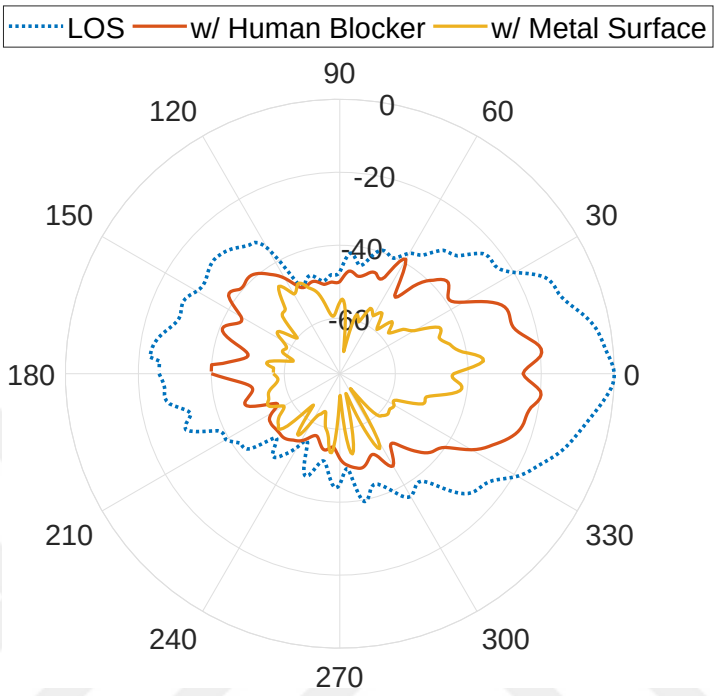


Figure 4.3: RSS in each azimuth angle for both LOS and penetration measurements in the absence of reflector in the system

literature [71, 72]. As expected, the LOS path is exposed to the highest power loss compared to indirect paths. Then, the reflectors are added as shown in Fig. 4.2 to increase multipath richness in the environment, and the observed results are shown in Fig. 4.4. An enhancement on angular power dispersion is observed in the presence of the reflectors due to the multipath richness. The improvement is due to energy reception from NLOS paths, which can be a beneficial solution to maintain the link connectivity under the obstacle for mmWave bands.

The received powers shown in Fig. 4.3 and Fig. 4.4 are interpolated to increase its resolution from 5° to 1°. Beam optimization approach is evaluated in two phases. As expressed in (4.4), PAS is obtained from the measurement results by removing Rx antenna pattern effect over RSS, and then obtained PAS is circularly convolved by different antenna patterns $\mathcal{G}_{\theta_{3dB}}$, as in (4.3). Fig.4.5 shows relative received power levels for various Rx antenna beamwidths. As seen in the figure, the HPBW is optimized to 27° for 1.5 dB power gain when there is a human blockage but no reflector in the environment. Similarly, when there are the reflectors in the environment, the HPBW is optimized to 55° for the gain of

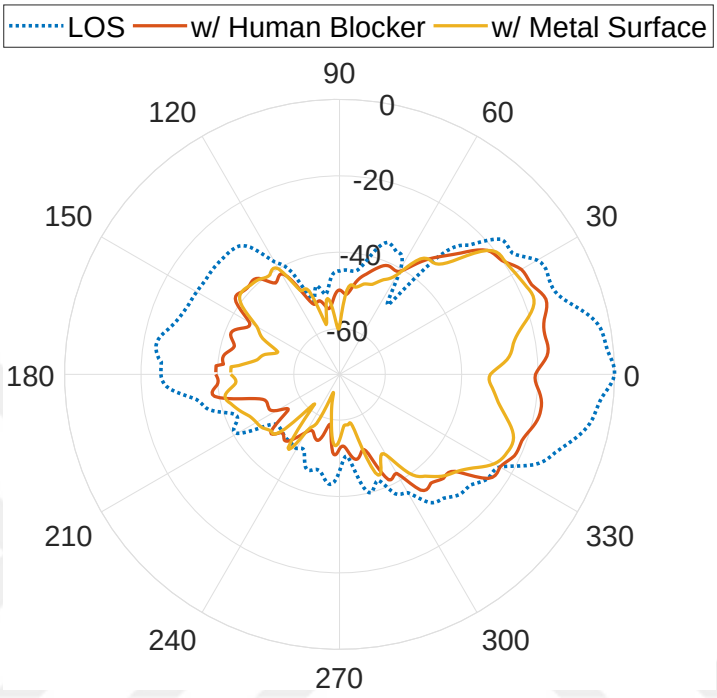


Figure 4.4: RSS in each azimuth angle for both LOS and penetration measurements in the presence of reflector in the system

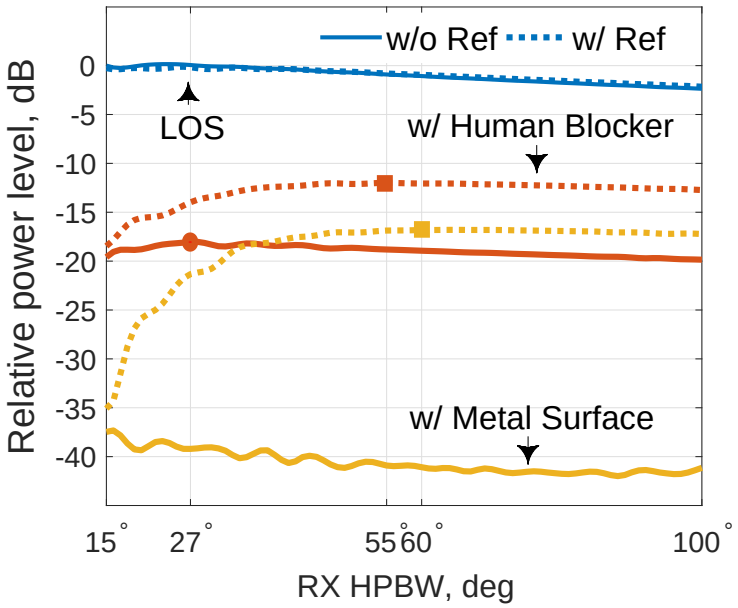


Figure 4.5: RSS in direct path regarding to Rx antenna HPBW

8 dB. In the case where there is the metal blockage between the transceivers, 18 dB gain is obtained by increasing HPBW from 15° to 60° because of multipath richness. The measurement results show that higher power level at the receiver is achieved by antenna patterns with larger HPBW under the blockage conditions, due to their abilities to capture the energy from the NLOS paths. However, in the measurement environment without reflector, there is no gain observed under metal blockage effect due to short link range. Table 4.1 shows the optimum HPBW $\hat{\theta}_{3dB}$ and the achieved power gain for a given measurement scenario in comparison to 15° Rx HPBW.

Table 4.1: Optimal decision on Rx HPBW with its gain

Scenario		$\hat{\theta}_{3dB}$ (deg)	Gain (dB)
w/ Human Blocker	w/o Ref	27	1.5
	w/ Ref	55	8
w/ Metal Surface	w/o Ref	15	-
	w/ Ref	60	18

4.4.2 Statistical Results

NYUSIM channel model is valid for carrier frequencies between 500 MHz and 100 GHz. In this work, 60 GHz NLOS environment is considered. Distance between Tx and Rx antennas is adjusted as $200m$, which has been considered as a cell size in mmWave bands [62]. Tx antenna HPBW is chosen as 120° due to its practical form for a user equipment, while Rx antenna HPBW is 7° which is the minimum valid HPBW defined in the channel model. We perform the simulation over 10,000 users as explained in Section 4.3.2. It is observed that 40% of the users require beam expansion, as depicted in Fig. 4.6. In addition, Fig. 4.7 shows probability distribution of the decided optimum HPBW and the achieved gain over the users who need a larger HPBW. The statistical results show that 2 dB gain is observed in average, while 13 dB gain is also achieved as a maximum gain using the beam expansion and optimization approach.

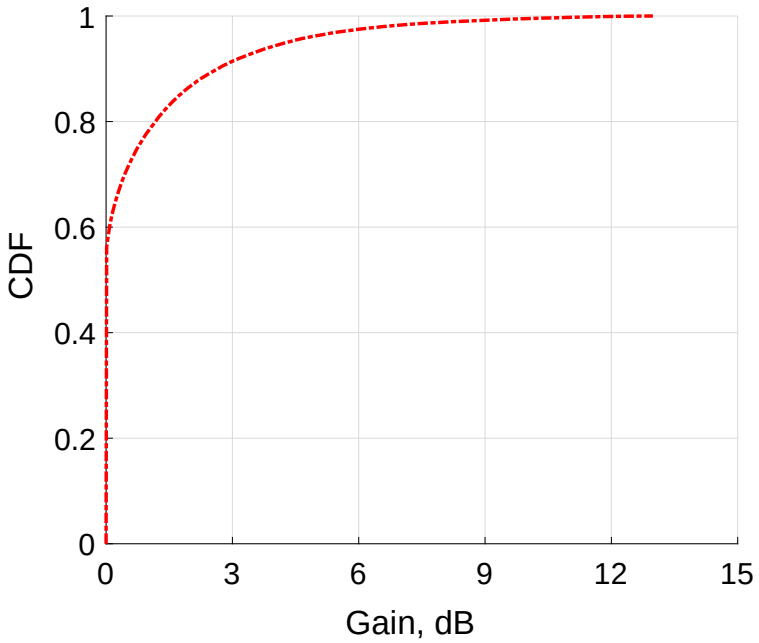


Figure 4.6: Cumulative distribution function (CDF) of observed gain as a result of optimizing HPBW.

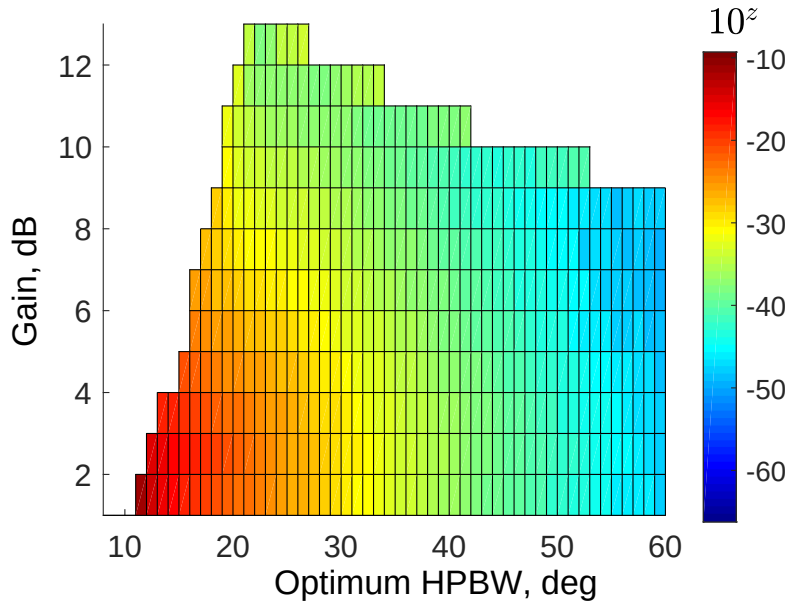


Figure 4.7: Probability distribution of optimized HPBW and its corresponding observed gain.

4.5 Conclusion

In this study, weak penetration problem of mmWave frequencies is addressed, and beam optimization approach is proposed. In contrast to the conventional belief, where wider beamwidth antennas lead to lower power at the receiver, a vice versa phenomena on the RSS is observed for NLOS conditions. Through our analysis, it is confirmed that RSS is improved by increasing antenna HPBW, which results in more energy captured from the NLOS paths. Indoor measurement results show that in rich scattering environment beam expansion and optimization approach significantly increases signal strength at the receiver due to indirect paths. Statistical results obtained from well-known channel model validate that the proposed approach can provide up to 13 dB RSS gain with an average of 2 dB in NLOS environment. Blockage detection mechanisms and application of the proposed optimization approach within received power decaying time will be studied as future works to prevent link drop caused by a blockage.

Chapter 5

Multidimensional Index Modulation for 5G and Beyond Wireless Networks

5.1 Introduction

The rapid growth of smart devices and services, such as sensors, smartphones, ultra-high-definition video streaming, wearable electronics, autonomous driving, drones, internet-based smart homes, and a broad range of augmented reality & virtual reality applications, leads to enormous data traffic that cannot be handled by fourth generation (4G) Long Term Evolution (LTE)-based communication systems [80]. Nearly ten-fold increase in the global mobile data traffic is envisioned from 2020 (57 exabytes/month) to 2030 (5016 exabytes/month) [81–83]. In an effort to support this overwhelming data volume and variety in fifth generation (5G) New Radio (NR) systems, International Telecommunication Union-Radio classifies numerous applications and use-cases into three main services, named enhanced mobile broadband (eMBB), massive machine-type communication (mMTC), and ultra-reliable low-latency communication (URLLC) [84, 85]. eMBB use-case is a continuation of 4G LTE systems with moderate reliability and

high data rate requirements. In mMTC, providing service to a massive number of user equipment (UE) is the main priority, while URLLC is the most challenging service for 5G New Radio (NR) systems due to the strict requirements for ultra-reliability with low-latency [16, 84–86]. In line with this trend, securing communication is essential for wireless networks, but it is disregarded during 5G standardizations. Thus, security is one of the pivotal requirements that need to be satisfied in the 6th generation (6G) and beyond networks, especially for scenarios with URLLC [87]. In short, a surprisingly diverse range of requirements poses two main challenges for researchers and engineers worldwide: *1) providing service in the presence of intensive data traffic over the current communication systems,* and *2) supporting a wide range of applications and use-cases.*

5.1.1 IM Can Revive Wireless Networks

Many researchers are putting tremendous effort on finding solutions to the aforementioned problems. In this spirit, plenty of work has been done to achieve flexibility in the medium access control (MAC) layer and physical layer (PHY) for the future generation systems [12, 32, 35]. In order to attain a high degree of freedom in the MAC layer, various radio resource management and multi-user scheduling techniques have been studied in the literature [5, 88, 89]. From the perspective of the PHY design, multi-numerology concept has been adopted for conventional orthogonal frequency division multiplexing (OFDM) systems [12,13]. Variable subcarrier spacings (SCSs) up to 120 kHz and mini-slot design that can consist of 2, 4 or 7 OFDM symbols have been introduced to meet different latency constraints.

In addition to the waveform-based approach, the use of different modulation options in the PHY has been also considered as the source of flexibility to support various UE demands. Three traditional modulation schemes, quadrature amplitude modulation (QAM), frequency shift keying (FSK), and phase shift keying (PSK) offer different performance under a variety of radio channel conditions [90, 91]. Specifically, transmission with lower order modulations provides

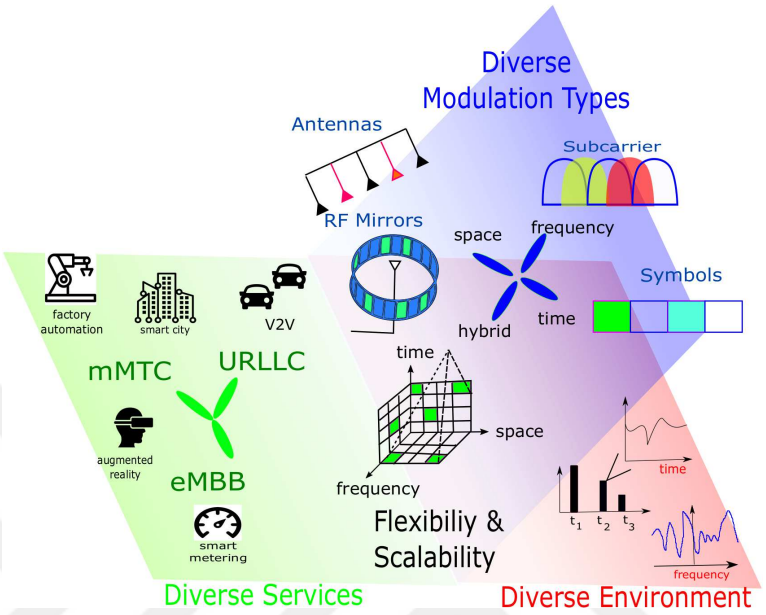


Figure 5.1: Diverse IM variants for various services and channel conditions.

robustness against channel impairments at the cost of decrease in SE, while the use of higher modulation orders maximizes achievable data rate under satisfactory channel conditions. Therefore, adaptive modulation selection with respect to the channel conditions has been adopted in modern communication systems [90]. However, flexibility stemming from the adaptive selection of modulation schemes is limited by the modulation order in these traditional schemes. On the other hand, recently reputed index modulation (IM) techniques have drawn substantial attention from the researchers because of their inherently flexible structure and promising advantages in terms of SE, energy efficiency (EE), complexity and reliability [25, 26, 92].

The main idea of IM is the utilization of the available transmit entities, such as antenna indices in space, subcarrier indices in frequency, and slot indices in time, to convey additional information bits along with the conventional M-ary symbols [25, 26, 92]. Application of IM in various domains enables an attractive trade-off among SE, EE, transceiver complexity, interference immunity, and transmission reliability [58, 93]. Therefore, the concept of IM has introduced new research opportunities for 5G and beyond wireless systems. Inspired by the performance of one-dimensional IM types, such as spatial modulation (SM) and

OFDM with IM (OFDM-IM), the multidimensional IM concept, which is composed of various combinations of one-dimensional IM options, has been introduced in recent studies. Despite the ongoing active research on IM techniques, the following important questions remain unanswered within the context of emerging IM solutions: how can the vast flexibility of IM be utilized for 5G and beyond systems, and how can IM solutions fulfill the broad range of user and application demands, as delineated in Fig. 5.1.

5.1.2 Related Works

Until today, several survey and magazine articles have appeared in the literature to shed light on the prominent members of the IM family, as listed in Table 5.1. SM represents an early stage of the IM concept and thus Di Renzo *et al.* [94] have introduced the working principle of SM associated with its superiority over the mature MIMO technology in terms of hardware and cost-efficiency. Moreover, beneficial insights have been provided on the exploitation of a wireless channel as a possible modulation unit. Besides SM-based MIMO investigation, in [98], the potential of space-time shift keying (STSK) with MIMO has been elaborated in a comprehensive manner. Specifically, a flexible framework allowing accommodation of multiple sub-mechanisms, i.e., space shift keying (SSK), SM, orthogonal space-time block coding (STBC), Vertical Bell Laboratories Layered Space-Time (V-BLAST), and linear dispersion codes (LDC), has been introduced as a unified STSK scheme. Di Renzo *et al.* [99] not only have presented different aspects of SM-MIMO including its principles, transceiver design, and hardware implementation, but also have paid attention to its integration with the emerging communication systems, such as relay-aided designs, small-cells, cooperative networks, mmWave systems, and visible light communications (VLC). Additionally, design guidelines for SM-MIMO have been discussed with the emphasis on receiver design, spatial constellation optimization, and link adaptation techniques, in [100]. Different from the aforementioned studies, Basar [25] has evaluated not only the future potentials and implementation feasibility of SM-MIMO architectures, but also frequency domain IM-based multicarrier systems,

Table 5.1: Summary of the existing magazine articles on IM techniques

Type	Ref.	Year	IM Domain(s)	Main Contributions
Magazine Articles	[94]	2011	Space	The principles of SM have been introduced and its advantages & disadvantages have been compared with the conventional MIMO.
	[25]	2016	Space, and Frequency	The potentials and implementation of IM techniques including SM and OFDM-IM for multi-user MIMO and multi carrier communication systems have been investigated.
	[95]	2018	Space, Time, and Frequency	Space, time, frequency, space-time and space-frequency IM options have been compared in terms of SE and EE.
	[96]	2018	Space, and Frequency	Space and frequency domain IM techniques have been subsumed by considering vehicular and railway communications.
	[97]	2020	Frequency	Frequency domain IM types including OFDM-IM, DM-OFDM, and ZTM-OFDM-IM have been evaluated for future wireless networks including cognitive radios, relay networks and multi-user communications.
Survey Articles	[98]	2012	Space, and Time	The potentials of MIMO signaling through STSK have been discussed, and unified STSK framework has been introduced.
	[99]	2014	Space	General aspects of SM-MIMO, its experimental evaluation and its integration with the promising communication systems have been presented.
	[100]	2015	Space	Transceiver design, spatial constellation optimization and link adaptation techniques for SM have been assessed.
	[26]	2016	Space, Time, Frequency, and Channel	Practical application of SM, OFDM-IM, and CM have been elaborated, and practical issues such as ICI, PAPR have been discussed.
	[101]	2017	Space, Time, and Frequency	Benefits and fundamental limitations have been discussed for SM, OFDM-IM and SC-IM.
	[102]	2018	Space, Time, Frequency, and Channel	Potential challenges and open issues for channel domain IM types have been provided in addition to space, time and frequency domain IM techniques.
	[103]	2018	Space, Time, Frequency, Code, and Channel	50 years history of SM and IM concepts, and the road from permutation modulation to OFDM-IM have been revealed.
	[104]	2019	Space	The integration of recent SM variants with promising technologies, such as CS theory, and their application in the future emerging systems, such as optical wireless communications, have been discussed.

i.e., OFDM-IM and MIMO-aided OFDM-IM. Also, the author has reviewed advanced SM technologies, such as generalized SM (GSM), enhanced SM (ESM), and quadrature SM (QSM). In [26], Basar *et al.* have provided an overview of the IM variants present in the literature and elaborated on the advantages of SM, OFDM-IM, and channel modulation (CM). They have assessed the application of these modulation techniques to different networks and systems and reviewed some practical concerns for OFDM-IM, such as peak-to-average power ratio (PAPR), inter-carrier interference (ICI), and achievable rate. Sugiura *et al.* [101] have discussed the limitations of IM in space, time, and frequency. They have compared single-carrier (SC) transmission with OFDM and examined the importance of time-limited pulses for SM. The challenges that occurred by the acquisition of channel state information (CSI) have been revealed for the SM technology. In [102], CM, which is media-based modulation (MBM), has been discussed in addition to space, time, and frequency domain IM variants. In [96], authors have classified space and frequency domain IM techniques for vehicular and railway communications. Cheng *et al.* [95] have compared space, frequency, space-time, and space-frequency domain IM variants in terms of SE and EE. Future directions to further increase the SE of IM techniques have been also suggested. Ishikawa *et al.* [103] have shed light on the historical background of permutation modulation, SM, and IM concepts, and have disclosed the road from permutation modulation to OFDM-IM. Research progresses on SM variants, performance enhancement schemes for SM, its integration with promising technologies, such as compressed-sensing (CS) theory and NOMA-aided systems, and its application in emerging systems, such as mmWave and optical wireless communications, have been presented in [104]. Recently, Li *et al.* [97] have evaluated frequency domain IM types including OFDM-IM, dual-mode OFDM (DM-OFDM), and zero-padded tri-mode IM-aided OFDM (ZTM-OFDM-IM) for future wireless networks including cognitive radio (CR) networks, relay-aided networks and multi-user communications.

5.1.3 Contributions

Against this background, the main contributions of this work are listed as follows:

- A comprehensive review of the existing IM approaches in the literature is presented and dimensional-based categorization is performed.
- To the best of authors' knowledge, this study is the first for both providing a survey and comparison of one-dimensional and multidimensional IM options.
- To further extend the understanding of these IM schemes, their differences and the trade-off among them are identified with respect to the achievable data rate, power consumption, transmission reliability, and practical implementation.
- The reviewed IM techniques are categorized considering the requirements of eMBB, mMTC, and URLLC to shed light on the application of IM techniques for future use-cases and applications.
- The main benefits and shortcomings of available IM domains are quantified.
- Finally, potential challenges and future directions on the integration of IM concept into the prominent wireless technologies, such as CR networks, cooperative systems, and non-orthogonal communications, are elaborated.

5.1.4 Organization

The organization of the survey is given in Fig. 5.2 via the chart flow. Section 5.2 revises the requirements of 5G and beyond services in wireless networks. Section 5.3 presents a comprehensive taxonomy of the existing IM schemes in the literature and then provides useful insights on future multidimensional IM

variants. In Section 5.4, enabling IM techniques for 5G and beyond services are provided, and key advantages & disadvantages of the available IM domains are revealed. Section 5.5 provides the potential challenges and future directions for IM-aided communication networks. Finally, Section 5.6 concludes the work. [1]

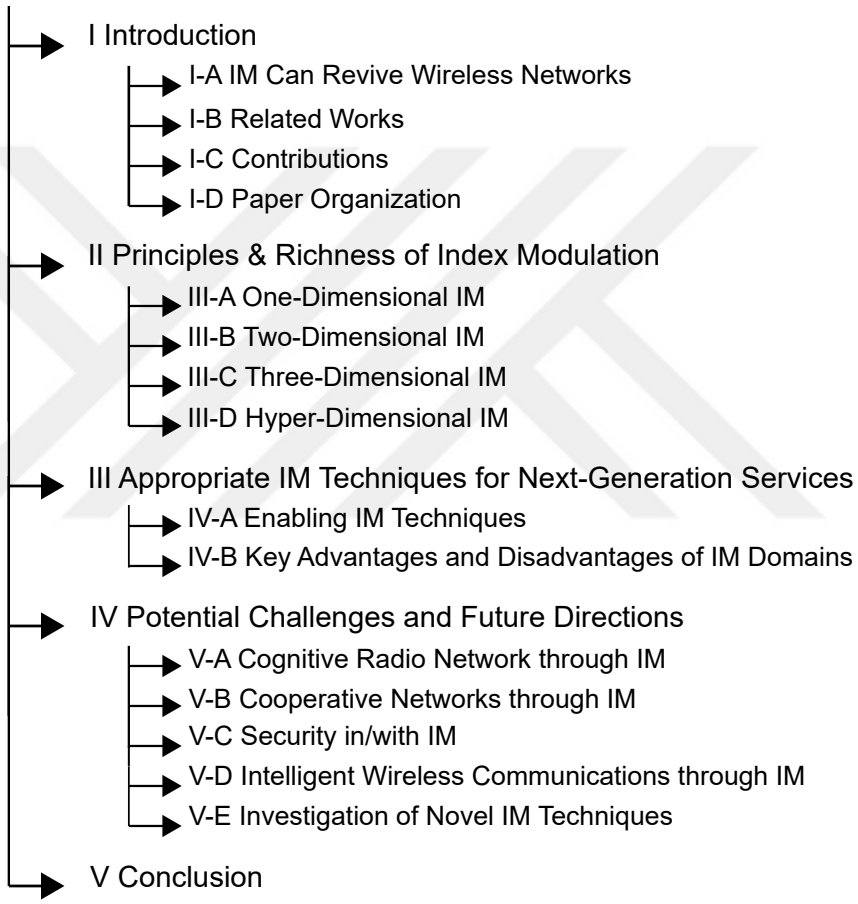


Figure 5.2: Organization of the survey.

[1] *Notation:* Bold, capital and lowercase letters are used for matrices and column vectors, respectively. $(.)^T$ and $(.)^H$ denote transposition and Hermitian transposition, respectively. E[.] stands for expectation and $\mathbb{C}$ is the ring of complex numbers. $\binom{\cdot}{\cdot}$ denotes the binomial coefficient and $\lfloor . \rfloor$ is the floor function.

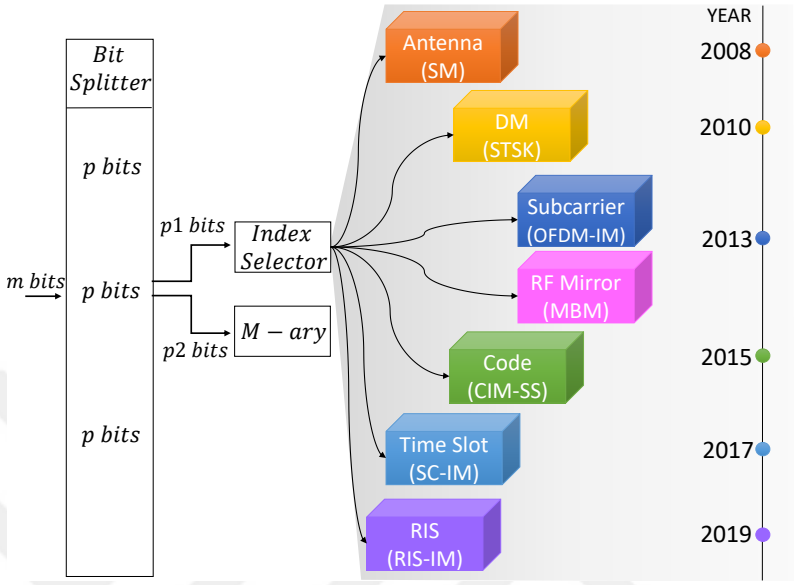


Figure 5.3: Basic implementation of IM, and the timeline of substantial IM techniques.

5.2 Principles and Richness of Index Modulation

IM deals with the mapping of data bits to information-bearing transmit entities, such as antennas, subcarriers, radio frequency (RF) mirrors, dispersion matrices (DMs), codes, time slots, and different combinations thereof. In order to convey additional information bits along with conventional M-ary symbols, partial activation of the entities in a given domain is performed through IM. Although the initial proposal of IM concept dates back to almost the beginning of the century, it has drawn substantial attention from the research community over the last decade [105]. Fig. 5.3 illustrates the timeline of the substantial IM variants in the literature.

In spite of the fact that one-dimensional IM methods are well-known, a comprehensive overview of the multidimensional IM methods is lacking in the literature. In view of this, firstly, this section reveals the applied multidimensional IM domains in the literature and provides their dimensional-based categorization

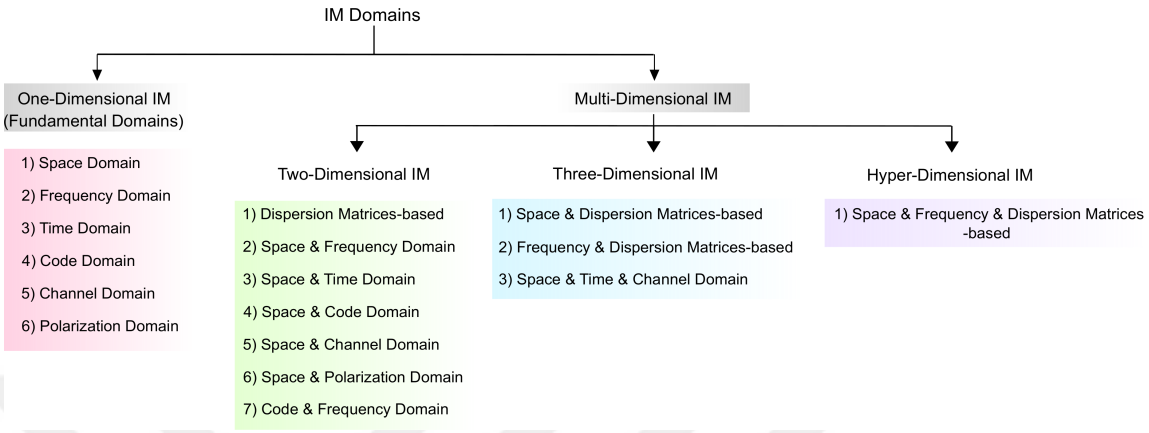


Figure 5.4: Dimensional-based categorization of the existing IM domains in the literature.

in detail, as illustrated in Fig. 5.4. Later, the existing IM techniques are subsumed regarding the dimensional-based categorization. In Table 5.2, the right-angled triangle demonstrates the available IM options in the literature regarding their application domains, where the diagonal and off-diagonal cells correspond to one-dimensional and multidimensional IM schemes, respectively. Note that two-dimensional IM placed in diagonal cells is only DMs-based IM types, and their combinations with the other IM schemes are minimum three-dimensional IM. Also, the unfilled cells denote the unexplored multidimensional IM variants.

5.2.1 One-Dimensional IM

One-dimensional IM corresponds to fundamental IM techniques that lay the foundations for multidimensional IM types. As illustrated in Fig. 5.4, space, frequency, time, code, channel, and polarization domains are elaborated under this category.

5.2.1.1 Space Domain IM

Two different physical entities consisting of antennas, and reconfigurable intelligent surfaces (RIS) are evaluated in the context of space domain IM.

Spatial multiplexing (SMX) and spatial diversity (SD) are well-known techniques for boosting transmission rate through sending independent information bits over independent channels and increasing reliability through emitting the same information bits over independent channels for conventional $N_t \times N_r$ MIMO systems, respectively [106, 107]. N_t and N_r represent the number of transmitter (Tx) and receiver (Rx) antennas, respectively. However, 1) hardware complexity, 2) strict synchronization requirement between Tx antennas, and 3) decoding complexity should be alleviated to reap the advantages of MIMO systems. Firstly, activation of N_t Tx antennas at each transmission interval requires N_t RF chains, which might be impractical for mMTC devices. Secondly, all data symbols should be transmitted at the same time, thus inter-antenna synchronization (IAS) is needed. Thirdly, the Rx is subject to a heavy decoding process due to the active N_t Tx antennas.

5.2.1.1.1 IM via Antennas Space domain IM is introduced via SSK which utilizes a single antenna out of N_t Tx antennas [105, 140]. The index of the active antenna conveys $m = \log_2(N_t)$ information bits, while the antenna itself does not carry M-ary symbol. There are N_t different combinations of the information bits to decide the active antenna. For the i-th combination, transmission vector $\mathbf{x_i}$ presents the status of N_t antennas, and it is expressed as

$$\mathbf{x_i} \triangleq \begin{bmatrix} 0 & 0 & 0 & 1 & 0 & \cdots & 0 \end{bmatrix}^T, \tag{5.1}$$

where the active antenna has unit transmission power while 0 refers to the inactive antennas. SSK attains a logarithmic increase on SE with N_t while SE of conventional SMX methods linearly increases with N_t. Thus, achieving higher data rates through SSK can be impractical due to the need for higher number of Tx antennas. Generalized SSK (GSSK) allows the utilization of multiple Tx antennas to carry the information bits [108]. For N_k active antennas, $\lfloor \log_2 \binom{N_t}{N_k} \rfloor$

Table 5.2: One-dimensional and multidimensional IM Variants

Modulation Domain	**Space**	**Frequency**	**Time**	**Code**	**DM**
Space	SSK* [105] GSSK* [108] SM* [109] GSM* [110] MA-SM* [111] QSM* [112] ESM* [113] STBC-SM* [114] DSM* [115] MBM^{+} [116] DMBM^{+} [117] RIS-IM^{-} [**?**]	SIM-OFDM [54] ESIM-OFDM [23] OFDM-IM [24] OFDM-ISIM [27] CI-OFDM-IM [31] OFDM-GIM [121] DM-OFDM [29] MM-OFDM [30] GFDM-IM [122]			
Frequency	ISM-OFDM [118] GSFIM [119] GFDM-SFIM [120]	...	SC-IM [125] FTN-IM [126] DM-SCIM [127]		
Time	TI-SM [123] TI-MBM [124] TI-SM-MBM [124]	...	...	CIM-SS [129] GCIM-SS [130] IM-OFDM-SS [131]	
Code	CIM-SM [128]	...	...	...	STSK [135] GSTSK [136] STFSK [137] OFDM-STSK [138] SFSK [139]
DM	MS-STSK [132]	OFDM-STSK-IM [133] MSF-STSK [134]	...	...	

Note - (.)*: IM via antennas, (.)$^{+}$: IM via RF mirrors, and (.)$^{-}$: IM via RIS

data bits are conveyed by the indices of multiple active antennas. Hence, $\mathbf{x_i}$ corresponds to

$$\mathbf{x_i} \triangleq \begin{bmatrix} 0 & \frac{1}{\sqrt{N_k}} & \cdots & 0 & \frac{1}{\sqrt{N_k}} & 0 & \cdots & 0 \end{bmatrix}^T. \tag{5.2}$$

Since multiple Tx antennas are active, IAS is a necessity for GSSK. Otherwise, the system performance is affected by IAI. Moreover, channels between the activated Tx and Rx antennas should be as independent as possible to achieve a performance gain via spatial selectivity. Thus, the distance between Tx antennas in an array should be more than half of the wavelength ($\frac{\lambda}{2}$).

The invention of the SM is an important breakthrough that not only paves the way for the introduction of the general IM concept to the wireless communication realm but also sheds light on its development [109, 141–143]. Besides conveying information bits via the index of active Tx antenna, SM also performs conventional M-ary symbol transmission. In this case, the transmission vector $\mathbf{x_i}$ is expressed as

$$\mathbf{x_i} \triangleq \begin{bmatrix} 0 & 0 & 0 & s_l & 0 & \cdots & 0 \end{bmatrix}^T, \tag{5.3}$$

where $s_l \in \mathcal{S}$, where $\mathcal{S}$ is the set of M-ary symbols $\mathcal{S} = \{s_0 \;\; s_1 \;\; \cdots \;\; s_{M-1}\}$. For each transmission interval, $\log_2(N_t)$ and $\log_2(M)$ bits are carried by the active antenna index and M-ary symbol, respectively. Thus, the number of transmitted bits per channel use (bpcu) for SM is

$$\eta = \log_2(N_t) + \log_2(M) \text{ [bpcu]}. \tag{5.4}$$

SM provides better SE than SSK while protecting the zero IAI feature. To improve both SE and achievable performance, GSM activates N_k Tx antennas for the transmission of the same data symbol, given that $1 \leq N_k < N_t$ [110]. Thus, $\mathbf{x_i} \triangleq \begin{bmatrix} 0 & s_l & \cdots & 0 & s_l & 0 & \cdots & 0 \end{bmatrix}^T$, and the SE rises to

$$\eta = \lfloor \log_2 \binom{N_t}{N_k} \rfloor + \log_2(M) \text{ [bpcu]}. \tag{5.5}$$

The transmission of different data symbols through the activated antennas is

performed by multiple active SM (MA-SM) [111]. As a result of the efficient implementation of IM with the conventional QAM/PSK, the achievable rate increases to

$$\eta = \lfloor \log_2 \binom{N_t}{N_k} \rfloor + N_k \log_2(M) \text{ [bpcu]}. \tag{5.6}$$

A new perspective to SM is introduced through QSM where in-phase and quadrature parts of complex data symbols are transmitted by two different Tx antennas [112, 144]. The selection of two Tx antennas requires $2\log_2(N_t)$ data bits. Hence, the transmission rate for QSM equals

$$\eta = 2\log_2(N_t) + \log_2(M) \text{ [bpcu]}. \tag{5.7}$$

Although not emphasized sufficiently in the literature, a particular strength of the QSM is that it exploits the spatial selectivity by conveying the real and imaginary parts of the data symbol separately. In order to further boost the data rate of SM, ESM proposes the transmission of information bits by the use of two different QAM/PSK sets, i.e., $\mathcal{S}_1$ and $\mathcal{S}_2$, for the two active Tx antennas [113]. It should be ensured that the same number of data bits is transmitted at each transmission interval. Otherwise, error propagation occurs due to asynchronization between the data blocks. Therefore, higher order modulation $\mathcal{S}_2$ is used when one of the two antennas is activated, while lower order modulation $\mathcal{S}_1$ is utilized in the presence of two active antennas. Moreover, the selected modulation types decide the BER performance of ESM. If Euclidean distance between the symbols modulated with $\mathcal{S}_1$ and $\mathcal{S}_2$ is higher than that of SM, better BER performance is achieved than SM, and vice versa. The aforementioned space domain IM types suffer from a lack of diversity gain. In [145], Trellis coded spatial modulation (TCSM) is presented with the implementation of Trellis coded modulation (TCM) over the antenna combinations of SM. In this way, the spatial distance between antennas within the same subblock is maximized without increasing the power consumption. Also, in [146], TCM is incorporated with QSM (TC-QSM) to further improve the error performance of SM systems. On the other hand, in order to achieve transmit diversity gain for any number of Tx antennas, STBC

with SM (STBC-SM) and STBC with QSM (ST-QSM) are proposed in [114] and [147, 148], respectively. ST-QSM divides the existing N_t antennas into two subsets (N_{t1} and N_{t2}) to carry two complex symbols. The real and imaginary parts of the symbols are transmitted over the subcarriers that are independently chosen from the first and second subsets. The total number of the active subcarriers in each set corresponds to (N_{k1} and N_{k2}). Moreover, IM concept is applied to Rx antennas via preprocessing/precoding of the transmission vector with the knowledge of CSI at Tx and named precoded SM (PSM) or receiver SM [149,150]. Generalised precoding-aided SM (GPSM) and QSM (GPQSM) are introduced in [151] and [152], respectively. GPSM corresponds to SM at Rx, while GPQSM is the QSM with multiple active antennas at Rx.

5.2.1.1.2 IM via RISs RIS concept has been extensively investigated in the past few years. Intelligent surfaces consist of small, low cost and a high number of passive elements which control the reflection features of the incoming signals. For a comprehensive overview of RIS concept, interested readers are referred to [153–155]. RIS-assisted IM concept is introduced in [156]. It is shown that IM can be applied on the passive elements as well as Tx and Rx antennas.

5.2.1.2 Frequency Domain IM

Indexing of the subcarriers in the frequency domain is proposed to improve both SE and EE of the conventional OFDM systems. Subcarrier index modulation OFDM (SIM-OFDM) divides incoming data bits into two parts [54]. On-off keying data bits decide the status of N_{sc} subcarriers in an OFDM block, and the remaining bits are conveyed through N_a subcarriers whose status is on. However, the inconsistent number of the total bits per OFDM block results in error propagation and degrades the BER performance of SIM-OFDM. Enhanced SIM-OFDM (ESIM-OFDM) splits the OFDM block to $N_{sc}/2$ subblocks with two subcarriers, and it only activates a single subcarrier ($N_a = 1$) per subblock to avoid error propagation [23]. Inspired by the SM, SIM-OFDM and ESIM-OFDM are the early

attempts for frequency domain IM. However, their performances are not satisfactory, and their implementations are impractical. Hence, the general concept for frequency domain IM is firstly introduced by OFDM-IM [24].

In OFDM-IM, available subcarriers are partitioned into N_G subblocks, and each subblock includes $N_b = N_{sc}/N_G$ subcarriers. N_a subcarriers out of N_b subcarriers are activated according to $p_1 = \lfloor \log_2 \binom{N_b}{N_a} \rfloor$ bits. The remaining $p_2 = N_a \log_2(M)$ bits are utilized to modulate the active subcarriers. The number of transmitted bits per OFDM-IM subblock is

$$p = p_1 + p_2 = \lfloor \log_2 \binom{N_b}{N_a} \rfloor + N_a \log_2(M). \tag{5.8}$$

Then, OFDM-IM subblocks are concatenated to generate an OFDM block, and the remaining process is the same as conventional OFDM. Inverse fast Fourier transform (IFFT) is applied to the OFDM block, and cyclic prefix (CP) is added to avoid inter-symbol interference (ISI). Thus, the SE of OFDM-IM is

$$\begin{aligned} \eta = \frac{N_G}{N_{sc} + N_{cp} - 1} \Bigg(& \lfloor \log_2 \binom{N_b}{N_a} \rfloor \\ & + N_a \log_2(M) \Bigg) \text{ [bits/s/Hz]}, \end{aligned} \tag{5.9}$$

where N_{cp} is the CP size in the frequency domain. At Rx, maximum likelihood (ML) detector is used for joint estimation of the active subcarriers and the QAM/PSK symbols after CP removal and fast Fourier transform (FFT) process. However, ML detector is impractical for large N_{sc} values. Hence, in [24] log-likelihood ratio (LLR) detector is proposed for OFDM-IM. In order to both reduce correlation and exploit frequency diversity, interleaving for an OFDM block is employed by OFDM with interleaved subcarrier index modulation (OFDM-ISIM) [27]. Lower correlation between the active subcarriers improves the detection performance at Rx, and consequently the BER. Coordinate interleaved OFDM-IM (CI-OFDM-IM) achieves an additional diversity gain through the transmission of real and imaginary parts of a complex data symbol over two active subcarriers via the CI orthogonal design. Therefore, CI-OFDM-IM provides higher reliability than both OFDM-IM and OFDM-ISIM [31]. Additionally,

OFDM with I/Q index modulation (OFDM-I/Q-IM) utilizes different information bits to generate the I/Q parts of data symbols [121, 157].

In OFDM-IM, N_a value is fixed for all OFDM subblocks. On the other hand, OFDM with generalized index modulation (OFDM-GIM) allows varying N_a values for the different subblocks to enhance the SE of OFDM-IM [121,158]. Further SE improvement is achieved with DM-OFDM that uses two different QAM/PSK sets $\mathcal{S}_1$ and $\mathcal{S}_2$ for N_a and $N_b - N_a$ subcarriers, respectively [29]. In this way, all the subcarriers are modulated within a subblock. Hence, the achieved SE by DM-OFDM equals

$$\eta = \frac{N_G}{N_{sc} + N_{cp} - 1} \Bigg(\lfloor \log_2 \binom{N_b}{N_a} \rfloor + N_a \log_2(M_1) + (N_b - N_a) \log_2(M_2) \Bigg) \text{ [bits/s/Hz]} \tag{5.10}$$

where M_1 and M_2 are the constellation size of $\mathcal{S}_1$ and $\mathcal{S}_2$, respectively. Inspired by DM-OFDM, two promising schemes including multiple-mode OFDM-IM (MM-OFDM) and zero-padded tri-mode index modulation aided OFDM (ZTM-OFDM-IM) are introduced in the literature [30, 159]. MM-OFDM uses multiple QAM/PSK sets within a subblock to enhance the SE, while ZTM-OFDM-IM performs fractional subcarrier activation by two different QAM/PSK sets. In order to further increase the SE of the OFDM-IM systems, in [160], layered OFDM-IM (L-OFDM-IM) is proposed by division of p incoming bits into L layers, where N_{a_L} out of N_{b_L} subcarriers are activated, given that $N_b = N_{b_L} + N_{a_L}(L-1)$.

The aforementioned frequency domain IM types are based on OFDM technology. In [122], IM is applied to generalized frequency division multiplexing (GFDM), instead of OFDM. GFDM performs block-based transmission over T time slots, and each block consists of K sub-symbols composed by N_{sc} subcarriers. Moreover, each block can include different number of sub-symbols. GFDM alleviates the strict synchronization requirement of OFDM since non-orthogonal pulse shaping is allowed. In this regard, GFDM with IM (GFDM-IM) combines the benefits of GFDM with IM flexibility.

5.2.1.3 Time Domain IM

Inspired by the frequency domain IM, single carrier with IM (SC-IM) is proposed in the time domain [125]. A SC block with K_s symbols is divided into K_G subblocks which consist of $K_b = K_s/K_G$ symbols. Data transmission is performed at the time intervals corresponding to active K_a symbols, and the remaining $K_b - K_a$ symbols are set to zero. SC subblocks are concatenated to generate a SC block, and then CP is added before its transmission over a multi-path channel. The SE of SC-IM is

$$\eta = \frac{K_G}{K + K_{cp} - 1}\left(\lfloor \log_2 \binom{K_b}{K_a} \rfloor + K_a \log_2(M)\right) \text{ [bits/s/Hz]}, \tag{5.11}$$

where K_{cp} refers to the CP size in the time domain. At Rx, ML or LLR detector is utilized to find the non-zero symbols after CP removal and frequency domain equalization [24]. It is worth mentioning that interleaving at Tx is needed to tear the correlation between the active symbols if the channel is non-selective in time. Thus, de-interleaving is required at Rx. Faster-than-Nyquist signaling with IM (FTN-IM) has been proposed since the passive symbols in the SC block alleviate the effect of ISI [126, 161]. Furthermore, dual-mode single carrier with index modulation (DM-SCIM) utilizes two different QAM/PSK sets for further increasing the SE of SC-IM, as in DM-OFDM [127].

5.2.1.4 Code Domain IM

By taking the advantage of direct-sequence spread spectrum (DS-SS) technology, code index modulation SS (CIM-SS) has been proposed in [129]. The information-bearing unit is the spreading code available in a predefined table of spreading codes. In [129], two orthogonal Walsh codes (w_1 and w_2) are stored in the look-up table. The incoming two bits are combined to generate a subblock, and one bit in each subblock chooses a code (N_{ac}) to spread the remaining bit over a time duration. In-phase and quadrature parts of a complex symbol are modulated by orthogonal Walsh codes. Generalized CIM-SS (GCIM-SS) uses the code table

with N_{ct} size, where $\lfloor \log_2(N_{ct}) \rfloor$ defines the number of bits required for choosing a code [130, 162]. Hence, the SE of GCIM-SS is

$$\eta = \frac{1}{N_{ct}} \left(2 \lfloor \log_2(N_{ct}) \rfloor + \log_2(M) \right) \text{ [bits/s/Hz]}. \tag{5.12}$$

At Rx, distinct N_{ct} correlators are used for the in-phase and quadrature parts of the complex symbol. The correlator that gives the maximum absolute value corresponds to the utilized code at Tx. Later, de-spreading and conventional QAM/PSK demodulation are applied to obtain the transmitted information bits. CIM is also applied in the frequency domain with the aid of OFDM and named index modulated OFDM-SS (IM-OFDM-SS) [131,163]. In order to obtain diversity gain, IM-OFDM-SS spreads data symbol over several subcarriers via spreading codes. ML and maximum ratio combining (MRC)-based detectors are used at Rx. Also, a generalized framework for multi-user scenarios is introduced in [163].

5.2.1.5 Channel Domain IM

Media-based modulation (MBM) transmits information bits via different channel realizations generated by the on-off status of the available RF mirrors, which are located in the vicinity of the Tx antenna [116, 143, 164–166]. In other words, each channel realization corresponds to a different point in the constellation diagram at the Rx. No additional energy is required to transmit the bits by MBM. Moreover, it is shown that $1 \times N_r$ single-input multiple-output (SIMO) systems with MBM can harvest the same energy as $N_t \times N_r$ MIMO systems, yielding $N_t = N_r$ [116]. Unlike SSK, SE of MBM linearly increases with the number of RF mirrors (N_{rf}). Thus, the transmission rate of MBM with a single RF mirror activation ($N_{am} = 1$) is

$$\eta = N_{rf} + \log_2(M) \text{ [bpcu]}. \tag{5.13}$$

The main issue for MBM is the requirement of CSI at Rx. $2^{N_{rf}}$ channel realizations need to be estimated in the presence of N_{rf} mirrors. Usually, the estimation

of CSI is performed through training process. However, it leads to severe signaling overhead for the system especially in the case of a higher number of RF mirrors. To overcome this, differential MBM (DMBM) is proposed in the literature, where the estimation process is avoided by encoding consecutive data blocks at the cost of performance degradation [117]. In [167] and [168], space-time channel modulation (STCM) and space-time MBM (ST-MBM) incorporate STBCs into channel domain IM for the purpose of achieving diversity gain. Specifically, STCM adopts Alamouti's STBC as the core, and ST-MBM amalgamates the Hurwitz-Radon family of matrices [32] with the MBM principles to allow a single RF chain-based transmission.

5.2.1.6 Polarization Domain IM

In order to provide both higher multiplexing gain and higher SE for the single RF MIMO systems, polarization shift keying (PolarSK) is introduced in [169]. PolarSK uses the available P polarization states, i.e., linear polarization, circular polarization, and elliptic polarization, to transmit the incoming bits as in SSK. In a recent study, a novel IM scheme, i.e, polarization modulation (PM), utilizes polarization characteristics to carry extra information bits along with the complex data symbols. Specifically, not only vertical and horizontal polarizations but also the axial ratio and tilt angle of elliptic polarization are used for conveying the information bits through IM [170].

5.2.2 Two-Dimensional IM

Two-dimensional IM corresponds to the simultaneous activation of information-bearing units in two different dimensions, such as space & frequency, and space & time, as given in Fig. 5.4.

5.2.2.1 Dispersion Matrices-based IM

Space-time shift keying (STSK) introduces an innovative information-bearing unit, i.e., DMs, for conventional MIMO systems [135, 171]. STSK exploits the time domain along with the space domain through block-based transmission as $\mathbf{Y} = \mathbf{HX} + \mathbf{N}$, where $\mathbf{Y} \in \mathbb{C}^{N_r \times T}$, $\mathbf{H} \in \mathbb{C}^{N_t \times N_r}$, and $\mathbf{X} = \mathbf{D}s \in \mathbb{C}^{N_t \times T}$ denote the received block, the multi-path channel, and the transmitted block, respectively. $\mathbf{D} \in \mathbb{C}^{N_t \times T}$ refers to the DM to spread the M-ary symbol (s) over space and time dimensions, and T is a block duration. A STSK block ($\mathbf{X} = \mathbf{D}s$) is generated by the different combinations of Q DMs with the M-ary symbols in a given modulation set. Also, SSK and SM can be assessed as the special cases of STSK, given that $T = 1$. Thus, STSK provides diversity gain along with multiplexing gain by adjusting the number of DMs (Q), STSK block duration (T), and the number of Tx and Rx antennas (N_t, N_r). To exemplify, a single DM and the modulation set with $M = M_1$ complex symbols, or two DMs and the modulation set with the $M = M_1/2$ complex symbols can generate different STSK blocks to transmit $\frac{\log_2(QM)}{T}$ bits [135]. It should be noted that the correlation between Q DMs should be as low as possible to improve the detection performance at Rx. This is one of the ongoing research areas pertaining to the design of DMs [172, 173]. Generalized STSK (GSTSK) is developed to choose P DMs at each transmission interval [136]. Hence, the achievable rate by GSTSK is

$$\eta = \frac{\lfloor \log_2 \binom{Q}{P} \rfloor + P \log_2(M)}{T} \text{ [bpcu]}. \tag{5.14}$$

The BER performance of STSK is affected by ISI under frequency-selective channel conditions. Therefore, space-frequency shift keying (SFSK) proposes the utilization of the conventional F-FSK to spread the data symbol in space, time, and frequency, instead of M-QAM/PSK [137]. A SFSK block corresponds to the multiplication of the F-FSK symbol with the DM. At Rx, square-law and ML detectors are used to detect the active frequencies and the DM, respectively. Moreover, space-time-frequency shift keying (STFSK) amalgamates STSK and SFSK. The information bits are modulated by M-QAM/PSK, F-FSK, and the index of active DM.

To exploit the robustness of OFDM against the frequency-selective channels, STSK has been combined with OFDM, and named OFDM-STSK [138]. Before the conventional OFDM transmission, $J = N_{sc}/T$ STSK blocks of size $N_t \times T$ are concatenated, where it is assumed that N_{sc} is the multiple of T. Thereafter, IFFT is applied, followed by CP addition. In other words, STSK block are modulated by OFDM. In this way, each column of the STSK block is transmitted by a subcarrier, corresponds to the frequency-flat channel. The transmission rate of STSK and OFDM-STSK is equal, given that $N_{sc} \gg N_{cp}$. Different from the SFSK in [137], OFDM-based SFSK (OFDM-SFSK) approach is proposed in [139], where the data symbol is spread over space and frequency dimensions. Indeed, OFDM-SFSK and OFDM-STSK follow the same idea of achieving robustness against time-varying OFDM channels. Differently, DMs in OFDM-SFSK are generated by the circular shifting of sparse vectors that also provides robustness against ICI for OFDM systems. In [174], the layered multi-group steered STSK (LMG-SSTSK) is proposed for multi-user MIMO downlink systems by combining OFDM, STSK, and Tx beamforming. Moreover, differential SM (DSM) avoids heavy channel estimation by differentially encoding two successive data blocks at Tx [115]. For this purpose, DSM exploits the time domain along with the space domain through block-based transmission as in STSK. In DSM, it is assumed that $T = N_t$. Each column of $\mathbf{X}$ corresponds to a transmission interval in which a single antenna is activated.

5.2.2.2 Space & Frequency Domain IM

Two transmit entities, i.e., antennas and subcarriers are used simultaneously to carry the information. Incoming bits are divided into three parts for antenna indexing, subcarrier indexing, and conventional M-ary modulation [118, 119, 175]. SM-OFDM with subcarrier index modulation (ISM-OFDM) is proposed to alleviate the ICI impact for vehicle-to-everything (V2X) communication [118]. Since a single antenna is activated at each transmission interval, the transmission rate of ISM-OFDM considering (5.4) and (5.9) equals

$$\eta = \frac{N_G}{N_{sc}+N_{cp}-1}\Bigg(\lfloor \log_2 N_t \rfloor + \lfloor \log_2 \binom{N_b}{N_a} \rfloor + \log_2(M)\Bigg) \text{ [bpcu]}. \tag{5.15}$$

Instead of the conventional SM, generalized space-frequency IM (GSFIM) combines OFDM-IM with MA-SM in order to activate multiple Tx antennas and subcarriers at each transmission interval [119]. Regarding (5.6) and (5.9), the achieved rate by GSFIM corresponds to the total number of transmitted bits by OFDM-IM and MA-SM. Moreover, GSFIM has been evaluated in the context of GFDM, named GFDM with SFIM (GFDM-SFIM) that provides higher SE than GSFIM for a given BER performance [120].

5.2.2.3 Space & Time Domain IM

Simultaneous indexing of the transmission entities in both space and time is evaluated in [123, 124]. Considering the time slots, Tx antennas and RF mirrors as separate units, two different space& time domain IM schemes are presented: time-indexed SM (TI-SM) and time-indexed MBM (TI-MBM).

In TI-SM, Tx is equipped with N_t antennas and one RF chain, while Rx contains N_r antennas. As in (5.11), the active symbols for SC-IM are chosen by $\lfloor \log_2 \binom{K_b}{K_a} \rfloor$ bits. Then, $K_a \log_2(N_t)$ bits corresponding to (5.4) decide the active Tx antenna. TI-MBM only requires a single Tx antenna supported by N_{rf} RF mirrors. MBM is applied to transmit the additional bits, instead of SM. Hence, considering (5.13), The number of information bits conveyed by TI-MBM equals the total number of information bits carried by both SC-IM and MBM.

5.2.2.4 Space & Channel Domain IM

SM with MBM (SM-MBM) and quadrature channel modulation (QCM) are employed through the combination of MBM with SM and QSM, respectively

[123, 176]. Basically, SM-MBM and QCM perform transmission through indexing both Tx antennas and RF mirrors. Therefore, N_t antennas are equipped with N_{rf} RF mirrors at Tx. The transmission rate of SM-MBM corresponds to $\eta = \log_2(N_t) + N_{rf} + \log_2(M)$ [bpcu]. Considering the QSM principles, QCM transmists $\eta = 2\log_2(N_t) + N_{rf} + \log_2(M)$ [bpcu].

5.2.2.5 Space & Code Domain IM

A novel MIMO transmission scheme is developed based on IM in space and code domains [128]. The transmission rate of CIM with SM (CIM-SM) is given by

$$\eta = \frac{1}{N_{ct}}\left[2\lfloor \log_2 N_{ct} \rfloor + \log_2\left(N_t\right) + 2\log_2\left(M\right)\right] \text{ [bpcu]}, \tag{5.16}$$

which corresponds to the total number of bits conveyed by CIM and SM. Firstly, the Rx process of CIM is employed, followed by ML detector to decide the utilized antenna and the transmitted data symbols.

5.2.2.6 Space & Polarization Domain IM

In [177], space-polarization shift keying (SPSK) is introduced via the utilization of dual-polarized antennas. Besides the active antenna, the utilized polarization type also carries information bits. Moreover, SM and PM are combined in SM with dual-polarized antennas (DP-SM) to avoid the spatial correlation in SM-MIMO systems [178, 179]. As a result, the achievable SE is also increased since the space limitation in SM-MIMO systems due to the required distance between the adjacent antennas is alleviated.

5.2.2.7 Code & Frequency Domain IM

Joint code-frequency index modulation (CFIM) is presented in [180] by simultaneous indexing in frequency and code domains in order to support multi-user communication with low-power consumption.

5.2.3 Three-Dimensional IM

Three-dimensional IM types are the enhanced IM types that would serve diverse requirements of 5G and beyond networks. The existing three-dimensional IM types are the combinations of space & DMs, frequency & DMs, and time & space & frequency domains, as given in Fig.5.4.

5.2.3.1 Space & Dispersion Matrices-based IM

The conventional STSK uses all of the available N_t Tx antennas for a transmission. In order to enhance the system reliability, partial antenna activation for the transmission of STSK block is presented in multi-set STSK (MS-STSK) [132]. Moreover, the columns of the STSK block corresponding to different time intervals are multiplied by different phase shifts for reducing the correlation amongst the transmissions. In [181], joint alphabet STSK (JA-STSK) and joint-alphabet MS-STSK (JA-MS-STSK) are performed by using a joint alphabet that corresponds to the utilization of different DMs and antenna combinations over multiple time slots for increasing the throughput gain of the STSK systems. In [182], a generalized framework that can accommodate all DM-based IM techniques is introduced and named layered multi-set GSTSK (LMS-GSTSK). Specifically, LDC, BLAST, SM, GSM, QSM, SSK, GSTSK, and MS-STSK can be implemented by the proper adjustment of LMS-GSTSK's parameters. Indeed, LMS-GSTSK provides adaptive dimensional IM due to its scalable structure.

5.2.3.2 Frequency & Dispersion Matrices-based IM

CS-aided OFDM-STSK with frequency index modulation (OFDM-STSK-IM) is presented for further improving the SE and BER performance of OFDM-STSK [133, 183]. At first, incoming m bits are divided into N_G groups, and each group

Table 5.3: IM techniques with the aid of dimension(s) exploitation

IM Techniques	Exploited Domain(s)				IM Domain(s)					IM Type
	Space	Time	Freq.	I/Q	Space	Time	Freq.	Code	Chan.	
QSM[1] [114]				✓	✓					1 Dim.
STBC-SM [114]	✓	✓			✓					1 Dim.
ST-QSM [147]	✓	✓		✓	✓					1 Dim.
OFDM-I/Q-IM [121]				✓			✓			1 Dim.
IM-OFDM-SS [163]			✓					✓		1 Dim.
STCM [167]	✓	✓							✓	1 Dim.
ST-MBM [168]	✓	✓							✓	1 Dim.
SFSK [137]			✓		✓	✓				2 Dim.
STFSK [137]			✓		✓	✓				2 Dim.
OFDM-STSK [138]			✓		✓	✓				2 Dim.
OFDM-SFSK [139]			✓		✓	✓				2 Dim.

[1]It is also valid for QSM-based IM techniques, such as QCM and GPQSM.

contains $\lfloor \log_2 \binom{N_b}{N_a} \rfloor$ and $\log_2(QM)$ bits to activate N_a subcarriers and select a DM, respectively. Then, coordinate interleaved STSK blocks are mapped to active N_a subcarriers. A virtual domain with N_v subcarriers is introduced by CS for transmitting additional energy-free $\lfloor \log_2 \binom{N_v}{N_a} \rfloor$ bits per subblock, given that $N_v \gg N_b$. At Rx, the signal is first compressed from the virtual domain to the frequency domain and then ML detector is utilized to obtain the transmitted bits. In [184], generalized space, time, and frequency index modulation (GSTFIM) combines GSTSK with OFDM-IM to achieve higher SE for STSK systems.

5.2.3.3 Space & Time & Channel Domain IM

In [124], Time-indexed SM with MBM (TI-SM-MBM) allows joint utilization of SC-IM, SM, and MBM for the purpose of increasing SE. Accordingly, the achieved SE by TI-SM-MBM equals the summation of each individual data rate.

5.2.4 Hyper-Dimensional IM

Hyper-dimensional IM types are relatively less investigated in the literature

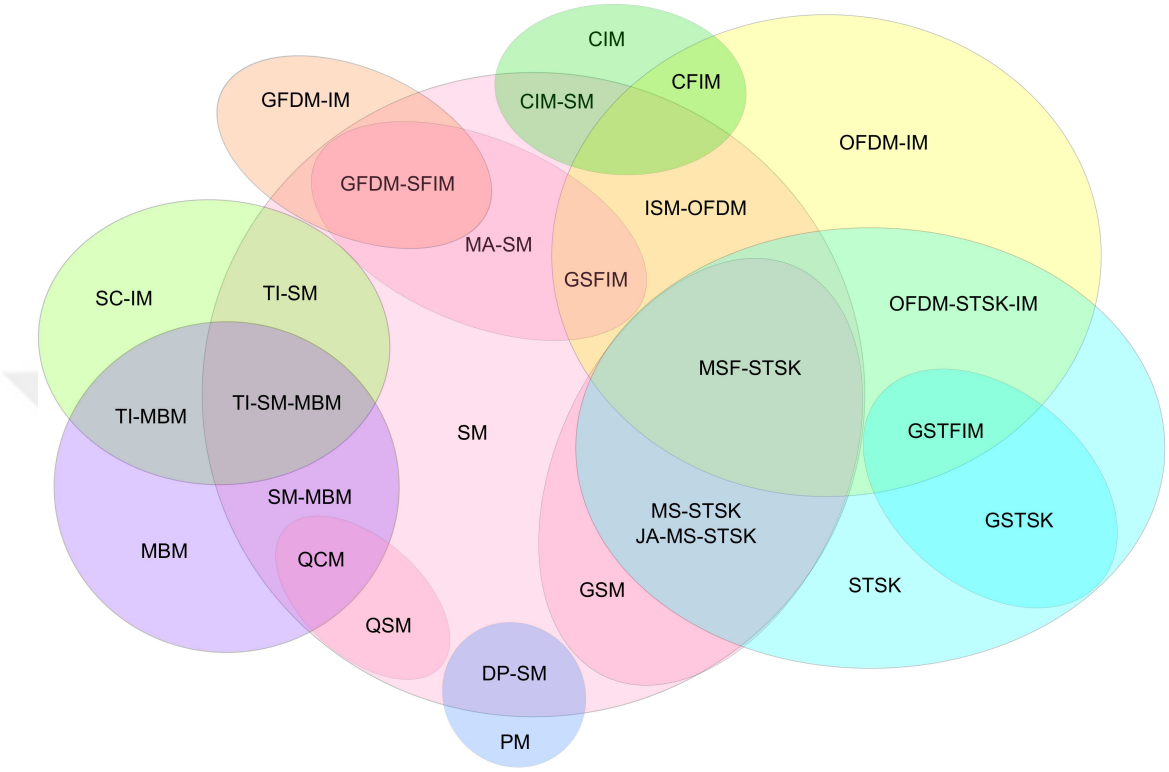


Figure 5.5: Corresponding fundamental IM variants for the existing multidimensional IM schemes.

when compared to the lower-dimensional IM types due to their complex structure, as shown in Fig. 5.4.

5.2.4.1 Space & Frequency & Dispersion Matrices-based IM

Multi-space-frequency STSK (MSF-STSK) combines OFDM-IM, GSM, and STSK to attain interference immunity and diversity gain [134]. Besides conventional M-ary symbols, incoming bits are carried by the indices of active DMs in space & time domains, active subcarriers in the frequency domain, and active antennas in the space domain.

Fig. 5.5 illustrates the multidimensional IM techniques and their constituent single domain ones. Since GSM, MA-SM and QSM are the advanced versions of SM, they are shown with the same color. According to Fig. 5.5, one-dimensional IM schemes without intersection regions provide insights about possible novel

multidimensional IM schemes.

Remark 1. *IM schemes, such as QSM, STBC-SM, IM-OFDM-SS, SFSK, OFDM-STSK, and OFDM-I/Q-IM, exploit different domain(s) alongside the IM domain(s) in order to serve diverse user demands. To exemplify, STBC-SM exploits space and time dimensions for the purpose of achieving transmit diversity gain for SM systems. In the same vein, OFDM-STSK utilizes the frequency domain aiming to overcome the ISI encountered in STSK transmission, while IM is applied in space and time domains. On the other hand, QSM and OFDM-I/Q-IM utilize I and Q dimensions for enhancing the SE of OFDM-IM systems. Therefore, these IM techniques are categorized considering the number of domains in which IM is employed. Table 5.3 illustrates the IM techniques that provide dimension(s) exploitation to alleviate the shortcomings of a particular IM type.*

5.3 Appropriate IM techniques for Next Generation Services

Although the variety of IM types promises appealing trade-offs amongst SE, EE, BER, and flexibility, the integration of diverse IM techniques into the current communication systems bring different challenges for the Tx and Rx sides of modern communication systems due to the requirement of numerous hardware design and signal processing techniques. In this section, promising IM types are subsumed considering the requirements of eMBB, mMTC, and URLLC. Thereafter, the advantages and disadvantages of a given IM domain are quantified for establishing a clear distinction between them, and its fidelity is evaluated in terms of practical implementation.

Table 5.4: Data rate and computational complexity assessment of space domain IM techniques

IM Techniques	**# RF Chain (N_{rc})**	**Data Rate** [bpcu]	**Processing Complexity at Rx**
SM [109]	1	$\log_2(N_t) + \log_2(M)$	MRC $\rightarrow 2N_rN_t - N_t$ Opt. $\rightarrow N_tM(3N_r+1)$
GSM [110]	$1 \leq N_{rc} = N_k < N_t$	$\lfloor \log_2 \binom{N_t}{N_k} \rfloor + \log_2(M)$	ML $\rightarrow N_r 2^{\lfloor \log_2 \binom{N_t}{N_k} \rfloor} M(N_k+2)$
MA-SM [111]	$1 \leq N_{rc} = N_k < N_t$	$\lfloor \log_2 \binom{N_t}{N_k} \rfloor + N_k \log_2(M)$	ML $\rightarrow N_r 2^{\lfloor \log_2 \binom{N_t}{N_k} \rfloor} M^{N_k}$ (N_k+2) LC $\rightarrow (2N_k^3 + 3N_k^2 - 5N_k)/6$ $+N_rN_k(2N_k+1)$
QSM[1] [110, 144]	1	$\log_2(N_t^2) + \log_2(M)$	ML $\rightarrow 4N_rN_t^2M$ LC $\rightarrow 4N_t^3 + 4N_{MPA}^2MN_r$
ESM[2] [113]	1, 2	$\lfloor \log_2 \left(\binom{N_t}{N_{k_1}} + \binom{N_t}{N_{k_2}} + \binom{N_t}{N_{k_3}} \right) \rfloor +$ $+ \log_2(M_1)$	ML $\rightarrow \binom{N_t}{N_{k_1}} M_1^{N_{k_1}} \binom{N_t}{N_{k_2}} M_2{}^{N_{k_2}}$ $+\binom{N_t}{N_{k_3}} M_3{}^{N_{k_3}}$
TCSM [145]	1	$\frac{1}{R}(\log_2(N_t) + \log_2(M))$, ($R$ = Code Rate)	Opt. $\rightarrow N_tM(3N_r+1)$
TC-QSM [146]	1	$\frac{1}{R}(\log_2(N_t^2) + \log_2(M))$	LC $\rightarrow 4N_t^3 + 4N_{MPA}^2MN_r$
STBC-SM [114]	2	$\frac{1}{2}\lfloor \log_2 \binom{N_t}{N_k} \rfloor + \log_2(M), (N_k = 2)$	ML $\rightarrow 2^{\lfloor \log_2 \binom{N_t}{2} \rfloor} M^2$ LC $\rightarrow 2^{\lfloor \log_2 \binom{N_t}{2} \rfloor} M$
ST-QSM [147, 148]	$2 \leq N_{rc} < N_t$	$\log_2(N_{t1}) + \log_2(N_{t2}) + \log_2(M)$	ML $\rightarrow M^2 2^{\lfloor \log_2(N_{t1}) \rfloor}$ $+M^2 2^{\lfloor \log_2(N_{t2}) \rfloor}$
PSM [150]	1	$\log_2(N_r) + \log_2(M)$	ML $\rightarrow N_rM$
GPSM [151]	$1 \leq N_{rc} = N_k < N_t$	$\lfloor \log_2 \binom{N_r}{N_k} \rfloor + N_k \log_2(M)$	ML $\rightarrow 2^{\lfloor \log_2 \binom{N_r}{N_k} \rfloor} M^{N_k}$ LC $\rightarrow N_r + 3N_kM + M$
GPQSM [152]	$1 \leq N_{rc} = N_k < N_t$	$2\lfloor \log_2 \binom{N_r}{N_k} \rfloor + N_k \log_2(M)$	ML $\rightarrow 2^{2\lfloor \log_2 \binom{N_r}{N_k} \rfloor} M^{N_k}$ LC $\rightarrow 10N_r + 3N_rM + M$

[1] N_{MPA} corresponds to the number of the most probable active antenna indices ($2 \leq N_{MPA} < N_t$).
[2] The generalization of the computational complexity for ESM is not possible due to the variable number of antenna combinations. Here, the complexity calculation is given in order to achieve the same data rate (8 [bpcu]) with SM ($M = 64QAM, N_t = 4, N_r = N_r$). Thus, $\mathcal{S}_1, \mathcal{S}_2$, and $\mathcal{S}_3$ are used with the size of $M_1 = 16$, and $M_2 = M_3 = 4$, respectively, while $N_{k_1} = 1$, and $N_{k_2} = N_{k_3} = 2N_{k_1} = 2$.

Table 5.5: Data rate and computational complexity assessment of frequency domain IM techniques

IM Techniques	**# Act. Subcarriers (N_a)**	**Data Rate** [bpcu]	**Comp. Complexity at Rx**
OFDM-IM [24]	$1 \leq N_a < N_b$	$N_G\big(\lfloor \log_2 \binom{N_b}{N_a} \rfloor + N_a \log_2(M)\big)$	ML $\rightarrow N_G 2^{\lfloor \log_2 \binom{N_b}{N_a} \rfloor} M^{N_a}$ LLR $\rightarrow N_G N_b M$
OFDM-ISIM [27]	$1 \leq N_a < N_b$	$N_G\big(\lfloor \log_2 \binom{N_b}{N_a} \rfloor + N_a \log_2(M)\big)$	ML $\rightarrow N_G 2^{\lfloor \log_2 \binom{N_b}{N_a} \rfloor} M^{N_a}$ LLR $\rightarrow N_G N_b M$
CI-OFDM-IM [31]	$1 \leq N_a < N_b$	$N_G\big(\lfloor \log_2 \binom{N_b}{N_a} \rfloor + N_a \log_2(M)\big)$	ML $\rightarrow N_G 2^{\lfloor \log_2 \binom{N_b}{N_a} \rfloor} M^{N_a}$ LLR $\rightarrow N_G N_b M$
OFDM-GIM[1] [121]	$1 \leq N_{a_\psi} < N_b$	$\sum_{\psi=1}^{\Psi} N_{G_\psi}\big(\lfloor \log_2 \binom{N_b}{N_{a_\psi}} \rfloor + N_{a_\psi} \log_2(M)\big)$	ML $\rightarrow \sum_{\psi=1}^{\Psi} N_{G_\psi} 2^{\lfloor \log_2 \binom{N_b}{N_{a_\psi}} \rfloor} M^{N_{a_\psi}}$ LLR $\rightarrow \sum_{\psi=1}^{\Psi} N_G N_b M$
OFDM-I/Q-IM [121]	$1 \leq N_a < N_b$	$2N_G\big(\lfloor \log_2 \binom{N_b}{N_a} \rfloor + N_a \log_2(M)\big)$	ML $\rightarrow 4N_G 2^{\lfloor \log_2 \binom{N_b}{N_a} \rfloor} M^{N_a}$ LLR $\rightarrow 4N_G N_b M$
DM-OFDM [29]	$N_{a_1} = N_{a_1}$, $N_{a_2} = N_b - N_{a_1}$	$N_G\big(\lfloor \log_2 \binom{N_b}{N_{a_1}} \rfloor + N_{a_1} \log_2(M_1) + (N_b - N_{a_1}) \log_2(M_2)\big)$	ML $\rightarrow N_G 2^{\lfloor \log_2 \binom{N_b}{N_{a_1}} \rfloor} {M_1}^{N_{a_1}} {M_2}^{(N_b - N_{a_1})}$ LLR $\rightarrow N_G N_b (M_1 + M_2)$
MM-OFDM [30]	$N_a = N_b$	$N_G\big(\lfloor \log_2(N_b!) \rfloor + N_b \log_2(M)\big)$	ML $\rightarrow N_G 2^{\lfloor \log_2(N_b!) \rfloor}$ LLR $\rightarrow \frac{N_G N_b M}{2}(N_b + 1)$
GFDM-IM [122]	$1 \leq N_a < N_b$	$TN_G\big(\lfloor \log_2 \binom{N_b}{N_a} \rfloor + N_a \log_2(M)\big)$	ML $\rightarrow TN_G 2^{\lfloor \log_2 \binom{N_b}{N_a} \rfloor} M^{N_a}$
ZTM-OFDM-IM [122]	$N_{a_1} + N_{a_2} = N_a$, $N_a \leq N_b$,	$N_G\Big(N_{a_1} \log_2(M_1) + N_{a_2} \log_2(M_2) \lfloor \log_2 \big(\binom{N_b}{N_a}\binom{N_a}{N_{a_1}}\big) \rfloor \rfloor\Big)$	ML $\rightarrow N_G 2^{\lfloor \log_2 \left(\binom{N_b}{N_a}\binom{N_a}{N_{a_1}}\right) \rfloor} {M_1}^{N_{a_1}} {M_2}^{N_{a_2}}$
L-OFDM-IM [160]	$N_{a_L} < N_{b_L} < N_b^2$	$N_G L\big(\lfloor \log_2 \binom{N_{b_L}}{N_{a_L}} \rfloor + N_{a_L} \log_2(M)\big)$	ML $\rightarrow N_G \big(2^{\lfloor \log_2 \binom{N_{b_L}}{N_{a_L}} \rfloor} M^{N_{a_L}}\big)^L$ LC $\rightarrow N_G \sum_{\psi=1}^{L} M(N_{b_L} + N_{a_L}(\psi - 1))$

[1] Ψ is the size of the allowed number of different subcarriers within an OFDM-IM block.

[2] $N_b = N_{b_L} + N_{a_L}(L-1)$

Table 5.6: Data rate and computational complexity assessment of time, code, and channel domain IM techniques

IM Techniques	**# Active Symbols (K_a)**	**Data Rate** [bpcu]	**Comp. Complexity at Rx**
SC-IM [125]	$1 \leq K_a < K_b$	$K_G(\lfloor \log_2 \binom{K_b}{K_a} \rfloor + K_a \log_2(M))$	ML $\rightarrow K_G 2^{\lfloor \log_2 \binom{K_b}{K_a} \rfloor} M^{K_a}$ LLR $\rightarrow K_G K_b M$
FTN-IM [126]	$1 \leq K_a < K_b$	$K_G(\lfloor \log_2 \binom{K_b}{K_a} \rfloor + K_a \log_2(M))$	ML $\rightarrow K_G 2^{\lfloor \log_2 \binom{K_b}{K_a} \rfloor} M^{K_a}$ LLR $\rightarrow K_G K_b M$

IM Techniques	**# Active Codes (N_{ac})**	**Data Rate** [bpcu]	**Comp. Complexity at Rx**
CIM-SS [129]	$N_{ac} = 1, N_{ct} = 2$	$2\lfloor \log_2(N_{ct}) \rfloor + \log_2(M) =$ $2 + \log_2(M)$	ML $\rightarrow 2N_{ct}M$ LC $\rightarrow 2N_{ct} + M$
GCIM-SS [130]	$N_{ac} = 1, 2 \leq N_{ct}$	$2\lfloor \log_2(N_{ct}) \rfloor + \log_2(M)$	ML $\rightarrow 2N_{ct}M$ LC $\rightarrow 2N_{ct} + M$
IM-OFDM-SS [131]	$N_{ac} = 1, 2 \leq N_{ct}$	$2\lfloor \log_2(N_{ct}) \rfloor + \log_2(M)$	ML $\rightarrow 2N_{ct}M$ LC $\rightarrow 2N_{ct} + M$

IM Techniques	**# Active RF Mirrors (N_{am})**	**Data Rate** [bpcu]	**Comp. Complexity at Rx**
MBM [116]	$N_{am} = 1$	$N_{rf} + \log_2(M)$	ML $\rightarrow N_r 2^{N_{rf}} M, N_t = 1$
STCM [167]	$N_{am} = 1$	$2N_{rf} + 2\log_2(M)$	ML $\rightarrow 4N_r 2^{2N_{rf}} M^2, N_t = 2$ LC $\rightarrow 4N_r 2^{2N_{rf}} M$

5.3.1 Enabling IM Techniques for Next-Generation Services

The presented IM techniques in Section 5.2 are categorized considering the requirements of three main services.

5.3.1.1 eMBB

The crucial requirement for eMBB is the efficient spectrum utilization, as explained in Section 2.1.1. Therefore, the IM schemes are assessed according to their SE performance. Table 5.4, 5.5, and 5.6 present the data-rate and the computational complexity assessment of space, frequency, time, code and channel domains. The computational complexity at Rx is provided for both available low-complex (LC) and ML detectors, and is calculated in terms of complex multiplications. It is readily seen that one-dimensional main IM types in space, frequency, time, code, and polarization domains lead to a decrease in SE due to both the partial transmission and the logarithmic increase on SE with the number of active information-bearing entities. Additionally, in comparison to conventional schemes, the reduction in SE becomes suddenly high in the case of high-order modulation usage. To exemplify, OFDM-IM with ($N_b = 8$, $N_a = 4$) corresponds to $2^{\lfloor \log_2 \binom{8}{4} \rfloor} = 64$ legitimate subcarrier combinations that enable the transmission of maximum number of bits through the subcarriers' indices, i.e., IM bits, for $N_b = 8$. However, it results in %12 and %32 SE loss for $M = 4$ and $M = 16$, respectively with respect to OFDM. Hence, these types of IM require an additional mechanism that allows the transmission with a higher number of M-ary symbols in support of eMBB application and use-cases.

GSM increases the number of IM bits, from $\log_2(N_t)$ to $\lfloor \log_2 \binom{N_t}{N_a} \rfloor$, but the number of M-ary symbols remains the same and equals one [35]. Therefore, it offers a moderate improvement in SE with the assistance of multiple antenna activation. As given in Table 5.4, MA-SM achieves higher SE than GSM via

transmitting different data symbols through these activated antennas at the expense of lower BER, which is not a primary concern for eMBB communication. It can be seen in Table 5.4 that QSM and its advanced versions provide increment only for IM bits. ESM enables the transmission of the data bits by both the active antennas' indices and the constellation type. On the other hand, achieving higher data rates with SM-based IM types is challenging in microwave frequency bands, since incorporating a higher number of Tx antennas becomes infeasible for both BS and UEs because of the required distance ($\frac{\lambda}{2}$) between the consecutive antennas. In the light of these considerations, the fundamental types of space domain IM are far from satisfying the requirements of eMBB use-cases.

DM-SCIM provides a higher data rate than the classical SC-IM by modulating the inactive data symbols with different modulation types. Although DM-SCIM improves the SE of SC-IM types as given in Table 5.6, its counterpart in the frequency domain, i.e., DM-OFDM, is superior to DM-SCIM owing to flexible resource allocation. ZTM-OFDM-IM combines OFDM-IM and DM-OFDM in order to boost the SE of OFDM-IM systems. As seen in Table 5.5, it provides a significant improvement in the number of information bits carried by the indices, but it poses a limit for competing with conventional schemes under high-order modulation conditions. MM-OFDM enables not only the modulation of all subcarriers by using multiple QAM/PSK sets but also the utilization of permutations of subcarriers' combinations. In other words, DM-OFDM and MM-OFDM activate all the subcarriers as in conventional OFDM and transmit IM bits as well. The number of legitimate subcarrier combinations is increased from $\lfloor \log_2 (N_b) \rfloor$ to $\lfloor \log_2 (N_b!) \rfloor$ by MM-OFDM-IM. OFDM-GIM provides a degree of freedom to control the number of IM bits and M-ary symbols adaptively. Thus, it supports both OFDM-IM and OFDM transmissions. In other words, L-OFDM-IM facilitates the improvement in both IM bits and M-ary symbols at the cost of the exponential increase in the processing complexity with L, as given in Table 5.5.

The SE of MBM linearly increases with the number of RF mirrors. Due to the linear increase in SE with N_{rf}, SM-MBM and TI-MBM provide higher data rates compared to TI-SM. TI-SM and TI-MBM need to utilize higher modulation orders than SM-MBM for the sake of achieving the same SE. However, the use of higher

modulation orders leads to degradation of the BER performance of TI-SM and TI-MBM. However, a high number of RF mirrors leads to high training overhead to estimate $2^{N_{rf}}$ channel realizations. Therefore, DMBM can be a candidate solution to satisfy the demand of high SE, since it removes the channel estimation at Rx, which is the UE in downlink transmission. On the other hand, receiver SM provides opportunities in downlink transmission for both reducing cost and increasing the EE at the UE side. GPSM can support the same throughput as conventional MIMO systems with the same processing complexity at Rx side [151, 185, 186].

Multidimensional IM types are more appealing for the purpose of fulfilling the requirements of eMBB service. GSFIM performs transmission through antenna indices, subcarrier indices, and M-ary symbols. Also, conventional MIMO-OFDM corresponds to the special case of GSFIM. It is shown that %20 rate gain can be achieved by GSFIM under the conditions of ($N_t = 32$, $N_r = 32$ and $M = 4$). In this regard, its advanced version GSTFIM can also be considered for eMBB use-cases. Additionally, current OFDM technology is one of the promising solutions for eMBB applications and use-cases. However, OFDM suffers from ICI in case of high mobility scenarios. To provide eMBB communications for the high mobility classes defined in Table 3.2, instead of the conventional OFDM, ISM-OFDM can alleviate the effect of ICI without compromising the SE.

Remark 2. *Amongst one-dimensional IM types, frequency domain IM types can compete with the conventional OFDM in terms of SE due to its flexible structure. The advanced versions of OFDM-IM, such as DM-OFDM, MM-OFDM, L-OFDM, are conducive to support eMBB service, even if high-order modulation types are considered. Space domain IM types are easily defeated by conventional SMX schemes due to not only the logarithmic increase with N_T but also the transmission of a limited number of M-ary symbols. In order to overcome this limitation, MBM is deemed to be promising, but it leads to the monumental complexity at Rx side, which can not be handled by UE in downlink transmission.*

Table 5.7: The comparison of space and channel domain IM techniques

IM Tech.	**Pros**	**Cons**	Performance Metrics						
			1	2	3	4	5	6	7
SM [109]	Single antenna activation, use of one RF chain at Tx, IAI free transmission	Logarithmic increase on SE with N_t, limited data rate	↓	↑	↓	↓	↓	↓	↑
GSM [110]	Multiple antenna activation to transmit the same data symbol, IAI free transmission	Logarithmic increase on SE with N_t, limited data rate, requirement of multiple RF chains and IAS at Tx	↓	↑	↑	↓	↓	↓	↑
MA-SM [111]	Multiple antenna activation to transmit the different data symbols, higher SE than SM/GSM	Logarithmic increase on SE with N_t, requirement of multiple RF chains and IAS at Tx, complex Rx process	↑	↑	↑	↑	↓	↑	↓
QSM [112]	Activation of two Tx antennas to transmit in-phase and quadrature parts of a complex symbol, exploiting spatial selectivity	Logarithmic increase on SE with N_t	↑	↑	↓	↓	↓	↓	↑
ESM [113]	Activation of a single and two Tx antennas for high order and low order modulations, increased Euclidean distance	Requirement of multiple RF chains and IAS at Tx, complex Rx process	↑	↑	↑	↑	↓	↑	↓
STBC-SM [113]	Use of two RF chains at Tx, achieving diversity and coding gains	Limited data rate	↓	↑	↓	↓	↑	↑	↑
MBM [116]	Linear increase on SE with N_{rf}, robustness against channel fading	Estimation of $2^{N_{rf}}$ channel realizations, high training overhead, complex Rx process	↑	↑	↓	↑	↓	↓	↑
DMBM [116]	Avoiding channel estimation at Rx	Increased processing time due to feedback mechanism, an error performance loss	↑	↑	↓	↑	↓	↓	↑

Performance Metrics - 1: SE, 2: EE, 3: Hardware Complexity at Tx, 4: Computational Complexity at Rx, 5: Tx Diversity Gain, 6: Multiplexing Gain, and 7: Interference Immunity
Sign - ↑: High ↓: Low

5.3.1.2 mMTC

Researchers in both academia and industry have been seeking technologies to provide large coverage area, low power consumption and low cost for mMTC services where latency, data rate, and reliability are not primary concerns, as explained in Section 2.1.2. In essence, IM provides high EE owing to the energy-free carried information bits by the indices of the transmit entities. For example, OFDM-IM with ($N_b = 4$ and $N_a = 2$) transmits $p_1 = 2$ bits by the subcarriers' indices and $p_2 = 2$ bits by the modulated subcarriers with binary phase-shift keying (BPSK). However, the classical OFDM requires 4 active subcarriers to transmit $p_1 + p_2 = 4$ bits. Hence, OFDM-IM with ($N_b = 4$ and $N_a = 2$) harvests 50% of the Tx power to transmit the same number of data bits. Utilization of the same Tx power for the OFDM-IM and conventional OFDM significantly extends the coverage area for OFDM-IM. Besides the high EE, hardware and computational complexity originated by IM should be considered for mMTC applications and use-cases. Please note that the SE and complexity of a given IM scheme are dependent on each other. Thus, Table 5.4, 5.5, and 5.6 provide the computational complexity of IM types considering the given SE. For instance, L-OFDM-IM and OFDM-IM offer the same complexity and SE, while $L = 1$.

One-dimensional space domain IM types including SSK and SM significantly reduce the hardware complexity due to the use of a single RF chain at Tx, as given in Table 5.4. In recent studies, it has been also demonstrated that SSK can be implemented even with a simple RF signal generator [166]. In this way, further reduction is achieved at both Tx and Rx sides. Therefore, SSK and SM provide a high EE, low hardware complexity at Tx, and low computational complexity at Rx for MIMO systems. Due to the increased antenna combinations, GSM and MA-SM require multiple RF chain activation and IAS at Tx and leads to the more complex Rx than that of SM.

The EE and computational complexity of frequency domain IM variants is dependent on the block size, the subblock size and the number of active subcarriers. Mainly, the ML detector is used for the detection of information bits carried by

Table 5.8: The comparison of frequency, time and code domain IM techniques

IM Techniques	**Pros**	**Cons**	Performance Metrics				
			1	2	3	4	5
OFDM-IM [24]	Robustness against ICI, hardware impairments including CFO and IQI	Lower SE than conventional OFDM for high-order modulations	↓	↑	↓	↓	↑
OFDM-ISIM [27]	Exploiting frequency diversity with the aid of interleaving, reliable transmission	Lower SE than conventional OFDM for high-order modulations	↓	↑	↓	↓	↑
CI-OFDM-IM [31]	Transmission of in-phase and quadrature parts of a symbol by different subcarriers, exploiting the real frequency diversity, reliable transmission	Lower SE than conventional OFDM for high-order modulations	↓	↑	↓	↓	↑
OFDM-GIM [121]	Allowing different number of active subcarriers for different subblocks, higher SE than OFDM-IM	Two-stage Rx process, error propagation, sensitivity to hardware impairments	↑	↓	↑	↑	↓
DM-OFDM [29]	Use of two different modulation schemes within a subblock, higher SE than OFDM-IM	Sensitivity to hardware impairments	↑	↓	↓	↓	↓
GFDM-IM [122]	Relaxed time and frequency synchronization	Complex Rx process	↑	↑	↓	↑	↑
SC-IM [125]	Robustness against ISI	Higher PAPR than conventional SC due to inherent sparsity	↓	↑	↓	↓	↑
CIM-SS [129]	Higher SE compared to DS-SS with lower energy consumption	Logarithmic increase on SE with N_c, complex Rx process	↓	↑	↓	↑	↑

Performance Metrics - 1: SE, 2: EE, 3: Computational Complexity at Tx, 4: Computational Complexity at Rx, and 5: Interference Immunity
Sign - ↑: High ↓: Low

the indices of active subcarriers and M-ary symbols. SIM-OFDM suffers from a complex Rx due to the block-based ML detection [54]. For example, in order to activate a quarter of the subcarriers in SIM-OFDM systems, ML detector should search over $2^{\lfloor \log_2 \binom{128}{32} \rfloor} = 2^{100}$ subcarrier combinations to find the correct active subcarriers for (N_{sc}= 128, $N_a = 32$). Thus, OFDM-IM divides the OFDM block into the subblocks to reduce the number of possible combinations for the ML detector. However, a larger subblock size still causes a higher complexity at Rx. Hence, OFDM-IM with the LLR detector is proposed in the literature. For OFDM-IM with ($N_{sc} = 128$, $N_b = 8$, $N_a = 2$, $M = 2$), LLR detector reduces the computational complexity four times than that of ML detector, as given in Table 5.5. Amongst one-dimensional IM types, spectral-efficient schemes such as DM-OFDM, MM-OFDM, L-OFDM-IM, and ZTM-OFDM-IM lead to the increased processing complexity at Rx. Due to the adaptive number of subcarrier activation, OFDM-GIM loses the inherent advantages of IM including EE and reliability. In fact, the achieved EE is limited due to the activation of the majority of existing subcarriers, i.e., $N_b/N_a \simeq 1$. In OFDM-IM, the obtained N_b/N_a power can be utilized for achieving a higher BER performance by increasing the power per subcarrier or can be harvested for achieving a higher EE by keeping the power per subcarrier as in OFDM. In [8], the power level is utilized to provide robustness against IUI in asynchronous mMTC networks, where the sporadic nature of mMTC originates time offset between the UEs and destroys the orthogonality among them. To satisfy the requirements of NB-IoT given in Table 3.2, the use of direct conversion Rx is proposed for the NB-IoT devices due to its simple structure [187]. However, the direct conversion causes in-phase and quadrature imbalance (IQI), and severely degrades the performance of the conventional OFDM. In [11], it is shown that the presence of inactive subcarriers in OFDM-IM allows easy estimation and compensation of the IQI.

For UL transmission, SC-IM provides higher EE than the conventional SC due to the transmission of additional informationbits through IM [188]. However, the inherent sparsity in the time domain leads to higher PAPR than that of classical SC. Multidimensional IM types have the complex transceiver structure for the

Table 5.9: The comparison of multidimensional IM techniques

IM Techniques	**Pros**	**Cons**	Performance Metrics						
			1	2	3	4	5	6	7
ISM-OFDM [118]	Robustness against IAI and ICI	Logarithmic increase on SE with N_t and N_{sc}	↓	↑	↑	↑	↓	↓	↑
GSFIM [119]	Robustness against ICI, multiple antenna activation to transmit the different data symbols	Logarithmic increase on SE with N_t and N_{sc}, requirement of multiple RF chains and IAS at Tx	↑	↑	↑	↑	↓	↑	↓
GFDM-SFIM [120]	Relaxed time and frequency synchronization	Complex transceiver process	↑	↑	↑	↑	↓	↑	↓
TI-SM [123]	Robustness against IAI and ISI	Limited data rate	↓	↑	↓	↓	↓	↓	↑
SM-MBM [123]	Robustness against IAI, linear increase on SE with N_{rf}	Estimation of $2^{N_{rf}}$ channel realizations, high training overhead, complex Rx process	↑	↑	↓	↑	↓	↓	↑
TI-MBM [123]	Robustness against ISI, linear increase on SE with N_{rf}	Estimation of $2^{N_{rf}}$ channel realizations, high training overhead, complex Rx process	↑	↑	↓	↑	↓	↓	↑
TI-SM-MBM [123]	Robustness against ISI and IAI, linear increase on SE with N_{rf}	Estimation of $2^{N_{rf}}$ channel realizations, high training overhead, complex Rx process	↑	↑	↑	↑	↓	↓	↑
CIM-SM [128]	Higher SE than SM	Complex Rx process	↑	↑	↑	↑	↓	↓	↑
DSM [115]	Robustness against IAI, avoiding channel estimation at Rx	Increased processing time due to feedback mechanism	↑	↑	↓	↓	↑	↑	↑
STSK [135]	Providing diversity gain as well as multiplexing gain	Requirement of $N_{rf} = N_t$ RF chains at Tx, complex Rx design, sensitivity to ISI	↓	↓	↑	↑	↑	↑	↓
OFDM-STSK [132]	Robustness against ISI	Requirement of $N_{rf} = N_t$ RF chains at Tx, complex Rx design	↓	↓	↑	↑	↑	↑	↑
OFDM-SFSK [139]	Robustness against ISI and ICI with the aid of sparse DMs	Requirement of $N_{rf} = N_t$ RF chains at Tx, complex Rx process	↓	↓	↑	↑	↑	↑	↑
OFDM-STSK-IM [133]	Robustness against ISI and ICI, high SE with the aid of CS,	Requirement of $N_{rf} = N_t$ RF chains at Tx, complex Rx process	↑	↓	↑	↑	↑	↑	↑
MS-STSK [132]	Increased SE by partial antenna activation, use of $N_{rf} \leq N_t$ RF chains at Tx	Complex Rx process	↑	↑	↓	↑	↑	↑	↓
MSF-STSK [134]	Robustess against ISI, ICI and IAI, increased SE by partial antenna activation, use of $N_{rf} \leq N_t$ RF chains at Tx	Complex Rx process	↑	↑	↓	↑	↑	↑	↑

Performance Metrics - 1: SE, 2: EE, 3: Hardware and Computational Complexity at Tx, 4: Hardware and Computational Complexity at Rx, 5: Tx Diversity Gain, 6: Multiplexing Gain, and 7: Interference Immunity
Sign - ↑: High ↓: Low

detection of active entities in multiple domains. Thus, among the multidimensional IM techniques, TI-SM, which has a moderate number of active entities in time and space, can be considered for mMTC.

The complexity of Rx in MBM is dependent on the number of RF mirrors, which determines both the SE and the system reliability via CSI estimation accuracy. Hence, it provides a trade-off among SE and complexity while ensuring high EE. The SE of MBM with a low number of RF mirrors is limited, but it significantly reduces the Rx complexity since the number of estimated channel realizations exponentially decreases with N_{rf}. In recent studies, a CS-based detection mechanism with low complexity is proposed at Rx to exploit the inherent sparsity of RF mirrors [189]. Besides, in [190], sparse user activity in mMTC, i.e., the intermittent and sporadic characteristics of mMTC, is exploited to improve the detection performance at Rx.

Remark 3. *One-dimensional space domain IM types can be considered as potential candidates for mMTC service due to low hardware complexity at TX and consequently low power consumption. MBM with a reasonable number of RF mirrors is also appropriate to obtain high EE at the UE side since no CSI is required at Tx. Partial activation in OFDM-IM and SC-IM provides robustness against IUI caused by asynchronous mMTC networks along with the high EE. Additionally, the channel and polarization domain IM types are more appealing when the UE is insufficient to accommodate multiple Tx antennas without spatial correlation between them.*

5.3.1.3 URLLC

As explained in Section 2.1.3, URLLC is the most challenging service due to the simultaneous yet conflicting demands of ultra-reliability and low-latency. In order to achieve the BLER values given in Table 3.2, IM schemes that provide diversity gain, interference immunity, and robustness against hardware impairments, such

as carrier frequency offset (CFO) and IQI, are the promising solutions for URLLC. Achieving high reliability via IM requires sufficient selectivity between the active entities in a given IM domain. Thus, space domain IM techniques require $\frac{\lambda}{2}$ separation distance between Tx antennas to improve the detection performance at Rx. Proper detection of the active antennas provides a high probability for the correct estimation of both the index bits and the M-ary symbols. Otherwise, the system performance severely reduces due to the high correlation between the utilized antennas. GSM enhances the BER performance of the SM by the transmission of the same data over the multiple active antennas. MA-SM requires an advanced Rx design to avoid IAI, which reduces reliability. However, its complex transceiver structure causes a long processing time. QSM exploits the spatial selectivity via the transmission of in-phase and quadrature parts of the complex data symbol separately. Hence, QSM ensures the achievement of a better BER performance than the conventional SMX and SM [112]. Also, STBC-SM, ST-QSM, TCSM, and TCQSM improve the performance of SM by additional diversity and coding gains. In MBM, the correct estimation of the transmitted bits relies on the exact CSI at Rx. Hence, the estimation error in CSI can lead to catastrophic BER performance. Even though DMBM removes the necessity of CSI at Rx, it reduces the system reliability and leads to latency due to the feedback mechanism for the encoding of two consecutive data blocks.

For the sake of supporting the desired reliability, frequency domain IM schemes require the exploitation of frequency diversity via proper mapping of the information bits to the subcarriers. In the conventional OFDM-IM, incoming data bits are directly mapped to the subcarriers within a subblock. Thus, the high correlation between the active subcarriers degrades the detection performance at Rx. Mapping of the data bits to the subcarriers located in different subblocks reduces the correlation between the activated subcarriers and enhances the BER performance. Therefore, OFDM-ISIM and CI-OFDM-IM attain higher reliability than the classical OFDM-IM by means of interleaving. Furthermore, CI-OFDM-IM provides an additional diversity gain with the aid of coordinate interleaving. For a given SE, DM-OFDM can provide better BER performance than OFDM-IM

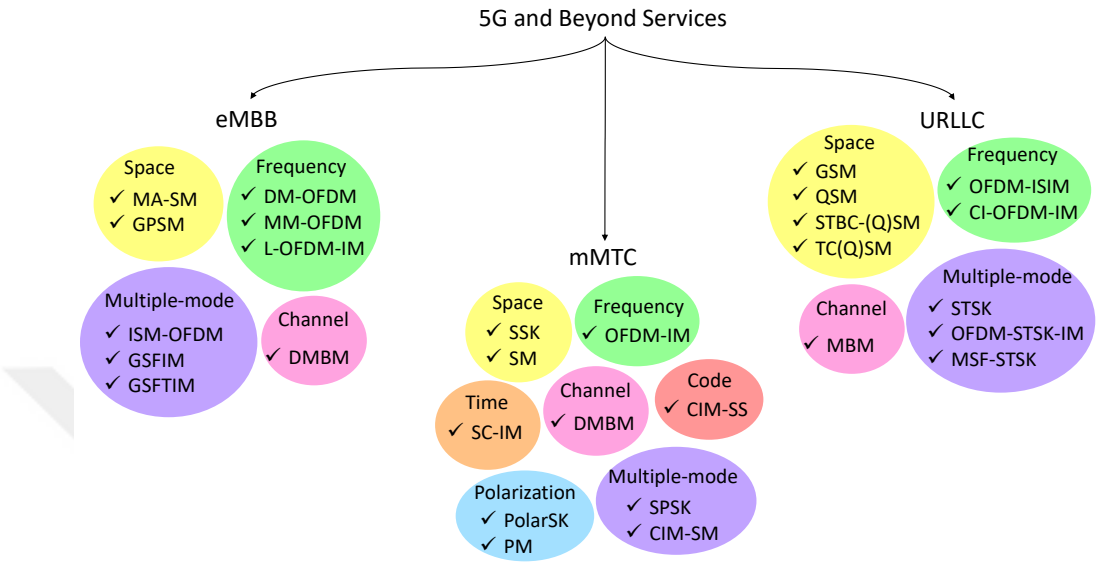


Figure 5.6: Promising IM variants for 5G and beyond services.

by proper selection of the used modulation sets [29]. However, DM-OFDM, MM-OFDM and OFDM-GIM are sensitive to the hardware and channel impairments since there is no idle subcarrier [191]. Due to the non-orthogonal transmission in GFDM-IM, attaining the ultra-reliability becomes a challenge. Moreover, resolving the ICI and ISI at Rx requires a complex Rx design that leads to extra latency. Recently, an interference immune OFDM-IM-based NOMA scheme is proposed in [192] to alleviate the effect of the collisions due to GF access of the URLLC UE.

If wireless channel is time-invariant, the interleaving of data symbols is a necessity for SC-IM to provide ultra-reliability. However, interleaving in the time domain requires storage and thus causes a long latency. Although space domain IM techniques provide multiplexing gain, they suffer from a lack of diversity gain which is of great importance for achieving ultra-reliability. Likewise, conventional SMX and STBC techniques maximize the multiplexing gain and diversity gain, respectively. STSK, which encompasses SMX, STBC, and SM, provides an attractive trade-off among complexity, multiplexing gain, and diversity gain through the spreading a given symbol in space and time dimensions. In this way, it is shown that STSK provides a significant improvement in BER performance [135].

To have robustness against frequency-selective channels, STSK is combined with conventional OFDM through OFDM-STSK. It should be noted that OFDM-STSK performs IM on DMs and exploits the frequency domain to improve system performance. MS-STSK increases the reliability of STSK by combining it with GSM. However, it suffers from ISI under dispersive channels. OFDM-IM and MS-STSK are coupled in MSF-STSK to provide robustness against ISI and ICI. So, DM-based IM types can provide the ultra-reliability by diversity gain, but the duration of the STSK block should be adjusted considering the latency constraint. In [123], it is shown that multidimensional IM schemes provide better BER performance than one-dimensional schemes for the same SE. This is due to a lower number of active entities in a single domain, which corresponds to a reduced correlation between them and consequently better detection performance at Rx. Lastly, in [156], it is shown that RIS-aided IM at Rx can provide up to 15 dB gain in the BER performance compared to the conventional MIMO schemes. Therefore, the RIS-aided IM concept is a promising approach for URLLC, but its usage for URLLC is still an open research area in the literature.

Remark 4. *The direct comparison of IM techniques in terms of BER performance is a difficult task since they should be assessed under the same SE. However, different QAM/PSK sets should be utilized for the achievement of the same SE and thus the performance of given IM type is directly affected. Therefore, IM techniques that can provide diversity gain are more prominent for URLLC. Additionally, frequency domain IM techniques provide the exploitation of frequency selectivity with the aid of interleaving, while conventional OFDM systems require a coding scheme at Tx, that leads to significant complexity at Rx, to further improve the BER performance.*

In view of the above considerations, space, frequency, time, channel, code and multidimensional IM variants are compared in Table 5.7, 5.8 and 5.9 in terms of SE, EE, Tx complexity, Rx complexity, transmit diversity gain, multiplexing gain, and interference immunity. The number of active entities given in Table 5.4, 5.5 and 5.6 determines the interference immunity of a given IM scheme, and also

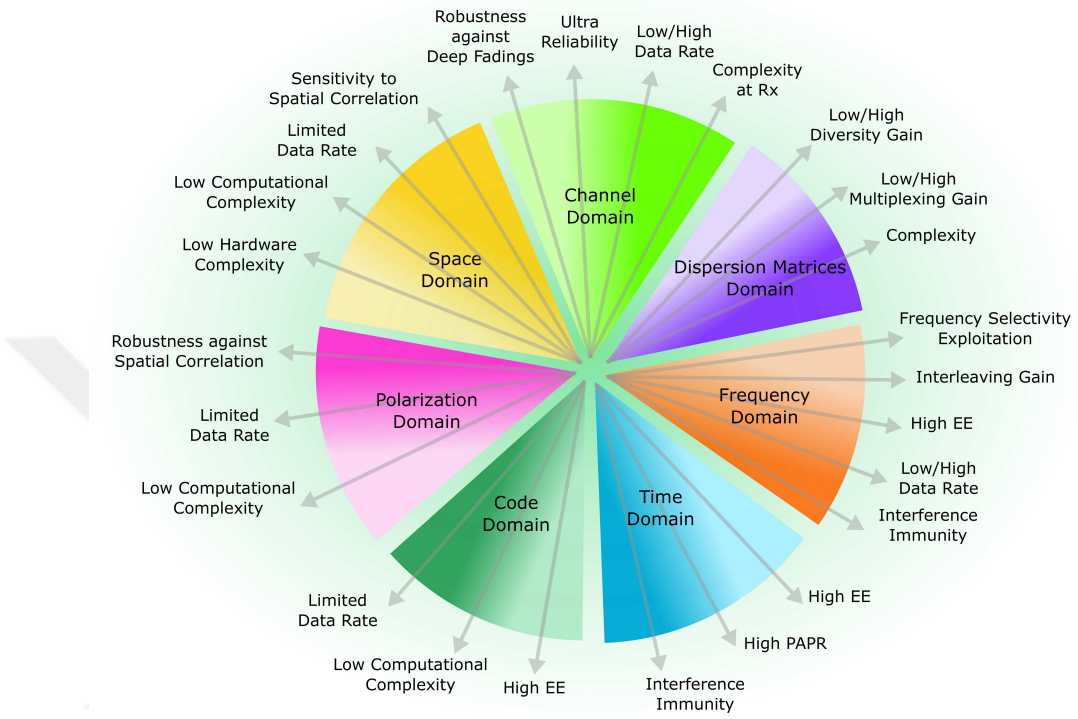


Figure 5.7: The key advantages and disadvantages of the existing IM domains.

defines the hardware complexity at Tx for space domain IM techniques. Lastly, Fig. 5.6 illustrates the categorization of promising IM variants for eMBB, mMTC, and URLLC.

5.3.2 Key Advantages and Disadvantages of Different IM Domains

In modern communication systems, the hardware complexity of the Tx is dependent on the number of used RF chains and antennas. Also, the required channel estimation and detection mechanisms in the Rx lead to additional computational complexity, especially in the presence of a higher number of antennas. The conventional MIMO systems, such as V-BLAST, have a complex structure due to the utilization of all Tx antennas and thus require an advanced Rx design. This structure makes its modification difficult for the diverse demands of 5G and

beyond networks.

In general, space domain IM schemes have similar transmission structure, i.e., the transmitted signals can be expressed in the vector form as in (5.1), (5.2), and (5.3), where ML is commonly utilized at Rx for the detection of active antenna indices and M-ary symbols, as given in Table 5.4. It is worth noting that the complexity of ML detector exponentially increases with N_t, while the achieved SE enhancement is logarithmic. Moreover, a higher number of Tx antennas is required to achieve higher data rates, but it leads to a larger transceiver size and higher power consumption. Therefore, space domain IM types are suitable for low data rates, high EE, and latency-critical transmission where the conventional MIMO technologies suffer. The spatial correlation between Tx antennas hurdles the performance of space domain techniques. In order to overcome this, its combination with polarization and channel domain IM types is promising. Considering the main benefits and shortcomings of space domain IM types given in Table 5.7, GSM, MA-SM, QSM, and ESM can be easily integrated into a given MIMO system for the purpose of meeting a wide range requirements of 5G and beyond.

Frequency, time and code domain IM types do not require additional hardware for practical implementation, as presented in Table 5.8. The complexity of conventional OFDM-IM using the LLR detector is in the same order as that of OFDM in terms of complex multiplications, as given in Table 5.5 [24]. In OFDM-ISIM and CI-OFDM-IM, block-interleaving, corresponding to the multiplication of OFDM block with an interleaving matrix, is easily applied in the frequency domain in order to break the correlation between the active subcarriers. Although DM-OFDM, MM-OFDM, and L-OFDM-IM result in a higher complexity than OFDM-IM, LC detectors are introduced and they can provide higher BER than OFDM due to the exploitation of frequency diversity. In this regard, frequency domain IM variants can easily serve different applications and use-cases with the proper type and parameter selection.

In contrast to the frequency domain, implementation of the interleaving in the time domain requires extra storage and increases the complexity at Tx. On the other hand, high reliability is difficult to achieve without interleaving gain. Thus,

time domain IM types provide a low data rate while maintaining high EE, which is the primary concern for mMTC. In the similar vein, code domain and polar domain IM offers limited data rate, but their combination with space domain IM types is one of the candidate solutions for avoiding spatial correlation between the active antennas, while improving the SE.

Channel domain IM provides a trade-off between ultra-reliability and complexity. The implementation of channel domain IM with the moderate number of RF mirrors is suitable for SIMO systems since the channel estimation at Rx becomes impractical in case of a higher number of RF mirrors.

The major concern for multidimensional IM types is their multi-stage transceiver architecture. Table 5.9 compares the reviewed multidimensional IM types in terms of SE, EE, complexity, transmit diversity gain, multiplexing gain, and interference immunity. Specifically, the complexity of ML detection tremendously increases due to the numerous possibilities of the active entities in different domains. A moderate Rx design can be achieved for ISM-OFDM with a lower number of Rx antennas. Fig. 5.7 summarizes the key advantages and disadvantages of available IM domains. Although multidimensional IM types are proposed for increasing the SE of IM systems, it is important to emphasize that proper combination of one-dimensional IM types can serve different requirements simultenously, as illustrated in Fig. 5.7.

5.4 Potential Challenges and Future Directions

In this section, potential challenges and future perspectives for the integration of IM into beyond 5G technologies are anticipated. Although the research world of academia and industry has shown a substantial and explicit emphasis on the capacity and reliability of IM technologies, its utilization in a flexible manner needs to be fully explored in emerging wireless networks.

5.4.1 Cognitive Radio Network through IM

CR has been heavily studied and considered as an enabling technology for dynamic spectrum access aiming to relax the problem of spectrum scarcity via a shared wireless channel between licensed and unlicensed users, i.e., primary user (PU) and secondary user (SU), respectively, and not to limit radio resources only to the license holders [193–195]. In the literature, three fundamental spectrum access methods named interweave, underlay, and overlay are adopted for CR technology [196]. Basically, SU is asked to sense and determine the possible availability of spectrum in which it can transmit without causing any interruption or endangering the legitimate user. The primary concern in such a system is handling the mutual interference originated by the overlapping of PU and SU. Here IM promises to control the interference through the fractional utilization of the available resources with different activation probabilities and with adaptive transmission power. On this basis, the application of SM in CR is relatively more understood in the literature [197, 198], while the superiority of different IM techniques against conventional schemes used in CR networks remains unknown in the literature. The authors in [199] exploit the space domain to allow CR communications with the improvement of the performance of PU. SU performs a retransmission of the data symbols of PU over conventional M-ary symbols, while its own data are conveyed by the activated antenna indices. In line with this, a novel dual-hop SM technique is proposed in [200], where relay conveys its own information. In recent studies, frequency domain IM is exploited for opportunistic spectrum sharing. In [201], SU senses the inactive subcarriers of PU with OFDM-IM and performs its transmission over these subcarriers. Moreover, the transmission of PU is supported by means of an amplify-and-forward relay in [202]. Flexible utilization of IM in CR reveals that the advantages of IM dominate its shortcomings when it is fully exploited. To exemplify, SE loss for SU becomes negligible as the reliability of PU is preserved or enhanced compared with conventional OFDM based technologies. Lastly, the utilization of different signal dimensions and types will be more prominent for the CR scenarios, where

PU and SU have different priorities. Spectrum sharing between LTE license-assisted access (LTE-LAA) and IEEE 802.11 Wi-Fi systems is an active research area in the literature that can be considered as an example scenario [203, 204]. It can be inferred from the above-mentioned scenarios that the study of IM in CR is at an incipient stage considering its multidimensional application, and there exist a plethora of trade-offs between PU and SU, which need to be exhibited by academia and industry.

5.4.2 Cooperative Networks through IM

Cooperative communication is an alternative enabling approach of exploring spatial diversity, which is achievable via the transmission of data from uncorrelated channels [205]. In other words, the transmitted signal is exposed to various channel fades and consequently reducing the possibility of facing deep fading. In particular, a cooperative user not only transmits its own data but also conveys the data of its corresponding partner, in order to improve diversity gain, coverage area, and data rate. Thus, investigation of mutual interest between cooperative networks and IM has brought a new interest in the literature. A significant reliability gain is achieved from the combination of SM and cooperative networks compared to conventional M-ary modulation [206]. Power allocation strategy is developed for frequency domain IM in cooperative networks to maximize the network capacity [207]. SM-aided cooperative NOMA scheme is investigated in order to provide effective multiple access while ensuring the low complexity and low power consumption [208]. In the same vein, information-bearing units of OFDM-IM, i.e., the utilized subcarriers and their indices, are used to carry the data of both paring users, respectively, in [209]. In this way, IUI is avoided in cooperative-based NOMA, alleviating the receiver complexity at the cost of a reduction in SE. The sparse representation of OFDM-IM is proposed to mitigate and control self-interference at relaying user while performing full-duplex (FD) communication in cooperative systems [210]. Furthermore, in [211], it is shown that the error performance of FD relay with media-based modulation outperforms

classical M-ary constellations due to extra channel diversity under the same SE. As observed from the aforementioned literature, a limited number of studies are available in the literature for the utilization of different IM domains, and a gap exists in the works assessing the performance of multidimensional IM in cooperative networks. Therefore, it is beneficial to give more attention to IM-aided cooperative networks for improving coverage area, cell-edge performance, and data rate under moderate system complexity and power consumption.

5.4.3 Security in/with IM

A doubtless trust is expected in beyond 5G wireless networks such as vehicular communications, health servicing, or other critical data information carriers. However, the broadcast nature of wireless systems makes the privacy and secrecy of these designs suspicious. For this reason, physical layer security (PLS) has emerged as a new powerful alternative that can complement or even replace cryptography-based approaches [212]. Basically, in the literature, the exploitation of channel features and the design of specific transceiver architectures are utilized in order to both provide reliable communication for the desired user and prevent the data detection by unwanted users, i.e., eavesdroppers. Although the possibility of ensuring reliability and security simultaneously has long excited the researchers, the performance of existing IM techniques is not elaborated from the perspective of security as it is ignored during 5G standardizations. Moreover, the mapping of data bits into the information-bearing entities in IM allows a chance to exploit the channel characteristics and consequently achieve the secrecy gap between the desired user and eavesdropper. For instance, in OFDM-IM, channel-based randomization is explored for the mapping of information bits to the entities in order to confuse the eavesdropper [213]. The secrecy gap is increased through the joint decision of modulation type and activation ratio regarding the SNR level at Rx side [214]. In the space domain, secrecy enhancement is offered for the data carried by antenna indices and data symbols via the rotation of the antenna indices and constellation symbols at the legitimate transmitter [215]. In

the case of time-division duplexing, the channel information of the legitimate user can not be learned by eavesdropper since the channel is reciprocal and not feed to Tx. It is expected that the exploitation of the reciprocal channel feature with time domain IM can provide further improvement in security. Additionally, PLS approaches based on artificial noise and transceiver impairments need to be investigated for different IM domains. Thus, considering the aforementioned possible applications of IM, enormous research potential challenges exist in this newly emerging research field of IM.

5.4.4 Intelligent Wireless Communications through IM

Here there are two standpoints that IM can be the pioneer for the smartness or assist the existing intelligent network. One of the main features of intelligent networks is the channel control capability. Channel domain IM, i.e., MBM, enables to create different channel realizations to transmit the data bits. These channel states allow us to have plenty of advantages including low complexity, high data rate, and ultra-reliability. However, the channel control capability of MBM is only dependent on the incoming bits. Therefore, channel domain modulation should be exploited not only for data transmission but also for the control of channel characteristics, such as delay and Doppler spread in order to overcome the problems of wireless communication systems. Although this requires profound thinking, channel domain modulation can be considered as a candidate solution to have intelligent communications over future systems. Furthermore, the recently reputed RIS concept controls the propagation environment to increase the quality of service at Rx [**?**, 216, 217]. In recent studies, IM is coupled with RIS to exploit the advantages of both technologies. In this regard, three scenarios including IM over Tx antennas, IM over RIS, and IM over Rx antennas are introduced in [156]. RIS-assisted beam-index modulation [218] and SSK [219] are proposed for avoiding line-of-sight blockage in mmWave frequency bands and achieving high EE with high reliability, respectively. Since the utilization of RIS is an early stage, its amalgamation with IM needs an intensive research effort to

speculate the potential benefits and drawbacks. Therefore, it is beneficial to give substantial attention to design smart communication systems via the combination of RIS and IM concepts.

5.4.5 Investigation of Novel IM Techniques

As presented throughout the survey, a plethora of studies on the IM concept is available in the literature. The majority of the studies provide their comparison with the well-adopted systems in terms of SE and BER. It should be noted that users had more or less the same priorities in previous wireless communication systems so that service providers had guaranteed their satisfaction. The emerge of different necessities hurdles the simultaneous happiness of the existing users in a network. IM concept reveals a novel perspective to wireless systems, where the physical entities can convey information. Moreover, it is adaptive and controlled by the incoming data bits. In other words, the rationale behind IM arises from the flexibility. Thus, it is essential and beneficial to overview the general picture and investigate novel IM technologies to serve multiple requirements simultaneously. For 6G and beyond networks, it is envisioned that there will be applications and use cases that can not be categorized under the eMBB, mMTC, and URLLC. Thus, the multidimensional application of IM opens the door for the system design to promote multiple demands. As can be seen in Fig. 5.5, IM application on both RF mirrors and subcarriers, i.e., corresponds to MBM with frequency domain IM, is not explored yet, and can be coupled to jointly support eMBB and URLLC services. Also, the potential of available IM techniques is not well-understood for serving the different combinations of these services. In addition to the foregoing approaches, sparse design in each dimension provides a degree of freedom in order to reap the advantages of multidimensional IM types and to facilitate the implementation of IM in current communication systems [220]. For instance, in [221], CS is integrated into Tx and Rx side of two dimensional IM scheme for the sake of increasing the data rate and system flexibility, while reducing the complexity of ML detector at Rx. Moreover, CS-aided IM are investigated

in the literature for SM [222], QSM [223], STBC-QSM [148], STSK [133, 224]. In recent study [225], neural network-based IM detector is introduced to relax ML complexity. As noticed from the above-reviewed literature, many CS-based research studies have been focusing on space domain IM types, but its applications for the other IM domains are missing in the literature. Moreover, the utilization of neural network-based strategies, machine learning, and deep learning for multidimensional IM types alongside one-dimensional IM types are noteworthy and virgin research area for the researchers worldwide. Hence, the researchers need to make further efforts on IM transceiver design to facilitate its implementation and the detection of active entities and M-ary symbols at Rx.

5.5 Conclusion

This study has presented the recent research progress on one-dimensional and multidimensional IM techniques. Moreover, considerations regarding the utilization of these IM schemes for next-generation wireless communication are provided. Specifically, IM schemes presented in the literature have been firstly grouped regarding their application dimensions. Later, we have categorized these IM techniques considering the requirements of eMBB, mMTC, and URLLC including SE, EE, system complexity, reliability, and latency.

In addition to the information bits carried by QAM/PSK, IM carries extra bits by utilizing the indices of information-bearing transmit entities. As a result, an increase in the number of utilized IM entities such as time slots, subcarriers, Tx antennas, and RF mirrors offers a high SE for IM-based schemes. Hence, multidimensional IM options have been considered as promising solutions for eMBB applications and use-cases. At this point, we conclude that further research on the joint utilization of other new possible entities will be beneficial to enhance SE of IM systems.

Additional bits conveyed over the indices of active entities do not require extra power for transmission and thus provide a high EE for IM-based systems. Transceiver complexity is increased by the distribution of information bits over

multiple domains, which specifically increases the Rx complexity. Thus, mainly one-dimensional IM variants appear as candidate solutions for mMTC applications and use-cases. Additionally, IM techniques with simple Rx structure, such as DMBM and TI-SM, can be also considered.

High diversity gain, interference immunity, and fast processing time are the main priorities for URLLC applications and use-cases. Thus, IM schemes, such as GSM, QSM, STBC-SM, and STSK are suitable candidates.

To sum up, it has been demonstrated that the presented categorization of IM techniques considering broad range demands of next-generation wireless systems can be considered as a reference point for new solutions in 5G and beyond technologies.

Chapter 6

Conclusions

This dissertation deals with three fundamental research directions 1) interference control mechanisms for coexistence of the existing users (waveform coexistence), 2) channel control mechanism against low penetration capabilities in millimeter wave (mmWave) frequency bands and 3) flexibility in the future communication systems via multidimensional signal transmission.

A novel perspective to NOMA, i.e., waveform domain NOMA, is introduced and the overlapping of orthogonal frequency division multiplexing (OFDM) and OFDM with IM (OFDM-IM) is proposed as a case study. The generalization of waveform domain NOMA concept is an open area and left for future studies. Adaptive beamwidth provides control of the propagation environment for mmWave communication. Indeed, the rationale behind the adaptive beamwidth concept with reflectors matches the idea of reconfigurable intelligent surfaces (RISs). Therefore, adaptive beamwidth utilization in RIS-empowered mmWave communication is an open issue for serving the different requirements. Lastly, IM-aided multidimensional transmission are assessed for satisfying the requirements of 5G services, i.e., eMBB, mMTC, and URLLC. The evaluation of the presented schemes in terms of achieving security and serving the different combinations of these services is left for future studies.

Bibliography

[1] E. Mohyeldin, "Minimum technical performance requirements for IMT 2020 radio interface(s)," tech. rep., Nokia, 2016.

[2] X. Meng, J. Li, D. Zhou, and D. Yang, "5G technology requirements and related test environments for evaluation," *China Commun.*, vol. 13, pp. 42–51, Jan. 2016.

[3] 3GPP R1-164006, "Design aspects of mMTC for NR," tech. rep., Samsung, May 2016.

[4] J. Schlienz and D. Raddino, "Narrowband Internet of Things," tech. rep., RohdeSchwarz, May 2016.

[5] C. Bockelmann *et al.*, "Massive machine-type communications in 5G: Physical and MAC-layer solutions," *IEEE Commun. Mag.*, vol. 54, pp. 59–65, Sep. 2016.

[6] C. Bockelmann *et al.*, "Towards massive connectivity support for scalable mMTC communications in 5G networks," *IEEE Access*, vol. 6, pp. 28969–28992, May 2018.

[7] A. Laya, L. Alonso, and J. Alonso-Zarate, "Is the random access channel of LTE and LTE-A suitable for M2M Communications? A survey of alternatives," *IEEE Commun. Surveys Tut.*, vol. 16, pp. 4–16, Jan. 2014.

[8] S. Dogan, A. Tusha, and H. Arslan, "OFDM with index modulation for asynchronous mMTC networks," *Sensors*, vol. 18, p. 1280, Apr. 2018.

[9] Y. E. Wang *et al.*, "A primer on 3GPP narrowband Internet of Things," *IEEE Commun. Mag.*, vol. 55, pp. 117–123, Mar. 2017.

[10] A. Hoglund *et al.*, "Overview of 3GPP Release 14 enhanced NB-IoT," *IEEE Network*, vol. 31, pp. 16–22, Nov. 2017.

[11] A. Tusha, S. Dogan, and H. Arslan, "IQI mitigation for narrowband IoT systems with OFDM-IM," *IEEE Access*, vol. 6, pp. 44626–44634, Aug. 2018.

[12] 3GPP, "IMT-2020 self-evaluation: UP latency in LTE," tech. rep., Ericson, Nov. 2018.

[13] 3GPP, "Study on latency reduction techniques for LTE ," tech. rep., 3rd generation partnership project (3GPP), May 2016.

[14] P. Schulz, M. Matthe, H. Klessig, M. Simsek, G. Fettweis, *et al.*, "Latency critical IoT applications in 5G: Perspective on the design of radio interface and network architecture," *IEEE Commun. Mag.*, vol. 55, pp. 70–78, Feb. 2017.

[15] H. Chen, R. Abbas, P. Cheng, M. Shirvanimoghaddam, *et al.*, "Ultra-reliable low latency cellular networks: Use cases, challenges and approaches," *ArXiv e-print*, Sep. 2017.

[16] J. Sachs, G. Wikstrom, T. Dudda, R. Baldemair, and K. Kittichokechai, "5G radio network design for ultra-reliable low-latency communication," *IEEE Netw.*, vol. 32, pp. 24–31, Apr. 2018.

[17] W. Saad, M. Bennis, and M. Chen, "A vision of 6G wireless systems: Applications, trends, technologies, and open research problems," *IEEE Network*, vol. 34, pp. 134–142, Aug. 2020.

[18] A. Yastrebova, R. Kirichek, Y. Koucheryavy, A. Borodin, and A. Koucheryavy, "Future networks 2030: Architecture & requirements," in *Int. Congr. Ultra Modern Telecommun. Control Syst. (ICUMT)*, pp. 1–8, Feb. 2018.

[19] A. Mourad, R. Yang, P. H. Lehne, and A. de la Oliva, "Towards 6G: Evolution of key performance indicators and technology trends," in *6G Wireless Summit (6G SUMMIT)*, pp. 1–5, May 2020.

[20] G. Berardinelli, P. Mogensen, and R. O. Adeogun, "6G subnetworks for life-critical communication," in *6G Wireless Summit (6G SUMMIT)*, pp. 1–5, Mar. 2020.

[21] S. Dang, B. Shihada, and M.-S. Alouini, "What should 6G be?," *Nat. Electron.*, vol. 3, pp. 20–29, Jan. 2020.

[22] R. Abu-alhiga and H. Haas, "Subcarrier-index modulation OFDM," in *Proc. IEEE Int. Symp. Pers., Indoor Mobile Radio Commun. (PIMRC)*, pp. 177–181, Sep. 2009.

[23] D. Tsonev, S. Sinanovic, and H. Haas, "Enhanced subcarrier index modulation (SIM) OFDM," in *Proc. IEEE Global Telecommun. Conf. (GLOBECOM)*, pp. 728–732, Dec. 2011.

[24] E. Basar, U. Aygolu, E. Panayirci, and H. V. Poor, "Orthogonal frequency division multiplexing with index modulation," *IEEE Trans. Signal Process.*, vol. 61, pp. 5536–5549, Nov. 2013.

[25] E. Basar, "Index modulation techniques for 5G wireless networks," *IEEE Commun. Mag.*, vol. 54, pp. 168–175, Jul. 2016.

[26] E. Basar, M. Wen, R. Mesleh, M. Di Renzo, Y. Xiao, and H. Haas, "Index modulation techniques for next-generation wireless networks," *IEEE Access*, vol. 5, pp. 16693–16746, Aug. 2017.

[27] Y. Xiao, S. Wang, L. Dan, X. Lei, P. Yang, and W. Xiang, "OFDM with interleaved subcarrier-index modulation," *IEEE Commun. Lett.*, vol. 18, pp. 1447–1450, Aug. 2014.

[28] R. Fan, Y. J. Yu, and Y. L. Guan, "Orthogonal frequency division multiplexing with generalized index modulation," in *Proc. IEEE Global Telecommun. Conf. (GLOBECOM)*, pp. 3880–3885, Dec. 2014.

[29] T. Mao, Z. Wang, Q. Wang, S. Chen, and L. Hanzo, "Dual-mode index modulation aided OFDM," *IEEE Access*, vol. 5, pp. 50–60, Aug. 2017.

[30] M. Wen, E. Basar, Q. Li, B. Zheng, and M. Zhang, "Multiple-mode orthogonal frequency division multiplexing with index modulation," *IEEE Trans. Commun.*, vol. 65, pp. 3892–3906, Sep. 2017.

[31] E. Basar, "OFDM with index modulation using coordinate interleaving," *IEEE Wireless Commun. Lett.*, vol. 4, pp. 381–384, Aug. 2015.

[32] 3GPP, "IMT vision - Framework and overall objectives of the future development of IMT for 2020 and beyond," tech. rep., Telecommun. Standardization Sector of ITU, 2015.

[33] A. Yazar and H. Arslan, "A flexibility metric and optimization methods for mixed numerologies in 5G and beyond," *IEEE Access*, vol. 6, pp. 3755–3764, Jan. 2018.

[34] Z. E. Ankarali, B. Pekoz, and H. Arslan, "Flexible radio access beyond 5G: A future projection on waveform, numerology, and frame design principles," *IEEE Access*, vol. 5, pp. 18295–18309, Mar. 2017.

[35] P. Popovski, K. F. Trillingsgaard, O. Simeone, and G. Durisi, "5G wireless network slicing for eMBB, URLLC, and mMTC: A communication-theoretic view," *ArXiv e-print*, Aug. 2018.

[36] ITU-R Working Party 5D, "Minimum requirements related to technical performance for IMT-2020 radio interface(s)," tech. rep., Radiocommun. Sector of ITU (ITU-R), Nov. 2017.

[37] J. C. S. Arenas, T. Dudda, and L. Falconetti, "Ultra-low Latency in next generation LTE radio access," in *Proc. Int. ITG Conf. on Syst., Commun. and Coding (SCC)*, pp. 1–6, Feb. 2017.

[38] D. Jiang, H. Wang, E. Malkamaki, and E. Tuomaala, "Principle and performance of semi-persistent scheduling for VoIP in LTE system," in *Int. Conf. on Wireless Commun., Netw. and Mobile Comput. (WiCom)*, pp. 2861–2864, Sep. 2007.

[39] G. Berardinelli, N. H. Mahmood, R. Abreu, T. Jacobsen, K. Pedersen, *et al.*, "Reliability analysis of uplink grant-free transmission over shared resources," *IEEE Access*, vol. 6, pp. 23602–23611, Apr. 2018.

[40] T. Jacobsen, R. Abreu, G. Berardinelli, K. Pedersen, P. Mogensen, *et al.*, "System level analysis of uplink grant-free transmission for URLLC," in *Proc. IEEE Global Telecommun. Conf. (GLOBECOM)*, Dec. 2017.

[41] 3GPP R1-1705246, "UL grant-free transmission for URLLC," tech. rep., Nokia, Apr. 2017.

[42] 3GPP R1-1701596, "Advanced grant-free transmission for URLLC ," tech. rep., ZTE, Feb. 2017.

[43] 3GPP RP-171043, "Revision of study on 5G non-orthogonal multiple access," tech. rep., ZTE, Jun. 2018.

[44] 3GPP R1-1811390, "Discussion on NOMA UL grant-free procedure ," tech. rep., Inst. for Inform. Ind., Dec. 2018.

[45] H. Arslan and K. Molnar, "Iterative co-channel interference cancellation in narrowband mobile radio systems," in *IEEE Emerging Technol. Symp. on Broadband, Wireless Internet Access. Digest of Papers (Cat. No.00EX414)*, pp. 1–5, Apr. 2000.

[46] M. B. Celebi, I. Guvenc, H. Arslan, and K. A. Qaraqe, "Interference suppression for the LTE uplink," *Physical Commun.*, vol. 9, pp. 23–44, May 2013.

[47] M. E. Sahin, I. Guvenc, and H. Arslan, "An iterative interference cancellation method for co-channel multicarrier and narrowband systems," *Physical Commun.*, vol. 4, pp. 13–25, Sep. 2011.

[48] H. Sari, F. Vanhaverbeke, and M. Moeneclaey, "Multiple access using two sets of orthogonal signal waveforms," *IEEE Commun. Lett.*, vol. 4, pp. 4–6, Jan. 2000.

[49] W. Shin, M. Vaezi, B. Lee, D. J. Love, J. Lee, and H. V. Poor, "Non-orthogonal multiple access in multi-cell networks: Theory, performance, and practical challenges," *IEEE Commun. Mag.*, vol. 55, pp. 176–183, Oct. 2017.

[50] A. Maatouk, E. al??kan, M. Koca, M. Assaad, G. Gui, and H. Sari, "Frequency-domain NOMA with two sets of orthogonal signal waveforms," *IEEE Commun. Lett.*, vol. 22, pp. 906–909, May 2018.

[51] S. M. R. Islam, N. Avazov, O. A. Dobre, and K. Kwak, "Power-domain non-orthogonal multiple access (NOMA) in 5G systems: Potentials and challenges," *IEEE Commun. Surveys Tut.*, vol. 19, pp. 721–742, Feb. 2017.

[52] M. Vaezi, Z. Ding, and H. V. Poor, *Multiple Access Techniques for 5G Wireless Networks and Beyond.* Springer, 2018.

[53] R. Abreu, G. Berardinelli, T. Jacobsen, K. Pedersen, and P. Mogensen, "A blind retransmission scheme for ultra-reliable and low latency communications," in *Proc. IEEE Veh. Technol. Conf. (VTC)*, pp. 1–5, Jun. 2018.

[54] R. Abu-alhiga and H. Haas, "Subcarrier-index modulation OFDM," in *Proc. IEEE Int. Symp. Pers. Indoor and Mobile Radio Commun.*, pp. 177–181, Sep. 2009.

[55] E. Memisoglu, E. Basar, and H. Arslan, "Low complexity peak-to-average power ratio reduction in OFDM-IM," in *IEEE Int. Black Sea Conf. Commun. and Netw. (BlackSeaCom)*, pp. 1–5, Jun. 2018.

[56] X. Cheng, M. Wen, L. Yang, and Y. Li, "Index modulated OFDM with interleaved grouping for V2X communications," in *Proc. Int. Conf. Intell. Transp. Syst. (ITSC*, pp. 1–8, Oct. 2014.

[57] G. D. Ntouni, V. M. Kapinas, and G. K. Karagiannidis, "On the optimal tone spacing for interference mitigation in OFDM-IM systems," *IEEE Commun. Lett.*, vol. 21, pp. 1019–1022, May 2017.

[58] Q. Ma, P. Yang, Y. Xiao, H. Bai, and S. Li, "Error probability analysis of OFDM-IM with carrier frequency offset," *IEEE Commun. Lett.*, vol. 20, pp. 2434–2437, Dec. 2016.

[59] M. Wen, Y. Zhang, J. Li, E. Basar, and F. Chen, "Equiprobable subcarrier activation method for OFDM with index modulation," *IEEE Commun. Lett.*, vol. 20, pp. 2386–2389, Dec. 2016.

[60] M.-S. Alouini and A. Goldsmith, "A unified approach for calculating error rates of linearly modulated signals over generalized fading channels," *IEEE Trans. Commun.*, vol. 47, no. 9, pp. 1324–1334, 1999.

[61] Y. Niu, Y. Li, D. Jin, L. Su, and A. V. Vasilakos, "A survey of millimeter wave communications (mmWave) for 5G: Opportunities and challenges," *Wireless Networks*, vol. 21, no. 8, pp. 2657–2676, 2015.

[62] T. S. Rappaport, S. Sun, R. Mayzus, H. Zhao, Y. Azar, K. Wang, G. N. Wong, J. K. Schulz, M. Samimi, and F. Gutierrez, "Millimeter wave mobile communications for 5G cellular: It will work!," *IEEE Access*, vol. 1, pp. 335–349, May 2013.

[63] S. Rangan, T. S. Rappaport, and E. Erkip, "Millimeter-wave cellular wireless networks: Potentials and challenges," *Proc. IEEE*, vol. 102, no. 3, pp. 366–385, 2014.

[64] Z. Pi and F. Khan, "An introduction to millimeter-wave mobile broadband systems," *IEEE Commun. Mag.*, vol. 49, pp. 101–107, Jun. 2011.

[65] Federal Communications Commission, "FCC takes steps to facilitate mobile broadband and next generation wireless technologies in spectrum above 24 GHz," tech. rep., Jul. 2016.

[66] T. S. Rappaport, G. R. MacCartney, M. K. Samimi, and S. Sun, " Wideband millimeter-wave propagation measurements and channel models for future wireless communication system design," *IEEE Trans. Commun.*, vol. 63, no. 9, pp. 3029–3056, 2015.

[67] T. S. Rappaport, S. Sun, and M. Shafi, "Investigation and comparison of 3GPP and NYUSIM channel models for 5G wireless communications," in *Proc. IEEE Veh. Technol. Conf. (VTC)*, pp. 1–5, Sep. 2017.

[68] M. Marcus and B. Pattan, "Millimeter wave propagation: Spectrum management implications," tech. rep., Aug. 2005.

[69] A. Maltsev, "Channel models for 60 GHz WLAN systems," tech. rep., Jun. 2010.

[70] T. Manabe, Y. Miura, and T. Ihara, "Effects of antenna directivity and polarization on indoor multipath propagation characteristics at 60 GHz," *IEEE J. Sel. Areas Commun.*, vol. 14, no. 3, pp. 441–448, 1996.

[71] S. Collonge, G. Zaharia, and G. E. Zein, "Influence of the human activity on wide-band characteristics of the 60 GHz indoor radio channel," *IEEE Trans. Wireless Commun.*, vol. 3, no. 6, pp. 2396–2406, 2004.

[72] H. Xu, V. Kukshya, and T. Rappaport, "Spatial and temporal characteristics of 60-GHz indoor channels," *IEEE J. Sel. Areas Commun.*, vol. 20, no. 3, pp. 620–630, 2002.

[73] G. R. MacCartney, T. S. Rappaport, and S. Rangan, "Rapid fading due to human blockage in pedestrian crowds at 5G millimeter-wave frequencies," in *Proc. IEEE Global Telecommun. Conf. (GLOBECOM)*, pp. 1–7, Dec. 2017.

[74] K. Sato and T. Manabe, "Estimation of propagation-path visibility for indoor wireless LAN systems under shadowing condition by human bodies," in *Proc. IEEE Veh. Technol. Conf. (VTC)*, vol. 3, pp. 2109–2113, May 1998.

[75] C. Leong, B. Lee, A. Nix, and P. Strauch, "A robust 60 GHz wireless network with parallel relaying," in *Proc. IEEE Int. Conf. Commun. (ICC)*, vol. 6, pp. 3528–3532, Jan. 2004.

[76] M. K. Samimi and T. S. Rappaport, "3-D millimeter-wave statistical channel model for 5G wireless system design," *IEEE Trans. Microw. Theor. Techn.*, vol. 64, no. 7, pp. 2207–2225, 2016.

[77] S. Sun, G. R. MacCartney, and T. S. Rappaport, "A novel millimeter-wave channel simulator and applications for 5G wireless communications," in *Proc. IEEE Int. Conf. Commun. (ICC)*, pp. 1–7, May. 2017.

[78] S. Sun, T. S. Rappaport, T. A. Thomas, A. Ghosh, H. C. Nguyen, I. Z. Kovcs, *et al.*, "Investigation of prediction accuracy, sensitivity, and parameter stability of large-scale propagation path loss models for 5G wireless communications," *IEEE Trans. Veh. Technol.*, vol. 65, no. 5, pp. 2843–2860, 2016.

[79] J. Li, X. Li, D. Zhou, and E. Zhang, "A novel method for estimating the power azimuth spectrum of the wireless channel," *IEEE Antennas Wireless Propag. Lett.*, vol. 5, pp. 11–14, Mar. 2006.

[80] J. Navarro-Ortiz, P. Romero-Diaz, S. Sendra, P. Ameigeiras, J. J. Ramos-Munoz, and J. M. Lopez-Soler, "A survey on 5G usage scenarios and traffic models," *IEEE Commun. Surveys Tut.*, vol. 22, pp. 905–929, Feb. 2020.

[81] ITU-R M.2370-0, "IMT traffic estimates for the years 2020 to 2030," tech. rep., ITU, 2015.

[82] Cisco, "Annual Internet Report (2018-2023)," tech. rep., Cisco, 2020.

[83] Cisco, "Global and Americas/EMEAR Mobile Data Traffic Forecast, 2017-2022," tech. rep., Cisco, 2019.

[84] ITU, "IMT vision - Framework and overall objectives of the future development of IMT for 2020 and beyond," tech. rep., Telecommun. Standardization Sector of ITU, 2015.

[85] I.-R. M.2412, "Guidelines for evaluation of radio interface technologies for IMT-2020," tech. rep., Telecommun. Standardization Sector of ITU, 2017.

[86] A. A. Zaidi, R. Baldemair, V. Moles-Cases, N. He, K. Werner, and A. Cedergren, "OFDM numerology design for 5G New Radio to support IoT, eMBB, and MBSFN," *IEEE Commun. Standards Mag.*, vol. 2, pp. 78–83, Jun. 2018.

[87] S. Dang, B. Shihada, and M.-S. Alouini, "What should 6G be?," *Nat. Electron.*, vol. 3, pp. 20–29, Jan. 2020.

[88] H. Zhang, N. Liu, X. Chu, K. Long, A. Aghvami, and V. C. M. Leung, "Network slicing based 5G and future mobile networks: Mobility, resource management, and challenges," *IEEE Commun. Mag.*, vol. 55, pp. 138–145, Aug. 2017.

[89] A. Yazar and H. Arslan, "A flexibility metric and optimization methods for mixed numerologies in 5G and beyond," *IEEE Access*, vol. 6, pp. 3755–3764, Jan. 2018.

[90] J. Oetting, "A comparison of modulation techniques for digital radio," *IEEE Trans. Commun.*, vol. 27, pp. 1752–1762, Dec. 1979.

[91] M. S. Alouini and A. J. Goldsmith, "A unified approach for calculating error rates of linearly modulated signals over generalized fading channels," *IEEE Trans. Commun.*, vol. 47, pp. 1324–1334, Sep. 1999.

[92] R. Y. Mesleh, H. Haas, S. Sinanovic, C. W. Ahn, and S. Yun, "Spatial modulation," *IEEE Trans. Veh. Tech.*, vol. 57, pp. 2228–2241, Jul. 2008.

[93] E. Memisoglu, E. Basar, and H. Arslan, "Fading-aligned OFDM with index modulation for mMTC services," *Phys. Commun.*, vol. 35, pp. 1–7, Aug. 2019.

[94] M. Di Renzo, H. Haas, and P. M. Grant, "Spatial modulation for multiple-antenna wireless systems: A survey," *IEEE Commun. Mag.*, vol. 49, pp. 182–191, Dec. 2011.

[95] X. Cheng, M. Zhang, M. Wen, and L. Yang, "Index modulation for 5G: Striving to do More with Less," *IEEE Wireless Commun.*, vol. 25, pp. 126–132, Apr. 2018.

[96] P. Yang, Y. Xiao, Y. L. Guan, M. D. Renzo, S. Li, and L. Hanzo, "Multidomain index modulation for vehicular and railway communications: A survey of novel techniques," *IEEE Veh. Technol. Mag.*, vol. 13, pp. 124–134, Sep. 2018.

[97] Q. Li, M. Wen, B. Clerckx, S. Mumtaz, A. Al-Dulaimi, and R. Qingyang Hu, "Subcarrier index modulation for future wireless networks: Principles, applications, and challenges," *IEEE Wireless Commun.*, vol. 27, pp. 1–8, Apr. 2020.

[98] S. Sugiura, S. Chen, and L. Hanzo, "A universal space-time architecture for multiple-antenna aided systems," *IEEE Commun. Surveys Tut.*, vol. 14, pp. 401–420, Feb. 2012.

[99] M. Di Renzo, H. Haas, A. Ghrayeb, S. Sugiura, and L. Hanzo, "Spatial modulation for generalized MIMO: Challenges, opportunities, and implementation," *Proc. IEEE*, vol. 102, pp. 56–103, Dec. 2014.

[100] P. Yang, M. Di Renzo, Y. Xiao, S. Li, and L. Hanzo, "Design guidelines for spatial modulation," *IEEE Commun. Surveys Tut.*, vol. 17, pp. 6–26, Sep. 2015.

[101] S. Sugiura, T. Ishihara, and M. Nakao, "State-of-the-art design of index modulation in the space, time, and frequency domains: Benefits and fundamental limitations," *IEEE Access*, vol. 5, pp. 21774–21790, Oct. 2017.

[102] T. Mao, Q. Wang, Z. Wang, and S. Chen, "Novel index modulation techniques: A survey," *IEEE Commun. Surveys Tut.*, vol. 21, pp. 315–348, Jul. 2018.

[103] N. Ishikawa, S. Sugiura, and L. Hanzo, "50 years of permutation, spatial and index modulation: From classic RF to visible light vommunications and data storage," *IEEE Commun. Surveys Tut.*, vol. 20, pp. 1905–1938, Mar. 2018.

[104] M. Wen, B. Zheng, K. J. Kim, M. Di Renzo, T. A. Tsiftsis, *et al.*, "A survey on spatial modulation in emerging wireless systems: Research progresses and applications," *IEEE J. Sel. Areas Commun.*, vol. 37, pp. 1949–1972, Jul. 2019.

[105] Y. A. Chau and Shi-Hong Yu, "Space modulation on wireless fading channels," in *Proc. IEEE Veh. Technol. Conf. (VTC)*, pp. 1–5, Oct. 2001.

[106] P. W. Wolniansky, G. J. Foschini, G. D. Golden, and R. A. Valenzuela, "V-BLAST: An architecture for realizing very high data rates over the rich-scattering wireless channel," in *Int. Symp. Signals Syst, and Electron.*, pp. 295–300, Oct 1998.

[107] V. Tarokh, A. Naguib, N. Seshadri, and A. R. Calderbank, "Space-time codes for high data rate wireless communication: Performance criteria in the presence of channel estimation errors, mobility, and multiple paths," *IEEE Trans. Commun.*, vol. 47, pp. 199–207, Feb. 1999.

[108] J. Jeganathan, A. Ghrayeb, and L. Szczecinski, "Generalized space shift keying modulation for MIMO channels," in *Proc. IEEE Int. Symp. Pers., Indoor Mobile Radio Commun. (PIMRC)*, pp. 1–5, Sep. 2008.

[109] R. Y. Mesleh, H. Haas, S. Sinanovic, C. W. Ahn, and S. Yun, "Spatial modulation," *IEEE Trans. Veh. Tech.*, vol. 57, pp. 2228–2241, Jul. 2008.

[110] A. Younis, N. Serafimovski, R. Mesleh, and H. Haas, "Generalised spatial modulation," in *Proc. Conf. Rec. Asilomar Conf. Signals. Syst. and Comput.*, pp. 1498–1502, Nov. 2010.

[111] J. Wang, S. Jia, and J. Song, "Generalised spatial modulation system with multiple active transmit antennas and low complexity detection scheme," *IEEE Trans. Wireless Commun.*, vol. 11, pp. 1605–1615, Apr. 2012.

[112] R. Mesleh, S. S. Ikki, and H. M. Aggoune, "Quadrature spatial modulation," *IEEE Trans. Veh. Technol.*, vol. 64, pp. 2738–2742, Jun. 2015.

[113] C. Cheng, H. Sari, S. Sezginer, and Y. T. Su, "Enhanced spatial modulation with multiple signal constellations," *IEEE Trans. Commun.*, vol. 63, pp. 2237–2248, Jun. 2015.

[114] E. Basar, U. Aygolu, E. Panayirci, and H. V. Poor, "Space-time block coded spatial modulation," *IEEE Trans. Commun.*, vol. 59, pp. 823–832, Mar. 2011.

[115] Y. Bian, X. Cheng, M. Wen, L. Yang, H. V. Poor, and B. Jiao, "Differential spatial modulation," *IEEE Trans. Veh. Technol.*, vol. 64, pp. 3262–3268, Jul. 2015.

[116] A. K. Khandani, "Media-based modulation: A new approach to wireless transmission," in *Proc. IEEE Int. Symp. Inform. Theory*, pp. 3050–3054, Jul. 2013.

[117] Y. Naresh and A. Chockalingam, "A low-complexity maximum-likelihood detector for differential media-based modulation," *IEEE Commun. Lett.*, vol. 21, pp. 2158–2161, Oct. 2017.

[118] Y. Liu, M. Zhang, H. Wang, and X. Cheng, "Spatial modulation orthogonal frequency division multiplexing with subcarrier index modulation for V2X communications," in *Int. Conf., Comp. Netw. Commun. (ICNC)*, pp. 1–5, Feb. 2016.

[119] T. Datta, H. S. Eshwaraiah, and A. Chockalingam, "Generalized space and frequency index modulation," *IEEE Trans. Veh. Technol.*, vol. 65, pp. 4911–4924, Jul. 2016.

[120] E. Ozturk, E. Basar, and H. A. Cirpan, "Generalized frequency division multiplexing with space and frequency index modulation," in *Proc. IEEE Int. Black Sea Conf. Commun., Netw. (BlackSeaCom)*, pp. 1–5, Jun. 2017.

[121] R. Fan, Y. J. Yu, and Y. L. Guan, "Generalization of orthogonal frequency division multiplexing with index modulation," *IEEE Trans. Wireless Commun.*, vol. 14, pp. 5350–5359, Oct. 2015.

[122] E. Ozturk, E. Basar, and H. A. Cirpan, "Generalized frequency division multiplexing with index modulation," in *Proc. IEEE Global Telecommun. Conf. Workshops (GLOBECOM)*, pp. 1–6, Dec. 2016.

[123] S. Jacob, T. L. Narasimhan, and A. Chockalingam, "Space-time index modulation," in *Proc. IEEE Wireless Commun., Netw. Conf. (WCNC)*, pp. 1–6, Mar. 2017.

[124] B. Shamasundar, S. Bhat, S. Jacob, and A. Chockalingam, "Multidimensional index modulation in wireless communications," *IEEE Access*, vol. 6, pp. 589–604, Nov. 2018.

[125] M. Nakao, T. Ishihara, and S. Sugiura, "Single-carrier frequency-domain equalization with index modulation," *IEEE Commun. Lett.*, vol. 21, pp. 298–301, Feb. 2017.

[126] T. Ishihara and S. Sugiura, "Faster-than-Nyquist signaling with index modulation," *IEEE Wireless Commun. Lett.*, vol. 6, pp. 630–633, Oct. 2017.

[127] M. Nakao and S. Sugiura, "Dual-mode time-domain single-carrier index modulation with frequency-domain equalization," in *Proc. IEEE Veh. Technol. Conf. (VTC)*, pp. 1–5, Sep. 2017.

[128] F. Cogen, E. Aydin, N. Kabaoglu, E. Basar, and H. Ilhan, "A novel MIMO scheme based on code-index modulation and spatial modulation," in *Proc. Int. Conf. Telecommun., Signal Process. (TSP)*, pp. 1–4, May 2018.

[129] G. Kaddoum, M. F. A. Ahmed, and Y. Nijsure, "Code index modulation: A high data rate and energy efficient communication system," *IEEE Commun. Lett.*, vol. 19, pp. 175–178, Feb. 2015.

[130] G. Kaddoum, Y. Nijsure, and H. Tran, "Generalized code index modulation technique for high-data-rate communication systems," *IEEE Trans. Veh. Technol.*, vol. 65, pp. 7000–7009, Sep. 2016.

[131] Q. Li, M. Wen, E. Basar, and F. Chen, "OFDM spread spectrum with index modulation," in *Proc. IEEE Global Telecommun. Conf. Workshops (GLOBECOM)*, pp. 1–6, Dec. 2017.

[132] I. A. Hemadeh, M. El-Hajjar, S. Won, and L. Hanzo, "Multi-set space-time shift-keying with reduced detection complexity," *IEEE Access*, vol. 4, pp. 4234–4246, Jun. 2016.

[133] S. Lu, I. A. Hemadeh, M. El-Hajjar, and L. Hanzo, "Compressed-sensing-aided space-time frequency index modulation," *IEEE Trans. Veh. Technol.*, vol. 67, pp. 6259–6271, Jul. 2018.

[134] I. A. Hemadeh, M. El-Hajjar, S. Won, and L. Hanzo, "Multi-set space-time shift keying and space-frequency space-time shift keying for millimeter-wave communications," *IEEE Access*, vol. 5, pp. 8324–8342, Jun. 2017.

[135] S. Sugiura, S. Chen, and L. Hanzo, "Coherent and differential space-time shift keying: A dispersion matrix approach," *IEEE Trans. Commun.*, vol. 58, pp. 3219–3230, Nov. 2010.

[136] S. Sugiura, S. Chen, and L. Hanzo, "Generalized space-time shift keying designed for flexible diversity-, multiplexing- and complexity-tradeoffs," *IEEE Trans. Wireless Commun.*, vol. 10, pp. 1144–1153, Apr. 2011.

[137] H. A. Ngo, C. Xu, S. Sugiura, and L. Hanzo, "Space-time-frequency shift keying for dispersive channels," *IEEE Signal Process. Lett.*, vol. 18, pp. 177–180, Mar. 2011.

[138] M. Driusso, F. Babich, M. I. Kadir, and L. Hanzo, "OFDM aided space-time shift keying for dispersive downlink channels," in *Proc. IEEE Veh. Technol. Conf. (VTC)*, pp. 1–5, Sep. 2012.

[139] Z. Li and J. Zheng, "Space-frequency shift keying in rapidly time-varying MIMO OFDM channels," in *Proc. IEEE Veh. Technol. Conf. (VTC)*, pp. 1–5, Jun. 2018.

[140] J. Jeganathan, A. Ghrayeb, L. Szczecinski, and A. Ceron, "Space shift keying modulation for MIMO channels," *IEEE Trans. Wireless Commun.*, vol. 8, Jul. 2009.

[141] R. Mesleh, H. Haas, C. W. Ahn, and S. Yun, "Spatial modulation - A new low complexity spectral efficiency enhancing technique," in *Proc. First Int. Conf. Commun. Netw. China*, pp. 1–5, Apr. 2006.

[142] J. Jeganathan, A. Ghrayeb, and L. Szczecinski, "Spatial modulation: Optimal detection and performance analysis," *IEEE Commun. Lett.*, vol. 12, pp. 545–547, Aug. 2008.

[143] P. Yang, Y. Xiao, Y. L. Guan, K. V. S. Hari, A. Chockalingam, *et al.*, "Single-carrier SM-MIMO: A promising design for broadband large-scale

antenna systems," *IEEE Commun. Surveys Tut.*, vol. 18, pp. 1687–1716, Feb. 2016.

[144] Z. Yigit and E. Basar, "Low-complexity detection of quadrature spatial modulation," *Electron. Lett.*, vol. 52, pp. 1729–1731, Sep. 2016.

[145] R. Mesleh, M. D. Renzo, H. Haas, and P. M. Grant, "Trellis coded spatial modulation," *IEEE Trans. Wireless Commun.*, vol. 9, pp. 2349–2361, Jul. 2010.

[146] E. B. Z. Yigit and R. Mesleh, "Trellis coded quadrature spatial modulation," *Phys. Commun.*, vol. 29, pp. 147–155, Aug. 2018.

[147] Z. Yigit and E. Basar, "Space-time quadrature spatial modulation," in *Proc. IEEE Int. Black Sea Conf. Commun., Netw. (BlackSeaCom)*, pp. 1–5, Jun. 2017.

[148] L. Xiao, P. Xiao, Y. Xiao, I. Hemadeh, A. Mohamed, and L. Hanzo, "Bayesian compressive sensing assisted space?time block coded quadrature spatial modulation," *IEEE Trans. Veh. Technol.*, vol. 67, pp. 10044–10048, Oct. 2018.

[149] A. Stavridis, S. Sinanovic, M. Di Renzo, and H. Haas, "Transmit precoding for receive spatial modulation using imperfect channel knowledge," in *Proc. IEEE Veh. Technol. Conf. (VTC)*, pp. 1–5, May 2012.

[150] L. Yang, "Transmitter preprocessing aided spatial modulation for multiple-input multiple-output systems," in *Proc. IEEE Veh. Technol. Conf. (VTC)*, pp. 1–5, Jul. 2011.

[151] R. Zhang, L. Yang, and L. Hanzo, "Generalised pre-coding aided spatial modulation," *IEEE Trans. Wireless Commun.*, vol. 12, pp. 5434–5443, Nov. 2013.

[152] J. Li, M. Wen, X. Cheng, Y. Yan, S. Song, and M. H. Lee, "Generalized precoding-aided quadrature spatial modulation," *IEEE Trans. Veh. Technol.*, vol. 66, pp. 1881–1886, May 2017.

[153] Q.-U.-A. Nadeem, A. Kammoun, A. Chaaban, M. Debbah, and M.-S. Alouini, "Asymptotic analysis of large intelligent surface assisted MIMO communication," *ArXiv e-print*, Apr. 2019.

[154] A. Taha, M. Alrabeiah, and A. Alkhateeb, "Enabling large intelligent surfaces with compressive sensing and deep learning," *ArXiv e-print*, Apr. 2019.

[155] J. Zhao, "A survey of intelligent reflecting surfaces (IRSs): Towards 6G wireless communication networks with Massive MIMO 2.0," *ArXiv e-print*, Aug. 2019.

[156] E. Basar, "Reconfigurable intelligent surface-based index modulation: A new beyond MIMO paradigm for 6G," *IEEE Trans. Commun.*, vol. 68, pp. 3187–3196, Feb. 2020.

[157] B. Zheng, F. Chen, M. Wen, F. Ji, H. Yu, and Y. Liu, "Low-complexity ML detector and performance analysis for OFDM with in-phase/quadrature index modulation," *IEEE Commun. Lett.*, vol. 19, pp. 1893–1896, Aug. 2015.

[158] R. Fan, Y. J. Yu, and Y. L. Guan, "Improved orthogonal frequency division multiplexing with generalised index modulation," *IET Commun.*, vol. 10, pp. 969–974, Jan. 2016.

[159] T. Mao, Q. Wang, J. Quan, and Z. Wang, "Zero-padded tri-mode index modulation aided OFDM," in *Proc. IEEE Global Telecommun. Conf. (GLOBECOM)*, pp. 1–5, Dec. 2017.

[160] J. Li, S. Dang, M. Wen, X. Jiang, Y. Peng, and H. Hai, "Layered orthogonal frequency division multiplexing with index modulation," *IEEE Syst. J.*, vol. 13, pp. 3793–3802, Jun. 2019.

[161] M. Nakao, T. Ishihara, and S. Sugiura, "Dual-mode time-domain index modulation for Nyquist-criterion and faster-than-Nyquist single-carrier transmissions," *IEEE Access*, vol. 5, pp. 27659–27667, Nov. 2017.

[162] G. Kaddoum and E. Soujeri, "On the comparison between code-index modulation and spatial modulation techniques," in *Proc. Int. Conf. Information, Commun. Technol. Research (ICTRC)*, pp. 24–27, May 2015.

[163] Q. Li, M. Wen, E. Basar, and F. Chen, "Index modulated OFDM spread spectrum," *IEEE Trans. Wireless Commun.*, vol. 17, pp. 2360–2374, Jan. 2018.

[164] E. Seifi, M. Atamanesh, and A. Khandani, "Media-based MIMO: Outperforming known limits in wireless," in *Proc. IEEE Int. Conf. Commun. (ICC)*, pp. 1–7, May 2016.

[165] Y. Naresh and A. Chockalingam, "On media-based modulation using RF mirrors," *IEEE Trans. Veh. Technol.*, vol. 66, pp. 4967–4983, Jun. 2017.

[166] E. Basar, "Media-based modulation for future wireless systems: A tutorial," *ArXiv e-print*, Nov. 2018.

[167] E. Basar and I. Altunbas, "Space-time channel modulation," *IEEE Trans. Veh. Technol.*, vol. 66, pp. 7609–7614, Aug. 2017.

[168] Z. Yigit and E. Basar, "Space-time media-based modulation," *IEEE Trans. Sig. Process.*, vol. 67, pp. 2389–2398, Mar. 2019.

[169] J. Zhang, Y. Wang, J. Zhang, and L. Ding, "Polarization shift keying (PolarSK): System scheme and performance analysis," *IEEE Trans. Veh. Technol.*, vol. 66, pp. 10139–10155, Sep. 2017.

[170] I. A. Hemadeh, P. Xiao, Y. Kabiri, L. Xiao, V. Fusco, *et al.*, "Polarization modulation design for reduced RF chain wireless," *IEEE Trans. Commun.*, vol. 68, pp. 3890–3907, Mar. 2020.

[171] S. Sugiura, S. Chen, and L. Hanzo, "Space-time shift keying: A unified MIMO architecture," in *Proc. IEEE Global Telecommun. Conf. (GLOBECOM)*, pp. 1–5, Dec. 2010.

[172] R. Rajashekar, K. V. S. Hari, and L. Hanzo, "Structured dispersion matrices from division algebra codes for space-time shift keying," *IEEE Signal Process. Lett.*, vol. 20, pp. 371–374, Apr. 2013.

[173] S. Sugiura and L. Hanzo, "On the joint optimization of dispersion matrices and constellations for near-capacity irregular precoded space-time shift keying," *IEEE Trans. Wireless Commun.*, vol. 12, pp. 380–387, Jan. 2013.

[174] I. A. Hemadeh, M. El-Hajjar, S. Won, and L. Hanzo, "Layered multi-group steered space-time shift-keying for millimeter-wave communications," *IEEE Access*, vol. 4, pp. 3708–3718, Apr. 2016.

[175] B. Chakrapani, T. L. Narasimhan, and A. Chockalingam, "Generalized space-frequency index modulation: Low-complexity encoding and detection," in *Proc. IEEE Global Telecommun. Conf. (GLOBECOM)*, pp. 1–6, Dec. 2015.

[176] I. Yildirim, E. Basar, and I. Altunbas, "Quadrature channel modulation," *IEEE Wireless Commun. Lett.*, vol. 6, pp. 790–793, Aug. 2017.

[177] S. Dhanasekaran, "Space-polarization shift keying modulation for MIMO channels," *Wireless Pers. Commun.*, vol. 86, pp. 1509–1539, Aug. 2015.

[178] G. Zafari, M. Koca, and H. Sari, "Spatial modulation with dual-polarized antennas," in *Proc. IEEE Int. Conf. Commun. (ICC)*, pp. 2375–2380, Jun. 2015.

[179] G. Zafari, M. Koca, and H. Sari, "Dual-polarized spatial modulation over correlated fading channels," *IEEE Trans. Commun.*, vol. 65, pp. 1336–1352, Dec. 2017.

[180] M. Au, G. Kaddoum, M. S. Alam, E. Basar, and F. Gagnon, "Joint code-frequency index modulation for IoT and multi-user communications," *IEEE J. Sel. Topics Sig. Process.*, vol. 13, pp. 1223–1236, Aug. 2019.

[181] P. Botsinis, I. Hemadeh, D. Alanis, Z. Babar, H. V. Nguyen, *et al.*, "Joint-alphabet space time shift keying in mm-Wave non-orthogonal multiple access," *IEEE Access*, vol. 6, pp. 22602–22621, Aug. 2018.

[182] I. A. Hemadeh, M. El-Hajjar, and L. Hanzo, "Hierarchical multi-functional layered spatial modulation," *IEEE Access*, vol. 6, pp. 9492–9533, Feb. 2018.

[183] H. Zhang, L. Yang, and L. Hanzo, "Compressed sensing improves the performance of subcarrier index-modulation-assisted OFDM," *IEEE Access*, vol. 4, pp. 7859–7873, Oct. 2016.

[184] M. I. Kadir, "Generalized space?time?frequency index modulation," *IEEE Commun. Lett.*, vol. 23, pp. 250–253, Oct. 2019.

[185] R. Zhang, L. Yang, and L. Hanzo, "Error probability and capacity analysis of generalised pre-coding aided spatial modulation," *IEEE Trans. Wireless Commun.*, vol. 14, pp. 364–375, Jan. 2015.

[186] J. Luo, S. Wang, and F. Wang, "Joint transmitter-receiver spatial modulation design via minimum Euclidean distance maximization," *IEEE J. Sel. Areas Commun.*, vol. 37, pp. 1986–2000, Jul. 2019.

[187] A. Burdett, "Ultra-low-power wireless systems: Energy-efficient radios for the Internet-of-Things," *IEEE Solid-State Circuits Mag.*, vol. 7, pp. 18–28, Jun. 2015.

[188] J. Choi, "Single-carrier index modulation for IoT uplink," *IEEE J. Sel. Topics Sig. Process.*, vol. 13, pp. 1237–1248, Oct. 2019.

[189] B. Shamasundar, S. Jacob, L. N. Theagarajan, and A. Chockalingam, "Media-based modulation for the uplink in massive MIMO systems," *IEEE Trans. Veh. Technol.*, vol. 67, pp. 8169–8183, Sep. 2018.

[190] X. Ma, S. Guo, and D. Yuan, "Improved compressed sensing-based joint user and symbol detection for media-based modulation-enabled massive machine-type communications," *IEEE Access*, vol. 8, pp. 70058–70070, Apr. 2020.

[191] A. Tusha, S. Dogan, and H. Arslan, "Performance analysis of frequency domain IM schemes under CFO and IQ imbalance," in *Proc. IEEE Int. Symp. Pers., Indoor Mobile Radio Commun. (PIMRC)*, pp. 1–5, Sep. 2019.

[192] S. Dogan, A. Tusha, and H. Arslan, "NOMA with index modulation for uplink URLLC through grant-free access," *IEEE J. Sel. Topics Sig. Process.*, vol. 13, pp. 1–1, May 2019.

[193] T. Yucek and H. Arslan, "A survey of spectrum sensing algorithms for cognitive radio applications," *IEEE Commun. Surveys Tut.*, vol. 11, pp. 116–130, Mar. 2009.

[194] I. F. Akyildiz, W.-Y. Lee, M. C. Vuran, and S. Mohanty, "A survey on spectrum management in cognitive radio networks," *IEEE Commun. Mag.*, vol. 46, pp. 40–48, Apr. 2008.

[195] J. Wang, M. Ghosh, and K. Challapali, "Emerging cognitive radio applications: A survey," *IEEE Commun. Mag.*, vol. 49, pp. 74–81, Mar. 2011.

[196] A. Goldsmith, S. A. Jafar, I. Maric, and S. Srinivasa, "Breaking spectrum gridlock with cognitive radios: An information theoretic perspective," *Proc. IEEE*, vol. 97, pp. 894–914, Apr. 2009.

[197] A. Afana, T. M. N. Ngatched, O. A. Dobre, and S. Ikki, "Spatial modulation in MIMO cognitive radio networks with channel estimation errors and primary interference constraint," in *Proc. IEEE Global Telecommun. Conf. Workshops (GLOBECOM)*, pp. 1–6, Dec. 2015.

[198] I. A. Mahady, A. Afana, R. Mesleh, S. Ikki, and I. Atawi, "Cognitive MIMO quadrature spatial modulation systems with mutual primary-secondary co-channel interference," in *Proc. IEEE Wireless Commun. Netw. Conf. (WCNC)*, pp. 1–5, Sep. 2016.

[199] A. Alizadeh, H. R. Bahrami, and M. Maleki, "Performance analysis of spatial modulation in overlay cognitive radio communications," *IEEE Trans. Commun.*, vol. 64, pp. 3220–3232, Aug. 2016.

[200] Q. Li, M. Wen, M. D. Renzo, H. V. Poor, S. Mumtaz, and F. Chen, "Dual-hop spatial modulation with a relay transmitting its own information," *IEEE Trans. Wireless Commun.*, vol. 19, pp. 4449–4463, Apr. 2020.

[201] J. Li, Y. Peng, Y. Yan, X. Jiang, H. Hai, *et al.*, "Cognitive radio network assisted by OFDM with index modulation," *IEEE Trans. Veh. Technol.*, vol. 69, pp. 1106–1110, Nov. 2020.

[202] Q. Li, M. Wen, S. Dang, E. Basar, H. V. Poor, *et al.*, "Opportunistic spectrum sharing based on OFDM with index modulation," *IEEE Trans. Wireless Commun.*, vol. 19, pp. 192–204, Oct. 2020.

[203] S. Xu, Y. Li, Y. Gao, Y. Liu, and H. Gacanin, "Opportunistic coexistence of LTE and WiFi for future 5G system: Experimental performance evaluation and analysis," *IEEE Access*, vol. 6, pp. 8725–8741, Dec. 2018.

[204] E. Khorov, A. Kiryanov, A. Lyakhov, and G. Bianchi, "A tutorial on IEEE 802.11ax high efficiency WLANs," *IEEE Commun. Surveys Tut.*, vol. 21, pp. 197–216, Sep. 2019.

[205] A. Nosratinia, T. E. Hunter, and A. Hedayat, "Cooperative communication in wireless networks," *IEEE Commun. Mag.*, vol. 42, pp. 74–80, Jun. 2004.

[206] G. Altın, E. Başar, Ü. Aygölü, and M. E. Celebi, "Performance analysis of cooperative spatial modulation with multiple-antennas at relay," in *Proc. IEEE Int. Black Sea Conf. Commun. Netw. (BlackSeaCom)*, pp. 1–5, Jul. 2016.

[207] S. Dang, G. Chen, and J. P. Coon, "Power allocation for adaptive OFDM index modulation in cooperative networks," in *Proc. IEEE Global Telecommun. Conf. (GLOBECOM)*, pp. 1–6, Jan. 2017.

[208] Q. Li, M. Wen, E. Basar, H. V. Poor, and F. Chen, "Spatial modulation-aided cooperative NOMA: Performance analysis and comparative study," *IEEE J. Sel. Topics Sig. Process.*, vol. 13, pp. 715–728, Feb. 2019.

[209] X. Chen, M. Wen, and S. Dang, "On the performance of cooperative OFDM-NOMA system with index modulation," *IEEE Wireless Commun. Lett.*, vol. 1, pp. 1–1, Apr. 2020.

[210] J. Zhao, S. Dang, and Z. Wang, "Full-duplex relay-assisted orthogonal frequency-division multiplexing with index modulation," *IEEE Syst. J.*, vol. 13, pp. 2320–2331, Sep. 2019.

[211] Y. Naresh and A. Chockalingam, "Performance analysis of full-duplex decode-and-forward relaying with media-based modulation," *IEEE Trans. Veh. Technol.*, vol. 68, pp. 1510–1524, Dec. 2019.

[212] J. M. Hamamreh, H. M. Furqan, and H. Arslan, "Classifications and applications of physical layer security techniques for confidentiality: A comprehensive survey," *IEEE Commun. Surveys Tut.*, vol. 21, pp. 1773–1828, Oct. 2018.

[213] Y. Lee, H. Jo, Y. Ko, and J. Choi, "Secure index and data symbol modulation for OFDM-IM," *IEEE Access*, vol. 5, pp. 24959–24974, Nov. 2017.

[214] M. Furqan, J. Hamamreh, and H. Arslan, "Adaptive OFDM-IM for enhancing physical layer security and spectral efficiency of future wireless networks," *Wireless Commun. Mobile Comput.*, vol. 2018, pp. 1–16, 2018.

[215] X.-Q. Jiang, M. Wen, H. Hai, J. Li, and S. Kim, "Secrecy-enhancing scheme for spatial modulation," *IEEE Commun. Lett.*, vol. 22, pp. 550–553, Mar. 2017.

[216] E. Basar, M. Di Renzo, J. De Rosny, M. Debbah, M. Alouini, *et al.*, "Wireless communications through reconfigurable intelligent surfaces," *IEEE Access*, vol. 7, pp. 116753–116773, Aug. 2019.

[217] C. Liaskos, S. Nie, A. Tsioliaridou, A. Pitsillides, S. Ioannidis, *et al.*, "A new wireless communication paradigm through software-controlled metasurfaces," *IEEE Commun. Mag.*, vol. 56, pp. 162–169, Sep. 2018.

[218] S. Gopi, S. Kalyani, and L. Hanzo, "Intelligent reflecting surface assisted beam index-modulation for millimeter wave communication," Mar. 2020.

[219] A. E. Canbilen, E. Basar, and S. S. Ikki, "Reconfigurable intelligent surface-assisted space shift keying," Jan. 2020.

[220] Z. Gao, L. Dai, S. Han, C. I, Z. Wang, and L. Hanzo, "Compressive sensing techniques for next-generation wireless communications," *IEEE Wireless Commun.*, vol. 25, pp. 144–153, Feb. 2018.

[221] S. Lu, I. A. Hemadeh, M. El-Hajjar, and L. Hanzo, "Compressed sensing-aided multi-dimensional index modulation," *IEEE Trans. Commun.*, vol. 67, pp. 4074–4087, Jun. 2019.

[222] L. Xiao, Y. Xiao, C. Xu, X. Lei, P. Yang, *et al.*, "Compressed-sensing assisted spatial multiplexing aided spatial modulation," *IEEE Trans. Wireless Commun.*, vol. 17, pp. 794–807, Nov. 2018.

[223] L. Xiao, P. Xiao, Y. Xiao, H. Haas, A. Mohamed, and L. Hanzo, "Compressive sensing assisted generalized quadrature spatial modulation for massive MIMO systems," *IEEE Trans. Commun.*, vol. 67, pp. 4795–4810, Apr. 2019.

[224] I. A. Hemadeh, S. Lu, M. El-Hajjar, and L. Hanzo, "Compressed sensing-aided index modulation improves space-time shift keying assisted millimeter-wave communications," *IEEE Access*, vol. 6, pp. 64742–64756, Oct. 2018.

[225] T. Wang, F. Yang, J. Song, and Z. Han, "Deep convolutional neural network-based detector for index modulation," *IEEE Wireless Commun. Lett.*, vol. 1, pp. 1–1, Jun. 2020.

[226] J. G. Andrews, S. Buzzi, W. Choi, S. V. Hanly, A. Lozano, *et al.*, "What will 5G be?," *IEEE J. Select. Areas Commun.*, vol. 32, pp. 1065–1082, Jun. 2014.

[227] X. Zhang *et al.*, "Mixed numerologies interference analysis and inter-numerology interference cancellation for windowed OFDM systems," *IEEE Trans. Veh. Technol.*, vol. 67, pp. 7047–7061, Aug. 2018.

[228] J. Choi, B. Kim, K. Lee, and D. Hong, "A transceiver design for spectrum sharing in mixed numerology environments," *IEEE Trans. Wireless Commun.*, vol. 18, pp. 2707–2721, May 2019.

[229] A. B. Kihero, M. S. J. Solaija, and H. Arslan, "Inter-numerology interference for beyond 5G," *IEEE Access*, vol. 7, pp. 146512–146523, Oct. 2019.

[230] K. S. Chandran and C. K. Ali, "Filtered-OFDM with index modulation for mixed numerology transmissions," in *Proc. Int. Conf. Adv. Comp. Commun. Sys. (ICACCS)*, pp. 306–310, May 2020.

A Appendix: Copyright Notices

The copyright notices for the use of material in Chapter 3 is below.

7/23/2020 Rightslink® by Copyright Clearance Center

Copyright Clearance Center RightsLink®

Home | Help | Email Support | Sign in | Create Account

IEEE Requesting permission to reuse content from an IEEE publication

Optimization of Antenna Beamwidth under Blockage Impact in Millimeter-Wave Bands

Conference Proceedings:
2018 IEEE 29th Annual International Symposium on Personal, Indoor and Mobile Radio Communications (PIMRC)

Author: Seda Doğan

Publisher: IEEE

Date: Sept. 2018

Copyright © 2018, IEEE

Thesis / Dissertation Reuse

The IEEE does not require individuals working on a thesis to obtain a formal reuse license, however, you may print out this statement to be used as a permission grant:

Requirements to be followed when using any portion (e.g., figure, graph, table, or textual material) of an IEEE copyrighted paper in a thesis:

1) In the case of textual material (e.g., using short quotes or referring to the work within these papers) users must give full credit to the original source (author, paper, publication) followed by the IEEE copyright line © 2011 IEEE.
2) In the case of illustrations or tabular material, we require that the copyright line © [Year of original publication] IEEE appear prominently with each reprinted figure and/or table.
3) If a substantial portion of the original paper is to be used, and if you are not the senior author, also obtain the senior author's approval.

Requirements to be followed when using an entire IEEE copyrighted paper in a thesis:

1) The following IEEE copyright/ credit notice should be placed prominently in the references: © [year of original publication] IEEE. Reprinted, with permission, from [author names, paper title, IEEE publication title, and month/year of publication]
2) Only the accepted version of an IEEE copyrighted paper can be used when posting the paper or your thesis on-line.
3) In placing the thesis on the author's university website, please display the following message in a prominent place on the website: In reference to IEEE copyrighted material which is used with permission in this thesis, the IEEE does not endorse any of [university/educational entity's name goes here]'s products or services. Internal or personal use of this material is permitted. If interested in reprinting/republishing IEEE copyrighted material for advertising or promotional purposes or for creating new collective works for resale or redistribution, please go to http://www.ieee.org/publications_standards/publications/rights/rights_link.html to learn how to obtain a License from RightsLink.

If applicable, University Microfilms and/or ProQuest Library, or the Archives of Canada may supply single copies of the dissertation.

BACK CLOSE WINDOW

© 2020 Copyright - All Rights Reserved | Copyright Clearance Center, Inc. | Privacy statement | Terms and Conditions
Comments? We would like to hear from you. E-mail us at customercare@copyright.com

https://s100.copyright.com/AppDispatchServlet#formTop 1/1

The copyright notices for the use of material in Chapter 4 is below.

7/23/2020 Rightslink® by Copyright Clearance Center

Copyright Clearance Center RightsLink® Home Help Email Support Sign in Create Account

IEEE Requesting permission to reuse content from an IEEE publication

NOMA With Index Modulation for Uplink URLLC Through Grant-Free Access

Author: Seda Doğan
Publication: Selected Topics in Signal Processing, IEEE Journal of
Publisher: IEEE
Date: Oct. 2019

Copyright © 2019, IEEE

Thesis / Dissertation Reuse

The IEEE does not require individuals working on a thesis to obtain a formal reuse license, however, you may print out this statement to be used as a permission grant:

Requirements to be followed when using any portion (e.g., figure, graph, table, or textual material) of an IEEE copyrighted paper in a thesis:

1) In the case of textual material (e.g., using short quotes or referring to the work within these papers) users must give full credit to the original source (author, paper, publication) followed by the IEEE copyright line © 2011 IEEE.
2) In the case of illustrations or tabular material, we require that the copyright line © [Year of original publication] IEEE appear prominently with each reprinted figure and/or table.
3) If a substantial portion of the original paper is to be used, and if you are not the senior author, also obtain the senior author's approval.

Requirements to be followed when using an entire IEEE copyrighted paper in a thesis:

1) The following IEEE copyright/ credit notice should be placed prominently in the references: © [year of original publication] IEEE. Reprinted, with permission, from [author names, paper title, IEEE publication title, and month/year of publication]
2) Only the accepted version of an IEEE copyrighted paper can be used when posting the paper or your thesis on-line.
3) In placing the thesis on the author's university website, please display the following message in a prominent place on the website: In reference to IEEE copyrighted material which is used with permission in this thesis, the IEEE does not endorse any of [university/educational entity's name goes here]'s products or services. Internal or personal use of this material is permitted. If interested in reprinting/republishing IEEE copyrighted material for advertising or promotional purposes or for creating new collective works for resale or redistribution, please go to http://www.ieee.org/publications_standards/publications/rights/rights_link.html to learn how to obtain a License from RightsLink.

If applicable, University Microfilms and/or ProQuest Library, or the Archives of Canada may supply single copies of the dissertation.

BACK CLOSE WINDOW

© 2020 Copyright - All Rights Reserved | Copyright Clearance Center, Inc. | Privacy statement | Terms and Conditions
Comments? We would like to hear from you. E-mail us at customercare@copyright.com

https://s100.copyright.com/AppDispatchServlet#formTop 1/1

About The Author

Received her B.Sc. degree in electronics and telecommunication engineering from Kocaeli University, Kocaeli, Turkey, in 2015. She has been working towards her Ph.D. degree as a member of the Communications, Signal Processing, and Networking Center (CoSiNC) at Istanbul Medipol University, Istanbul, Turkey since 2015. Her research interests include index modulation (IM), millimeter-wave (mmWave) frequency bands, non-orthogonal multiple accessing (NOMA) schemes, and random access techniques for next-generation wireless networks.

INTERFERENCE AND CHANNEL CONTROL TECHNIQUES FOR THE FUTURE OF WIRELESS COMMUNICATIONS

ORIGINALITY REPORT

15%	11%	5%	10%
SIMILARITY INDEX	INTERNET SOURCES	PUBLICATIONS	STUDENT PAPERS

MATCH ALL SOURCES (ONLY SELECTED SOURCE PRINTED)

4%

★ scholarcommons.usf.edu

Internet Source

Exclude quotes	Off	Exclude matches	Off
Exclude bibliography	On		